



UNIVERSITÀ  
DEGLI STUDI  
DI PADOVA

Università degli Studi di Padova  
Department of Molecular Medicine

Ph.D. COURSE IN MOLECULAR MEDICINE  
CURRICULUM: REGENERATIVE MEDICINE  
SERIES XXXII

**Crosstalk between ECM mechanical cues and cellular  
metabolism**

**Coordinator:** Prof. Stefano Piccolo

**Supervisor:** Prof. Sirio Dupont

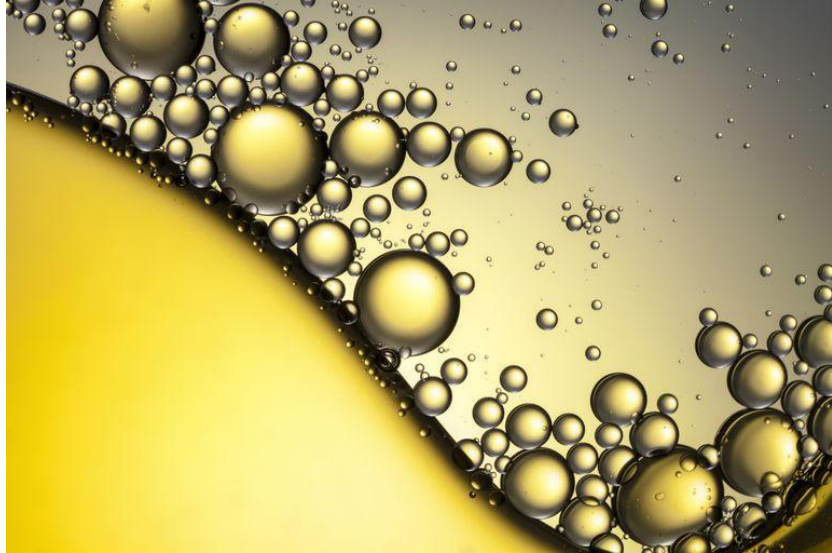
**PhD student :** Irene Brian



*Dedicated to myself and most importantly to my family, who has been supporting me in every aspect of life, without being too intrusive, and by letting me choose each single next step.*

*In such a way, they gifted me with the freedom to make important educative mistakes.*

*Dedicata a me stessa e alla mia famiglia, che mi ha supportata in tutto e per tutto in questi anni, senza fare troppe domande, lasciandomi la possibilità di scegliere ogni mio passo, e dandomi così anche la libertà, a volte, di sbagliare.*



## Summary

PUBLICATIONS .....	8
ABSTRACT.....	9
INTRODUCTION.....	10
A role for physical forces in biology.....	10
What physical forces act on cells and tissues?.....	10
Cells can sense physical forces .....	11
Mechanosensing .....	12
Mechanotransduction .....	13
Mechanoresponses .....	14
Cell metabolism .....	16
Cholesterol synthesis.....	19
Lipid and cholesterol homeostasis: The role for SREBP signalling pathway.....	20
Sterol-dependent regulation of SREBPs .....	21
SREBP regulation downstream of the mTOR kinase .....	23
The biology of the LIPIN-1 phosphatidate phosphatase .....	24
Mechanotransduction and Metabolism: State of Art.....	25
RATIONALE.....	29
RESULTS .....	30
Low actomyosin contractility induces lipid accumulation.....	30
Lipid accumulation is independent from YAP/TAZ transcriptional factors .....	31
Lipid accumulation in conditions of low tension correlates with activation of SREBP transcription factors.....	32
ECM mechanical cues regulate lipid accumulation through SREBP1/2.....	33
ECM mechanical cues regulate SREBP processing.....	33
SREBP activity is repressed in stiffened keloid tissues .....	34
ECM mechanical cues regulate SREBP through SCAP .....	35
Lipid synthesis contributes to the beneficial effects of ROCK inhibitors in hPSC.....	36
Lipin1 and ARF1 inhibition induce lipid accumulation and SREBP activation.....	37
ECM mechanical cues regulate Lipin1 and ARF1 activity .....	38
LIPIN1 mediates the effects of tension on SREBP activity .....	39
The Golgi apparatus: a mechanosensitive organelle? .....	40

FIGURES .....	46
FIGURE 1 .....	47
FIGURE 2 .....	49
FIGURE 3 .....	51
FIGURE 4 .....	53
FIGURE 5 .....	55
FIGURE 6 .....	57
FIGURE 7 .....	59
FIGURE 8 .....	61
FIGURE 9 .....	62
FIGURE 10 .....	64
FIGURE 11 .....	66
FIGURE 12 .....	68
FIGURE 13 .....	70
FIGURE 14 .....	72
FIGURE 15 .....	74
MATERIALS AND METHODS .....	77
Plasmids and recombinant plasmids .....	77
Recombinant retrovirus for stable transduction .....	77
Cell cultures .....	78
siRNA transfection.....	78
Reagents .....	80
RNA extraction .....	81
Retrotranscription protocol .....	81
RT-PCR.....	81
Western blot .....	83
Cell fractionation and pulldown.....	84
Luciferase Assay .....	84
Antibody and Microscopy.....	85
Oil red O and Filipin Staining .....	87
Alkaline Phosphatase Staining .....	88

EdU Incorporation Assay .....	89
Hydrogel Preparation .....	89
Metabolomics and metabolic analyses .....	90
Microarray .....	92
Intracellular optical micromanipulation, microrheological measurements and analysis .....	92
REFERENCES .....	96

## PUBLICATIONS

- Giulia Santinon, Irene Brian, Arianna Pocaterra, Patrizia Romani, Elisa Franzolin, Chiara Rampazzo, Silvio Bicciato, Sirio Dupont. dNTP metabolism links mechanical cues and YAP/TAZ to cell growth and oncogene-induced senescence. *EMBO J.* **37**, e97780 (2018).
- Patrizia Romani, Irene Brian, Giulia Santinon, Arianna Pocaterra, Matteo Audano, Silvia Pedretti, Samuel Mathieu, Mattia Forcato, Silvio Bicciato, Jean-Baptiste Manneville, Nico Mitro & Sirio Dupont. Extracellular matrix mechanical cues regulate lipid metabolism through Lipin-1 and SREBP. *Nat. Cell Biol.* **21**, 338–347 (2019)
- Arianna Pocaterra, Giulia Santinon, Patrizia Romani, Irene Brian, Andrea Dimitracopoulos, Andra Ghisleri, Alejandro Carnicer Lombarte, Mattia Forcato, Paola Braghetta, Marco Montagner, Francesca Galuppini, Mariaceleste Aragona, Gianmaria Pennelli, Silvio Bicciato, Nils Gauthier, Kristian Franze, Sirio Dupont. F-actin dynamics regulates mammalian organ growth and cell fate maintenance. *J. Hepatol.* **71**, 130–142 (2019)

## **ABSTRACT**

Mechanical cues coming from the extracellular matrix (ECM) are key factors in the control of tissue homeostasis in physiology and disease. Cells can sense these physical cues and measure external resisting forces by adjusting their actomyosin cytoskeleton, which in turn regulates intracellular signalling pathways to orchestrate a proper cell response. Thus, ECM stiffness is important for many biological aspects such as proliferation, differentiation and migration. Very little is known instead, about its impact on cellular metabolism, and the molecular players involved in this process are largely unknown. Starting from an unbiased metabolomics approach, we found lipid accumulation as a general response to mechanical signals and to low tension conditions. Mechanistically, this accumulation is associated with a decreased Lipin1 phosphatidate phosphatase localization at ER/Golgi membranes and decreased Lipin1 activity which ultimately lead to nuclear translocation and activation of SREBP1/2 transcription factors. This occurs independently of YAP/TAZ and mTOR, and in parallel to the feedback control by sterols. Led by our findings, we discovered a coherent regulation of SREBP in stiffened pathological human tissues, and identified SREBP as required for the pro-survival activity of ROCK inhibitors in embryonic stem cells. We thus propose that SREBP is a general mechanism that links the physical cell microenvironment to a key metabolic pathway.

# INTRODUCTION

## A role for physical forces in biology

It is well known that biochemical soluble signals are key players during cell and tissue development as well as in regulating adult cellular functions<sup>1,2</sup>. Indeed, throughout all the life of any living organism hormones, growth factors and cytokines continuously signal to cells, enabling cells to exchange information and coordinate their behaviour. However, multiple evidence led to the idea that additional inputs exist that regulate tissue development and cellular functions<sup>3,4</sup>. For example, cells and tissues are responsive to physical and mechanical forces that are embedded in their microenvironment. This is relevant to understand tissue physiology, because mechanical cues can be as important as chemical factors to regulate cell functions<sup>5,6</sup>. One of the first fields where scientists started to take into account physical forces is developmental biology. Here, mechanical forces are integral to many processes starting from early development to gastrulation and organogenesis<sup>3,5,7</sup>. This goes from spatial regulation of mitotic spindle orientation and cell division to the morphogenetic movements that shape embryonic tissues and structures<sup>3</sup>. Mechanical forces are not only required to shape tissues, but in turn drive cell and tissue differentiation: in vivo data also showed that lung, joint and heart development can be seriously compromised by the absence of tissue deformations provided by muscle contraction and the intracardiac blood flow<sup>3</sup>. More recently, also adult tissues and organs has been discovered to play by the rules of physics. Infact, the elasticity of the microenvironment can regulate stem cell lineage specification<sup>6,8</sup>, adult cell proliferation<sup>9,10</sup> and apoptosis<sup>11</sup>. Furthermore, it's been shown that cellular shape and tension controls the differentiation of human epidermal keratinocytes and human mesenchymal stem cell commitment<sup>6,8</sup>.

## What physical forces act on cells and tissues?

Cells and tissues are constantly subjected to mechanical forces from the external environment. Some examples of these forces are the contraction of muscles and skeletal muscles that deform neighbouring tissues, pumping of the heart and flowing of blood

exerting pressure and shear stresses on vessel's walls, gravity, stretching or contraction of whole tissues such as the lungs or, locally, of neighbouring cells within a tissue, such as cutaneous receptors for the sense of touch<sup>3,12</sup>. This also applies to hearing, where mechanical sound waves propagate to the inner ear where sound receptor cells are located. All these forces create different tensions in tissues and cells, modifying the status of the organ and perturbing cellular and tissue microenvironment. Physical forces can also come from the cells themselves. These endogenous forces are mainly due to the tension arising from the contractility of the cell cytoskeleton. Mechanobiology is an emerging field that focuses on understanding how cells can sense mechanical forces and convert them into biochemical signals, thus enabling cells to adapt to their physical surroundings. This phenomenon of signal conversion from mechanical to chemical is indicated by the name of mechanotransduction, and in the last years many studies have been carried out in this field, given its important role during cellular decision-making<sup>13</sup>.

## Cells can sense physical forces

Cells are geared with specific structures to sense external forces. For example, cells can sense the intensity and direction of liquid flowing at their surface by displacement of cilia, or by stretching of their cell-cell adhesions. Another example is the ability of cells to sense stretching of their plasma membrane thanks to tension-dependent ion channels, including TRPMs and the recently identified Piezo. Finally, cells are also able to sense the elasticity of the surrounding extracellular matrix (ECM). The ECM is a complex 3D network of fibrillary proteins (including collagens, elastin, proteoglycans, laminin and fibronectin) that surrounds most cells in animal bodies, and serves as physical scaffolds to provide structural support and biochemical signalling to cells<sup>5,14</sup>; cell attachment to this network is indeed fundamental for their correct function<sup>5</sup>.

Each tissue is characterized by a different ECM composition, due to the variable concentration of proteins and to the diverse degree of cross-linking between them. This diversity also confers different mechanical properties of the ECM, such as stiffness or elasticity. Thus, specific organs have a distinct stiffness which is instrumental for their physiological functions. For example, the adipose tissue, lung, breast and brain are among

the softest tissues, skeletal muscles are characterized instead by intermediate values, and bone exhibit higher stiffness<sup>5, 15</sup> (FIG. 1a). The physiological stiffness of a tissue can change during aging or in disease conditions<sup>5,16</sup>, for example during tissue fibrosis or during cancer growth, when tumour cells actively stiffen the surrounding ECM. Furthermore, an ischemic insult usually induce the degradation of the cardiac matrix, leaving a scar with very different composition<sup>17</sup>. These structural changes of the myocardial ECM affect cardiomyocyte function<sup>6</sup>, thus compromising the overall structure and function of the whole myocardium. Interestingly, remodelling of the physical properties of the cell microenvironment is not only an effect of the disease, but it is also a fundamental concurring factor as it can locally instruct cell behaviour<sup>16,18</sup>(see below), making it a fundamental regulator of cell behaviour.

So how do cells perceive ECM stiffness?

## Mechanosensing

The process by which cells sense an external mechanical cue is generally called *mechanosensing*. In the case of ECM stiffness, this mechanism is based on integrins and focal adhesion complexes that are found in the cell membrane at the ECM-cells contact sites<sup>15,16</sup>. These complexes acts as primary sensors and transduce the physical forces into biochemical signals, ultimately regulating intracellular signalling pathways and orchestrating a cell response<sup>14, 16</sup>. When cells adhere to the ECM, integrin receptors cluster together and start recruiting adaptor molecules such as focal adhesion kinases (FAKs), paxillin, and talin to induce focal adhesion assembly<sup>16</sup>. These structures constitute a physical bridge between the ECM and the cell interior, where they connect to the F-actin cytoskeleton. The cytoskeleton is a dynamic structure composed by actin fibers (F-actin), microtubules (MTs) and intermediate filaments (IFs). It functions as structural support to the cells and regulates their motility, shape and tension homeostasis<sup>15</sup>. Once the initial integrin clusters assemble and get stabilized by cytosolic adaptor proteins, the so-called focal points are established; this in turn enables the local polymerisation of actin filaments. F-actin attached to focal points typically form linear bundles, held together by a-actinin and fascin crosslinking proteins, that are able to contract thanks to the presence of the non-muscle

myosin II motor proteins<sup>14,19</sup>. By this process cells start the formation of contractile stress fibers and are thus able to pull on the ECM, probing its elasticity.

## Mechanotransduction

During the mechanotransduction process the pulling of cells on focal adhesions, resisted by ECM, enables cells to measure ECM stiffness. Even if the precise molecular mechanisms are not fully understood yet, it is indeed clear that cells need to develop internal traction forces to measure ECM stiffness and behave accordingly<sup>20</sup>. If the ECM is stiff enough to resist, this enables the conformational switch of some focal adhesion proteins, such as talins, and the subsequent recruitment of other adaptor proteins such as vinculin, to strengthen further the link with F-actin and to enable the development of higher traction forces. In turn, this enable the growth and maturation of focal points into larger and much more stable structures, i.e. focal adhesions. This means that only a stiff ECM induces full blown focal adhesion and stress fiber maturation, with maximal development of intracellular tension or contractility. Cells grown on very soft substrates show instead few/smaller focal adhesions and stress fibers, or no discernible focal adhesions at all, and ultimately less tension at the cell-ECM contact sites. Thus, mechanotransduction is an active process by which cells oppose extracellular forces, and in doing so they measure these forces.

Focal adhesion maturation under tension then enables the activation of multiple signalling events (FIG 1b). For example, activation of FAKs can induce cell proliferation and stem cell differentiation through ERKs and can regulate cell migration by acting on Src phosphorylation of p130 Cas and Grb7 proteins<sup>14</sup>. One crucial signalling pathway in the regulation of cell-matrix mechanotransduction is Rho/ROCK. The Rho GTPases protein family has a central role in regulating the actin cytoskeleton. The three main classes of this family are Rho itself (RhoA, RhoB, RhoC), Rac1 and Cdc42. The main function of RhoA is to induce stress fibers formation. It has been shown that Rho activity is regulated by ECM stiffness, and in particular, a stiff matrix induces Rho activity and thus cell contractility<sup>20,21</sup>. Thus, following transmission of physical forces across focal adhesions and activation of the small GTPase Rho, this activates two primary downstream effectors: ROCK (Rho-associated protein kinase) and the mDia family of F-actin polymerisation factors. ROCK is

a serine/threonine kinase that can phosphorylate the myosin-binding subunit of myosin phosphatase, preventing myosin inactivation, and the myosin regulatory light chain, directly stimulating myosin activity and enhancing actomyosin contractility. ROCK also phosphorylates and activates LIM-kinase<sup>20</sup>, which in turn phosphorylates and inactivates cofilin which is an actin depolymerizing factor, to stabilize existing actin filaments. Since RHO/ROCK signalling is required for the development of contractile actin bundles, inhibition of any of these players affects focal adhesion maturation, traction force development, and the ability of cells to measure ECM stiffness<sup>20,21</sup>.

## Mechanoresponses

Experimental evidence indicates that ECM mechanical cues can influence cell proliferation, migration, differentiation and death<sup>9,11</sup>. Initial studies unveiled how increasing availability of adhesion sites regulated cell geometry, with cells taking on a round shape in the presence of very few adhesion sites, and instead spreading against the substratum in the presence of abundant adhesion sites, and how, surprisingly, this was sufficient to drive, in a dose-dependent manner, multiple cell phenotypes<sup>22,23,24</sup>. This occurred in the absence of any cell-cell contact, ruling out a primary effect of cell-cell adhesions in mediating these effects, and by consequence ruling out the involvement of cell-cell adhesion associated molecules. Subsequent studies demonstrated in a more formal manner how the spacing, rather than the total amount, of the adhesion sites was the key parameter to support cell spreading and the associated phenotypes<sup>25</sup>, which importantly ruled out a simple quantitative (and, thus, “biochemical”) effect of the ECM. At the same time, others developed tools to modulate ECM elasticity specifically, without changing ECM composition and without changing the local concentration of ECM molecules available to cells: this was attained by the use of polyacrylamide hydrogels functionalized with ECM molecules<sup>26</sup>. In this case, a soft ECM promoted cell rounding and the associated phenotypes, while a stiff ECM promoted cell spreading. Bringing together the two similar but so far separate observations, it was later measured that both a soft ECM and a small adhesive area induce decreased cell traction forces against the substratum<sup>27</sup>, and that treating cells freely spreading on a stiff substratum with drugs inhibiting cell traction forces (RHO inhibition, ROCK inhibition, NMII inhibition) induced cell rounding and the associated phenotypes<sup>25,26,8</sup>. This overall suggested

the existence of biochemical signal transduction pathways regulated downstream of mechanical cues (FIG.1c), whose identity was unveiled in the following decade.

Initial studies focused on focal-adhesion associated signalling molecules such as the tyrosine kinase c-Abl, shuttling from the FAs to the nucleus in response to cell cycle cues<sup>28</sup>, or FAKs-dependent regulation of JNK or Rac1, which can induce cyclin D1 and E2F transcription and cell proliferation. Other players involved in the mechano-dependent regulation of proliferation are the PI3K/Akt and MEK/ERK signalling pathways, likely owing to the cross-talk between integrin complexes and RTKs. Other identified the MAL/MRTF coactivators, partners of the SRF (serum response factor) transcription factors, as nucleus/cytoplasmic factors regulated by the actin cytoskeleton: when cells are stimulated by serum, the activation of GPCRs (G-protein coupled receptors) stimulate the activity of RHO/ROCK leading to F-actin polymerisation, and a corresponding decrease in monomeric or globular G-actin; this unleashed MAL/MRTF, that directly bind G-actin, enabling them to bind SRF and stimulate gene transcription<sup>29,30</sup>. Despite these fundamental findings, none of these pathway was shown to regulate in a general manner and across different cell types the wide array of phenotypes induced by ECM mechanical properties, which were not limited to proliferation but also included skewed differentiation of keratinocytes, hepatocytes and mesenchymal stem cells<sup>23,24,26</sup>.

Recently, such a general effector of ECM mechanical properties has been finally discovered. In Dupont et al. 2011, it's been reported that cell geometry, ECM stiffness and the contractile actin cytoskeleton regulate YAP/TAZ localization, and that this accounts for the main phenotypes driven by ECM mechanical cues. Yes-associated protein (YAP) and transcriptional coactivators with PDZ-binding motif (TAZ) are two paralog mammalian transcriptional coactivators that shuttle between the cytoplasm and the nucleus<sup>31</sup>. In the nucleus, they act in combination with TEAD family of transcription factors and control gene expression. They were previously known as downstream transducers of the Hippo pathway, an important tumor suppressor pathway controlling organ and tissue size across animals. As such, YAP/TAZ play a fundamental role in regulating cell proliferation and exert a great impact on tumorigenesis and cancer progression<sup>32,33</sup>. Many upstream regulatory inputs of YAP/TAZ have been identified so far<sup>26</sup>. Among them, cell geometry and cytoskeletal tension

induced by ECM stiffness have been shown to potently boost YAP/TAZ activity<sup>10,34</sup>. This suggests that adhesion of a cell to its surroundings ECM, and tensional forces of the cytoskeleton, by acting on YAP/TAZ activity, can make cells aware about the properties of the tissue in which they are enclosed.

## Cell metabolism

The word metabolism originates from the Greek “to change” and accordingly defines the set of chemical reactions occurring in living organisms to match the different needs of cells and tissues (FIG. 1d). Metabolic reactions are aimed at producing the basic biochemical components of cells such as lipids, amino acids, carbohydrates and nucleotides (anabolic reactions) or at breaking them down to extract energy (catabolic reactions). Anabolism involves three basic stages: firstly, the production of precursors such as amino acids, monosaccharides, isoprenoids and nucleotides; secondly, their activation into reactive forms; and thirdly, the assembly of these precursors into complex molecules. These processes are tightly regulated and allow organisms to grow and reproduce, maintain their structures, and respond to environmental changes. Metabolism is organized into metabolic pathways, in which one molecule is transformed into another by a sequence of ordered reactions which are catalysed by dedicated enzymes; regulation of enzyme expression and activity is crucial for the fine regulation of metabolic pathways. Animal cells depend on nutrient uptake to replenish the pool of biochemical precursors that fuel metabolism and provides energy for cell survival, including carbohydrates, amino acids and lipids.

There is a very large number of metabolic pathways. In humans, the most important are:

**Glycolysis**, which drives anaerobic glucose oxidation, with the breakdown of glucose into pyruvic acid and ATP. Glycolysis takes place in the cytoplasm and splits each six-carbon glucose molecule into two three-carbon pyruvate molecules. Glycolysis does not require oxygen to occur, and provides precursor molecules for other anabolic and catabolic metabolic pathways, including mitochondrial tricarboxylic acid (TCA) or Krebs’s cycle and

oxidative phosphorylation, the pentose-phosphate pathway, synthesis of precursors for glycosylation reactions, synthesis of phospholipids.

**TCA cycle**, where acetyl coenzyme A (acetyl CoA) is oxidised to obtain precursors for some aminoacids, reducing equivalents in the form of NADH and FADH<sub>2</sub>, GTP and, indirectly (through oxidative phosphorylation) ATP. This pathway takes place in the mitochondria and is initiated by acetyl CoA, which mainly derives from pyruvate or from fatty acid breakdown. While the citric acid cycle does not itself produce much ATP, the major energy currency of the cell, the NADH and FADH<sub>2</sub> molecules act as electron carriers that shuttle into the electron transport chain for oxidative phosphorylation and production of ATP.

**Oxidative phosphorylation (OXPHOS)** is the reaction that transforms the reducing equivalents produced in the TCA cycle into ATP. OXPHOS also takes place in the mitochondria, across the inner mitochondrial membrane. There are five transmembrane enzyme complexes, known as the electron transport chain, that transfer electrons from one molecule to another in a series of redox reactions. The transfer of electrons releases energy that drives translocation of protons against their concentration gradient from the mitochondrial matrix into the intermembrane space. This forms an electrochemical gradient which is dissipated by the ATP synthase complex: protons are transported back into the mitochondrial matrix along their concentration gradient, and the energy associated to this transport is used to catalyze the addition of a phosphate group to the ADP precursor forming ATP. By this reactions, coupled to glycolysis and the TCA cycle, one glucose molecule yields up to 36 ATP molecules, which is far more efficient than the 2 ATP molecules yield of direct pyruvate to lactate fermentation.

**Pentose phosphate pathway**, produces pentose sugars, necessary for the synthesis of purines and pyrimidines, and reducing equivalents needed for anabolic reactions, in the form of NADPH. This pathway branches off glycolysis just after the conversion of glucose into glucose-6-phosphate, and is composed of two branches: the oxidative branch, where glucose is transformed into ribose-5-phosphate and NADPH is produced, and the non-oxidative branch, where ribose can be converted into xylose-5-phosphate or back in fructose-6-phosphate and glyceraldehyde-3-phosphate, that can be routed back into glycolysis. The

non-oxidative branch is bidirectional, and can also be used independently of the oxidative one, depending on the availability of nutrients and on the need for NADPH. NADPH is indeed used in redox reactions to regenerate glutathione, and thus to scavenge reactive oxygen species (ROS), or during the synthesis of fatty acids.

**Glutamine metabolism** is an important carbon source. Glutamine is transported into cells via a specific amino acid transporter and converted into glutamate. Glutamate can follow multiple fates: it can be converted into  $\alpha$ -ketoglutarate and transported into mitochondria, feeding the TCA cycle and thus either empowering oxidative phosphorylation or providing the precursors for non-essential amino acid synthesis; it can be oxidised in the cytoplasm to isocitrate, providing NADPH and cytoplasmic acetyl-coA (typically, for fatty acid synthesis); it can be used to drive cysteine uptake and glutathione synthesis.

**Gluconeogenesis** produces glucose from pyruvate by using the reverse reactions occurring during glycolysis. This pathway is typically used by cells to transform fatty acids or other macromolecules into glucose and to release it into the blood-stream during fasting, to keep circulating glucose levels stable.

**Fatty acid  $\beta$ -oxidation** results in the breakdown of fatty acids into acetyl-CoA, to be used by the TCA cycle. Fatty acid beta-oxidation required fatty acids to be converted to acyl-carnitines and transported across the mitochondrial membrane; in mitochondria, fatty acids are then broken down into their acetyl-CoA subunits, which is usually used to support oxidative phosphorylation.

**Fatty acid synthesis** is the initial step for production of the main lipid molecules, which are the basic constituents of cell membranes and can be used to storage energy as triacylglycerols. This reaction takes place in the cytosol and forms fatty acids by polymerizing acetyl-CoA and NADPH. Acetyl-CoA units that fuel fatty acid synthesis can derive from different sources including glucose and glutamine catabolism, but also by direct conversion of extracellular acetate. Glucose breakdown also provides the precursor for glycerol, which combines with fatty acyl chains to form phosphatidates, diacylglycerols and triacylglycerols. Phosphatidates are also the precursors for the synthesis of phosphatidyl-

inositols; diacylglycerols are also the precursors for the main phospholipids, phosphatidylcholines and phosphatidyl-ethanolamines.

## Cholesterol synthesis

Cholesterol is the principal sterol in animal cells. It is present in the form of free cholesterol or cholesterol-esters. Cholesterol is an essential structural component of animal cell membranes<sup>35</sup> and the precursor of all steroid hormones, bile acids and vitamin D. Due to its chemical properties, cholesterol inserts within the lipid bilayers, among the phospholipid fatty-acid chains, and alters the biophysical properties of the membranes by making it less fluid and more rigid, thus promoting membrane integrity<sup>36</sup>. It also reduces the permeability of the plasma membrane to neutral solutes, hydrogen ions, and sodium ions<sup>37</sup>. Within membranes, cholesterol usually concentrates into discrete patches, the so-called lipid rafts, which are essential for endocytosis<sup>38</sup> but also provide an important platform that promotes the activity of several transmembrane signalling receptors<sup>39,40</sup>. Given these important functions, cholesterol levels are tightly regulated in cells so that they remain around a very narrow range of concentrations.

Cells obtain cholesterol either by taking it up from extracellular fluids (in the body, almost 80% of total daily production occurs in the liver), or by direct synthesis. Cholesterol synthesis occurs in the endoplasmic reticulum by a fine-tuned biosynthetic pathway that starts with the mevalonate pathway. Two molecules of acetyl-CoA condense, forming acetoacetyl-CoA, which condenses further with a third molecule of acetyl-CoA to yield the six-carbon molecule  $\beta$ -hydroxy- $\beta$ -methylglutaryl-CoA (HMG-CoA). These first reactions, catalyzed by thiolase and HMG-CoA synthase (HMGCS), respectively, are reversible and do not commit the cell to the synthesis of cholesterol. The third reaction is the committed step and entails the reduction of HMGCoA to mevalonate, using up NADPH. HMG-CoA reductase (HMGCR), an integral membrane protein of the smooth endoplasmic reticulum, catalyses this reaction and is the major point of regulation on cholesterol synthesis. In the next stages mevalonate is converted to isoprene compounds by a series of multimerisation reactions that leads to formation of geranyl-pyrophosphate and then to farnesyl-pyrophosphate. Farnesyl-PP can be used for cholesterol synthesis or for alternative

pathways, namely the synthesis of heme and related compounds, the synthesis of dolichol (for N-glycosylation of proteins into the ER), or the post-translational modification of proteins with lipid moieties (farnesylation and geranylation). If farnesyl-PP is committed to cholesterol synthesis, it first forms squalene and then the four-ring steroid nucleus, which is the basic shared structure of all the sterols. Important enzymes of this pathway are the sterol-C5 desaturase (SC5D) and 7-dehydrocholesterol reductase (DHCR7), the latter promoting the last step of cholesterol synthesis.

## Lipid and cholesterol homeostasis: The role for SREBP signalling pathway

As stated above, lipids and cholesterol play fundamental functions in cells and, as such, their biosynthesis and uptake is tightly controlled to maintain their levels at homeostasis: cholesterol biosynthesis was indeed discovered as an anabolic pathway undergoing end-product feedback suppression<sup>41,42</sup>. Schoenheimer and Breusch more than 60 years ago demonstrated that mice synthesize less cholesterol after they have ingested it in the diet<sup>43</sup>. Gould et al., twenty years later, by incubating liver slices from dogs and rabbits with [<sup>14</sup>C]acetate, observed that its incorporation into acetyl coA and then cholesterol was reduced to less than 2% of the control value when cholesterol had been supplied in the diet<sup>44</sup>. The identification of the underlying molecular mechanisms that ensure cholesterol homeostasis in cells was worth Dr. Goldstein and Brown the Nobel Prize for Medicine in 1985. This is based on two parallel and converging regulatory mechanisms, acting on HMGCR and on the Sterol regulatory element-binding proteins (SREBPs). HMGCR protein stability is regulated by cholesterol levels in ER membranes, which provides a fast mechanism to turn on/off the mevalonate pathway. In addition, ER cholesterol levels also regulate SREBPs, a family of transcription factors which regulate the expression of multiple genes involved in lipid metabolism, and in fatty acid and cholesterol synthesis in particular<sup>42</sup>: when the cells contains enough cholesterol SREBP activation is prevented; when cholesterol levels decrease, SREBP activity is induced to replenish cholesterol. SREBP also regulates expression of LDL receptor, which supplies cholesterol and fatty acids through receptor-mediated endocytosis<sup>45</sup>. Thus, SREBPs coordinate the synthesis of the two major building

blocks of membranes, fatty acids and cholesterol, by directly activating the expression of more than 30 genes dedicated to the synthesis and uptake of cholesterol, fatty acids, triglycerides, and phospholipids, as well as of the NADPH required for synthesis<sup>45</sup>.

The human genome encodes for 3 different isoforms of SREBPs: SREBP-1a and SREBP-1c, are encoded as alternative transcripts of a single gene, *SREBF1*; the third member of the SREBP family is SREBP-2, that is encoded by the *SREBF2* gene. SREBP-1a is a potent activator of all SREBP-responsive genes, including those that mediate the synthesis of cholesterol, fatty acids, and triglycerides. Its high-level transcriptional activity is dependent on exon 1a, which encodes a longer acidic transactivation segment than the first exon of SREBP-1c. The roles of SREBP-1c and SREBP-2 are more restricted than that of SREBP-1a: SREBP-1c preferentially activates genes involved in fatty acid synthesis, while SREBP-2 preferentially activates cholesterol synthesis<sup>42</sup>. SREBP-1c is mainly expressed in the liver, white adipose tissue, adrenal gland, skeletal muscle and brain of mice and humans; but SREBP-1a is expressed in cell lines, spleen and intestinal tissues. In general, SREBP-1a and SREBP-2 are the predominant isoforms of SREBP in most cultured cell lines, whereas SREBP-1c and SREBP-2 predominate in the liver and most tissues in vivo. SREBP homologs are present in all eukaryotes, including yeasts. SREBP proteins are organized into three domains: (a) an NH<sub>2</sub>-terminal domain of about 480 amino acids that contains the basic helix-loop-helix-leucine zipper (bHLH-Zip) region for DNA-binding and transcriptional regulation, that faces the cytoplasm; (b) two hydrophobic transmembrane domains interrupted by a short loop of about 30 amino acids that projects into the lumen of the ER; and (c) a COOH-terminal domain of about 590 amino acids that performs essential regulatory functions<sup>45</sup>.

## Sterol-dependent regulation of SREBPs

SREBPs are bHLH-Zip transcription factors that are synthesized as inactive precursors at ER transmembrane proteins. Under normal cholesterol conditions, SREBPs are actively kept in the ER compartment by forming a complex together with the SCAP (SREBP cleavage-activating protein) and INSIG (Insulin induced gene 1 and 2) transmembrane proteins. SCAP bears a cholesterol-binding domain, while INSIG1 binds to oxysterols specifically, and

reinforces the activity of SCAP. SCAP is a multiple transmembrane protein with a long COOH-terminal extension that includes multiple copies of a WD-repeat sequence known to promote protein–protein interactions (FIG. 1e). A sequence that includes five transmembrane helices (TMs 2–6) bears homology to a sequence in the transmembrane domains of HMGCR, which is also regulated by cholesterol levels<sup>46</sup>, and is the site for cholesterol binding. When cells experience lower levels of sterols, absence of cholesterol binding allows a conformational change of SCAP, which induces the SCAP-SREBP complex to detach from INSIG proteins and its loading into COPII-coated vesicles for transport to the Golgi apparatus<sup>47</sup>. At the Golgi, SCAP dissociates from SREBP and its cytoplasmic N-terminal domain is cleaved by the sequential action of Golgi-two resident proteases, S1P and S2P. S1P is a membrane-bound serine protease that cleaves SREBP in the luminal loop between its two membrane-spanning segments, splitting the SREBP molecule in two (FIG 1f). The NH<sub>2</sub>-terminal bHLH-Zip domain is then released from the membrane via a second cleavage mediated by S2P, a membrane-bound zinc metalloproteinase. The NH<sub>2</sub>-terminal domain, now designated nuclear SREBP (nSREBP), translocates to the nucleus and activates transcription by binding to nonpalindromic sterol response elements (SREs) in the promoter/enhancer regions of multiple target genes<sup>45, 48</sup>. This model posits that in conditions of high sterols the SCAP/SREBP complex is maintained in the ER; as with every ER-resident protein, however, the concentration into the ER is also ensured by KDEL-receptor-mediated retrieval of proteins occasionally leaking to the Golgi apparatus, as demonstrated by the observation that SREBP displays Golgi-specific glycosylations also in conditions of high sterols, and that inhibition of COPI-mediated retrograde trafficking from the Golgi apparatus to the ER is sufficient to cause SREBP accumulation at the Golgi<sup>49,50,51</sup>.

Another important layer of regulation of SREBP activity occur at the level of *SREBF1* and *SREBF2* gene expression. SREBP-1a appears to be constitutively expressed at low levels in liver and most other tissues of adult animals<sup>45</sup>, while SREBP-1c and SREBP-2 are regulated by four main mechanisms: SREBP activity itself, liver X-activated receptors (LXRs), insulin and mTOR signalling. nSREBPs bind to their own gene promoters, which represents an additional mechanism to empower cholesterol synthesis when cells are in need of it. LXR

has a more complex function, as it regulates fatty acid vs. cholesterol synthesis and the systemic distribution of cholesterol between different tissues. LXR activity is promoted by oxysterols, and specifically activates SREBP-1c transcription<sup>52</sup>. This selective modulation preferentially enhances fatty acid synthesis for the formation of cholesteryl-esters, which are necessary for the secretion or the storage, within lipid droplets, of cholesterol. At the same time, LXR directly promotes expression of genes involved in cholesterol secretion, resulting in elimination of excess cholesterol from cells towards the bloodstream. LXR-mediated regulation of SREBP-1c appears also to be one mechanism by which unsaturated fatty acids suppress SREBP-1c transcription and thus fatty acid synthesis. Multiple lines of evidence suggest that also fatty acid synthesis induced by insulin, is mediated by an increase in SREBP-1c. For examples, in isolated rat hepatocytes, insulin treatment increases the amount of mRNA for SREBP-1c in parallel with the mRNAs of its target genes. And interestingly, the overexpression of nuclear SREBP-1c in livers of transgenic mice prevents the reduction in lipogenic mRNAs that normally follows a fall in plasma insulin levels.

## SREBP regulation downstream of the mTOR kinase

One important signalling pathway impacting on SREBPs activity is the one based on mTOR. The mechanistic target of rapamycin (mTOR) is a serine/threonine kinase that belongs to the phosphatidylinositol 3-kinase (PI3K)- related kinases (PIKKs) family. This kinase is part of a well conserved pathway that regulates cell growth, proliferation, survival, autophagy, and anabolic metabolism from yeast to mammals<sup>53</sup>. The mTOR kinase is the catalytic subunit of 2 different protein complexes, mTORC1 and mTORC2; these protein complexes are characterized by different subunits and they perform partially non-overlapping functions. The mTORC1 complex positively regulates SREBPs at multiples levels, including processing, trafficking, and transcription. For example, inhibition of mTORC1 by rapamycin prevents the Akt-mediated nuclear accumulation of mSREBP1 and the induction of lipogenesis in epithelial cells<sup>54</sup>. These results were confirmed also by other studies, supporting the importance of mTORC1 for SREBP1 activation<sup>55,56</sup>. Moreover, genetic deletion in cancer cells of the TSC1/2 (tuberous sclerosis complex 1 and 2) complex, a known inhibitor of mTORC1, induces mSREBP1 nuclear accumulation and de novo

lipogenesis in a rapamycin-dependent manner<sup>55</sup>. In vivo studies have also confirmed decreased SREBP processing and diminished expression of lipogenic genes in the liver upon treatment of mice with rapamycin<sup>57</sup>. The general idea is that mTOR, which signals to cells to grow in size and to proliferate, also ensures through SREBPs the correct levels of lipid synthesis required for the formation of new membranes and organelles. At the molecular level, several mechanisms have been proposed to explain the effects of mTOR on SREBPs, which include: stimulation of RPK2 and of lipogenic mRNA splicing<sup>58</sup>; phosphorylation of the p300 acetyltransferase, thus enhancing SREBP-dependent transcription<sup>59</sup>; defective trafficking of cholesterol from autophagic lysosomes to the ER<sup>60</sup>; AKT-dependent suppression of INSIG proteins<sup>57</sup> and of GSK3 activity<sup>54</sup>; mTOR-mediated phosphorylation of Lipin1<sup>61</sup>.

## The biology of the LIPIN-1 phosphatidate phosphatase

The LIPIN protein family consists of three members LIPIN-1, -2 and -3, which play important roles in regulating lipid metabolism. Lipin-1 was discovered first, by using a positional cloning approach to identify the gene mutated in fld (fatty liver dystrophic) mice, characterized by a severely reduced mass of adipose tissue, resulting in insulin resistance, and hypertriglyceridemia<sup>62</sup>. In humans, mutations of LIPIN-1 is associated with muscle weakness and rhabdomyolysis but without general signs of dyslipidemia observed in mice, likely due to redundancy between the Lipin isoforms<sup>63,64</sup> and to differential expression of the isoforms between mice and humans.

Lipin-1 is a phosphatidic acid (PA) phosphatase (PAP) enzyme that dephosphorylates PA to form diacylglycerol (DAG), which is the precursor of triglyceride (TG), phosphatidylcholine, and phosphatidyl-ethanolamine synthesis<sup>65</sup>. After the first identification of the yeast PAP enzyme, PAP activity was subsequently demonstrated for all three mammalian lipin proteins, with lipin-1 having the highest specific activity<sup>66,67</sup>. Regulation of PAP activity mainly occurs by partitioning the enzyme between the cytosol and the intracellular membranes, mostly of the ER, where they encounter PA and catalyze its conversion to DAG. Binding to intracellular membranes is stimulated by high levels of free fatty acids (FA), such that these are efficiently incorporated into DAG and more complex lipids. Lipin-1

localization is also regulated by multiple phosphorylations, and among these several insulin-stimulated mTOR sites. Phosphorylation of Lipin-1 does not directly inhibit the enzyme activity, but rather regulates its subcellular localization in a complex manner: phosphorylation inhibits the membrane-bound fraction of Lipin-1<sup>68</sup>, but at the same time it prevents the nuclear localization of Lipin-1<sup>61</sup>. Inhibition of Lipin-1 by insulin was described in adipocytes and is counterintuitive, because insulin promotes the synthesis of TAG, and Lipin-1 is required for DAG (and, thus, TAG) production; this discrepancy was resolved with the discovery that Lipin-1 is a negative regulator of SREBP activity<sup>41</sup>, such that mTOR-induced inhibition of Lipin-1 potentially induces lipid synthesis<sup>61</sup>. Thus, the signalling function of Lipin-1 is that of inhibiting lipid synthesis, and when Lipin-1 is inhibited this can anyway lead to enhanced TAG production thanks to the presence of the other Lipin isoforms, compensating for the enzymatic function. Surprisingly, the signalling function of Lipin-1 also depends on its enzymatic activity, perhaps suggesting that Lipin-1 and Lipin-2 and -3 are redundant for DAG production when/where this is necessary for TAG synthesis, but not for DAG production which regulates SREBP. What molecular mechanism mediates regulation of SREBP by Lipin-1 remains incompletely understood<sup>69</sup>.

In addition to its enzymatic and signalling functions just described, Lipin-1 may also have a direct role in the regulation of gene expression. Lipin1 can translocate into the nucleus in conditions of nutrient starvation<sup>67</sup> or upon strong inhibition of mTOR activity<sup>61</sup>. In the nucleus, lipin1 can interact with transcriptional factors and co-activators involved in metabolic gene expression, including peroxisome proliferator-activated receptor gamma coactivator 1-alpha (PGC1a), peroxisome proliferator-activated receptors alpha and gamma (PPARa, PPARc), and nuclear factor of activated T cells (NFAT)<sup>62,70</sup>. The functional relevance of these interactions remains poorly characterized.

## Mechanotransduction and Metabolism: State of Art

While several studies indicated an effect of ECM mechanical properties in regulating cellular proliferation, migration, and differentiation, much less is known on cell metabolism. Some explored the link between cell adhesion and metabolism by completely detaching cells from the substrate and growing them in suspension, which can be seen as an extremely soft

microenvironment, but also bear fundamental differences (e.g. complete lack of integrin attachment to the ECM). This is also due to the interest in understanding cancer cell metabolism, and to the related concept that survival upon cell detachment is considered a hallmark of transformation. Other compared cells growing on tissue culture dishes with cells growing as organoids, which usually entails the initial detachment of cells, followed by growth of cell aggregates of loosely defined composition and 3D arrangement, with extensive cytokine supplementation (including for example pituitary extracts) to support survival. Only more recently some groups started do address more specifically the effects of changing ECM mechanical properties in more controlled manner. Very few provided compelling evidence that these metabolic traits are actually regulated by actomyosin tension, and are thus bona-fide mechanoresponsive phenotypes. Briefly, what emerges is that:

- autophagy, a key metabolic pathway, is induced by ECM detachment to delay anoikis<sup>71</sup>. Multiple parallel pathways seemingly contribute to this phenotype, including activation of the PERK-mediated ER stress response and activation of the I $\kappa$ B kinase complex<sup>72,73</sup>. As such, forced activation of autophagy or of autophagy-promoting oncogenes in mammary epithelial cells undergoing 3D acinar morphogenesis in a soft ECM prevents the death of luminal cells. This contrasts with more recent findings, where a soft ECM impaired autophagosome formation<sup>74</sup>, which would indicate a biphasic control of autophagy by cell attachment strength.
- detachment of mammary epithelial cells from the ECM induces reduced glucose uptake, reduced glucose flux through the TCA cycle and reduced ATP synthesis<sup>75,76</sup>. This can be rescued by the Erbb2 oncogene acting through EGFR/PI3K signaling, owing not only to its ability to reinstall glucose uptake and the activity of pyruvate dehydrogenase, but also because it skewed the use of glucose towards the oxidative branch of the pentose-phosphate pathway to provide NADPH. Indeed suspended cells experience a surge of ROS which was counteracted by Erbb2-driven NADPH production, thus indirectly enabling suspended cells to resume fatty acid oxidation.

- again by using cell detachment, Gan and colleagues found that attachment-induced focal adhesion kinase (FAK) phosphorylates and inhibits tuberous sclerosis protein 2 (TSC2), which is a negative regulator of mTOR, resulting in its activation and in the activation of its downstream targets eIF4a and S6K. Other studies confirmed these results, by showing that in vivo and in vitro inhibition of FAKs decreases glucose uptake<sup>77</sup>.
- Jiang and colleagues<sup>78</sup> used lung cancer cells growing as floating spheroids and found this suppressed oxidation of glucose, in line with<sup>75</sup>, and glutamine. This was accompanied by increased reductive glutamine metabolism in the cytoplasm, driven by IDH1, which maintained mitochondrial oxidation of citrate by IDH2 and production of NADPH, ultimately counteracting increased mitochondrial ROS observed upon cell detachment and supporting cell fitness. Thus, the IDH1/2-dependent cycle that transmits NADPH from mitochondria to the cytosol in attached cells, upon cell detachment operates in reverse to transfer reducing equivalents from the pentose-phosphate pathway into mitochondria.
- Peck and colleagues<sup>79</sup> instead examined lipid metabolism during spheroid growth, and found increased levels of unsaturated fatty acids, which was dependent on SCD activity. This was important for cancer cell growth in spheroids and in orthotopic systems, because unsaturated FAs sustained the production of unsaturated cardiolipins and thus prevented mitochondrial release of cytochrome C. This suggests that a tissue-like microenvironment imposes on cancer cells the need to maintain fatty acid desaturation.
- some other studies provided evidence for indirect regulation of some metabolism traits due to regulation of mechano-responsive transcription factors such as YAP/TAZ; this includes dNTP metabolism<sup>33</sup> glutaminolysis<sup>80</sup>, aspartate/glutamate transport across the plasma membrane<sup>81</sup> and more recently autophagy<sup>82</sup> and ferroptosis<sup>83</sup>.

- Finally, Bays and colleagues explored a somewhat different type of forces, namely those developing at cadherin-dependent cell-cell junctions. They found that upon force application, E-cadherin stimulates the activity of liver kinase B1 (LKB1), which in turn recruits AMPK to cadherin complexes. This recruitment stimulated glucose uptake and ATP production, which are instrumental to maintain actomyosin contractility<sup>84</sup>.

## **RATIONALE**

The mechanical properties of the cell microenvironment are recognised as important inputs for controlling cell behaviour. While we know the basic mechanisms of mechanosensing, we are only starting to identify what intracellular pathways are differentially regulated by extracellular forces, and what cell processes and phenotypes they control. We focused our attention on how physical inputs can impact cell metabolism, and decided to approach this question with an unbiased metabolomic analysis of cells developing different degrees of cell contractility.

## RESULTS

### Low actomyosin contractility induces lipid accumulation

In order to uncover a possible crosstalk between mechanical cues and metabolism, we chose an experimental model to study the effects of decreased actomyosin contractility. For this, we treated MCF10ATk1 mechanosensitive mammary epithelial cells with Y27632 and ML7, two established small molecule inhibitors of ROCK (Rho kinase) and MLCK (myosin light chain kinase) respectively, that are two upstream regulators of NMII activity. NMII is the myosin isoform present in non-muscle cells that is responsible for developing actin contractility. As first and unbiased approach, we performed a global metabolomics by comparing cells seeded on plastics and cells treated with YM (Y27632 and ML7). We conducted the experiment at two time points, treating cells for 6h (early time point) and 24h (late time point), observing clear differences between the two conditions (FIG.2a), and in particular, we detect accumulation of several classes of lipids (FIG.2b). Among the most enriched, we found acylcarnitines, lysophospholipids, sterols, phospholipids, monoacylglycerols, diacylglycerols and sphingolipids. This accumulation was already significant at 6h and appeared sustained at 24h (FIG 2c). We then performed a targeted lipidomics at 24 h of treatment, in order to confirm the previous results and to have more specific information on what lipid species were altered. Indeed, we confirmed the accumulation of many of them, such as triglycerides, diacylglycerols, and ceramides (FIG 2d). This was further reinforced by the observation that both total fatty acid levels and cholesterol levels were increased in cell extracts (FIG 2e).

To validate the -omics data, we looked for a more direct way to observe lipids, so we stained our cells with filipin and ORO (Oil red O). Filipin is a naturally fluorescent cholesterol binding molecule detectable in the UV spectrum. The ORO staining is a fluorescent lysochrome preferentially soluble in lipids and thus used for the visualization of lipid droplets formed by neutral lipids. With both staining, we were able to confirm cholesterol and lipid accumulation in cells treated with YM for 6h and 24h (FIG 3a). Lipid accumulation was mainly due to lipid synthesis, since treatment of cells with cerivastatin and TOFA (fatty acid and cholesterol synthesis inhibitors, respectively) reverted the phenotype. Furthermore,

we found lipid accumulation to be a general response to ECM mechanical cues and actomyosin contractility. Indeed we could observe stronger filipin and ORO staining in cells plated on soft hydrogels compared to those plated on a stiff substratum (FIG 3b). Hydrogels, are ECM-functionalised polyacrylamide gels of tunable elasticity or stiffness and cells plated on Stiff hydrogels ( $E= 15$  KPa) can spread and develop actomyosin contractility, while cells plated on soft hydrogels ( $E= 0,5$  KPa) remain rounded and develop lower levels of contractility<sup>19</sup>. Moreover, the expression of RHO inhibitor C3, and treatment of cells with NMII small molecule inhibitor blebbistatin, showed similar results (FIG 3b). Importantly, we also tested several cell lines of different tissue origin and grade of transformation, and always confirmed lipid accumulation (FIG 3c).

## Lipid accumulation is independent from YAP/TAZ transcriptional factors

Looking for a molecular mechanism, we first considered YAP/TAZ and the Hippo pathway. Given that YAP/TAZ activity is inhibited in low tension conditions (FIG 4a), we tested whether knockdown of YAP/TAZ by siRNA transfection was sufficient to induce lipid accumulation, but we didn't observe any difference between YAP/TAZ-knockdown and control-siRNA transfected cells (FIG 4b). We also stably overexpressed a constitutive active form of TAZ in our cells, but this was not sufficient to prevent lipid accumulation upon treatment with YM (FIG 4b). Furthermore, by luciferase assays we tested the effects of YAP/TAZ on the activity of the LDLR (low density lipoprotein receptor) promoter, a gene related to lipid synthesis that was upregulated by inhibiting actomyosin contractility (see below): neither YAP/TAZ knockdown nor their inhibition obtained by overexpressing NF2/Merlin was sufficient to recapitulate the effects of YM treatment or to interfere with LDLR-reporter activation by YM treatment (FIG 4d).

## Lipid accumulation in conditions of low tension correlates with activation of SREBP transcription factors

We then asked whether the effects of ECM mechanical cues on lipid metabolism was direct (e.g. direct regulation of enzyme activity), or mediated by a transcriptional response. To this end we performed a microarray analysis in cells treated with YM for 6h (i.e. the minimal amount of time to see consistent lipid accumulation), and we observed upregulated expression of multiple enzymes involved in cholesterol and fatty acid synthesis (FIG 5a), suggesting a transcriptional response. Multiple transcription factors can control the expression of lipogenic enzymes, including LXR, SREBPs and possibly others. To identify which of these transcription factors was primarily involved, we performed Gene set enrichment analysis and observed a strong and specific upregulation of the signature of SREBP transcription factors (FIG 5a). Indeed among the upregulated genes, several were known direct SREBP target genes (FIG 5b). We first validated this data by RT-PCR in MCF10ATk1 cells treated with YM for 6h and 24 h, confirming the upregulation of multiple established SREBP target genes, including some that were not initially present in our microarray analysis (FIG.5c). Of note, we performed the same experiments in others cell lines, and obtained similar results (data not shown). We then performed RT-PCR on cells plated on hydrogels of differential stiffness and observed induction of the same set of SREBP target genes in cells cultured on a soft ECM (FIG 5d). Finally, we performed luciferase assays using the LDLR (low density lipoprotein receptor) and FASN (fatty acid synthase) luciferase reporters, bearing established serum-response elements bound by SREBP, and we confirmed early and sustained SREBP transcriptional activation in cells treated with YM (FIG 5e and data not shown).

## ECM mechanical cues regulate lipid accumulation through SREBP1/2

To test a causative role for SREBP in inducing lipid accumulation downstream of mechanical cues, we depleted our cells of both SREBP1 and SREBP2. We depleted both isoforms because our lipidomic and gene expression data suggested regulation of both fatty acid synthesis, a SREBP1-dependent process, and of cholesterol synthesis, a SREBP2-dependent process. As shown in FIG 6b, the knockdown of SREBP1/2 by the use of two independent siRNA mixes (used to rule out potential off-target effects of siRNAs) inhibited lipid accumulation in cells cultured on a soft matrix, indicating a requirement of SREBP1/2. SREBP1/2 knockdown was also sufficient to inhibit the induction of genes encoding for lipogenic enzymes observed in low contractility (FIG. 6c), and to counteract activation of the LDLR reporter in low tension (FIG. 6d). Of note, these assays were also used to further confirm the specificity of our knockdowns, as shown by the use of multiple independent siRNA mixes (FIG 6c), and by the ability of siRNA-resistant mouse SREBP1 and SREBP2 to rescue the effects of the SREBP1 siRNA mixes A and B (FIG 6d).

## ECM mechanical cues regulate SREBP processing

SREBP (Sterol regulatory element binding proteins) transcription factors are produced as precursor proteins resident in the ER membranes, where they form a complex with two sterol sensor proteins, SCAP and INSIG. Thus, in low sterol conditions, SCAP undergoes a conformational change which allows the SCAP-SREBP complex to detach from the ER and go to the Golgi apparatus. Here, SREBP is subsequently cleaved by two proteases, S1P and S2P, that allow the mature and active form of SREBP to translocate to the nucleus and induce the transcription of its target genes (FIG 7a). We then asked whether ECM mechanical cues regulate SREBP in a similar manner, or by different mechanisms.

By immunofluorescence on the endogenous protein, we observed SREBP2 at the ER membrane in control conditions, likely due to saturating amounts of lipids present in the serum and/or sufficient synthesis keeping SREBP2 inhibited (FIG 7a). Upon treatment with ROCK and MLCK inhibitors, we first observed SREBP2 concentration at the Golgi

apparatus after 2h of treatment, followed by its nuclear accumulation after 6h of treatment (FIG 7a). Coherently, we found SREBP2 translocation in the nucleus also in other conditions inducing low actomyosin contractility, including transfection of the C3 enzymatic RHO inhibitor and treatment with the NMII small-molecule inhibitor Blebbistatin (FIG. 7a). At later time-points, such as 24h and 48h of treatment, SREBP2 nuclear levels progressively decreased (FIG. 7b), likely due to activation of a negative feedback mechanism due to additional lipid accumulation. This indicated that the SREBP control system is not completely deregulated in conditions of low tension, as also indicated by disappearance of nuclear SREBP2 1h after the ROCK and MLCK inhibitors were washed out (FIG. 7b). We repeated similar observations with another antibody for SREBP2, but failed to find a suitable antibody to visualize SREBP1 endogenous levels in our cells (not shown). Collectively, these data indicate that mechanical cues shift the threshold for SREBP2 regulation by lipids, without hampering its ability to dynamically respond to other external stimuli.

A corollary of our observation is that in our culture conditions SREBP2 must be processed from its transmembrane form, at the Golgi apparatus, to accumulate into the nucleus. Indeed by western blotting we found accumulation of the cleaved/mature form of SREBP1 and SREBP2 in nuclear extracts of YM-treated cells (FIG 7c). Moreover, in line with the idea of a direct regulation of SREBP2 protein processing, nuclear accumulation of SREBP2 induced by YM treatment was not inhibited by blocking protein translation with cycloheximide (FIG. 7d and data not shown). Finally, YM treatment was not able to increase SREBP2 activity in cells engineered to express only the cleaved/mature form of SREBP2, excluding an effect of mechanical cues on nuclear SREBP2 stability and/or activity (FIG. 7e).

## **SREBP activity is repressed in stiffened keloid tissues**

We next sought to find evidence that the mechanism we observed in cell cultures is also observed *in vivo*. To this end chose keloids scars, benign dermal fibroproliferative disorders that are formed as a consequence of incorrect resolution of the scarring process and that occur in predisposed individuals spontaneously or following trauma, inflammation, surgery, or burns<sup>78</sup>. In this disorder, activated fibroblasts that migrate into the wound bed to

reconstitute the damaged tissue do not cease their activity, but instead continue to produce excess fibrotic ECM that expands beyond the original boundaries of the wound, recruiting more fibroblasts and growing into adjacent tissues. Importantly, keloid scars are often induced in the body regions more subjected to mechanical stresses, and are characterized by increased ECM stiffness, which locks fibroblasts in an activated state, thus making keloid scars an ideal model system to study cell mechanotransduction<sup>85,86</sup>. We took advantage of published gene expression data of patient-matched normal skin vs. keloid scars and analysed the relative expression levels of several known SREBP target genes, which we found were consistently and uniformly downregulated in stiffened keloids across all patients, supporting our model (FIG. 8a). Of note, this finding nicely parallels the so far unexplained decrease in lipids and cholesterol-esters observed in keloids by others<sup>87</sup>. As a control, we also found the expected upregulation of several YAP/TAZ target genes (Fig. 8a), in line with stiffness-induced YAP/TAZ activity during fibrosis<sup>88,89</sup>. Thus, cytoskeletal tension is a relevant input to regulate SREBP in vitro and in at least one human pathological tissue.

## ECM mechanical cues regulate SREBP through SCAP

Based on the notion that SREBP transport between the ER and the Golgi apparatus is usually regulated by the SCAP (SREBP cleavage activating protein) chaperone, we next explored whether SCAP was also involved in the regulation of SREBP by mechanical cues. By using transfected Myc-tagged SCAP, we observed SCAP colocalization with the Golgi apparatus after 6h of YM treatment, in cells cultured on a soft matrix, and upon C3 RHO inhibitor co-expression (FIG 9a). Importantly, in our experimental set up SCAP is required for SREBP regulation, because we observed inhibition of SREBP activity upon SCAP siRNA transfection (FIG 9b). We obtained similar results by treating cells with 25-hydroxycholesterol, a dominant inhibitor of SCAP transport to the Golgi apparatus (FIG. 9b). Furthermore, we also found that treatment of cells with ROCK and MLCK inhibitors was unable to induce LDLR luciferase activity in cells transfected with a small-molecule inhibitor of the SREBP protease S1P (PF429242); in this case we used Fasudil (F), an alternative ROCK inhibitor (FIG 9c). We then further confirmed these data by using the C3 RHO inhibitor (FIG. 9d).

## Lipid synthesis contributes to the beneficial effects of ROCK inhibitors in hPSC

Looking for a possible biological function for lipid accumulation in condition of low tension, we focused on Human Pluripotent Stem Cells (hPSCs), a cellular system that is strongly dependent on ROCK inhibition to survive single cell dissociation in vitro. hPSCs are derived from human embryos, retain indefinitely the ability to self-renew as undifferentiated stem cells, and can differentiate into any of the three embryonic germ layers. hPSCs represent a key experimental system to study how pluripotency is regulated, and an obligate intermediate during epigenetic reprogramming of somatic cells; however, and at difference with mouse pluripotent stem cells, hPSC are very vulnerable to apoptosis upon single-cell dissociation<sup>90</sup>, a fundamental assay to study their clonogenic ability and to isolate single-cell mutants during genome engineering procedures. A fundamental step forward was the implementation of ROCK inhibitors to reduce apoptosis and enhance the cloning efficiency of hPSCs when dissociated in single cells; the underlying molecular mechanism remain however incompletely understood<sup>90,91</sup>. Prompted by our findings, we tested the idea that ROCK inhibition could support single cell survival of hPSCs by sustaining SREBP-dependent lipid synthesis. For this we used an established hPSC line (Wi09 H9) that strongly requires ROCK inhibition for survival as single cells, while ROCK inhibition is dispensable when these cells are passaged as cluster<sup>88,89</sup>.

We first checked and confirmed lipid accumulation by filipin staining in hPSCs treated with ROCK inhibitor for 24h (FIG.10a). Then we challenged ROCK-induced single-cell survival by using a combination of Cerivastatin and TOFA to inhibit lipid synthesis, or by using 25-hydroxycholesterol to inhibit SCAP transport. In both conditions cell survival was unaffected when cells were plated as clusters (i.e. when ROCK inhibition is not required), but it was strongly affected when cells were plated as single cells (i.e. when ROCK inhibition is required) (FIG. 10b). Of note, in these experiments we used a dose of small-molecule inhibitors of lipid synthesis that was well below the active dose in most other cells, indicating how hPSC growing as single cells are extremely dependent on lipogenesis. Importantly, also SREBP1/2 downregulation by siRNA transfection was sufficient to inhibit ROCK inhibition-driven single cell survival (FIG. 10c). These results indicate that SREBP activity

is instrumental for ROCK inhibition-driven single cell survival in hPSCs, and provide a functional validation of our model.

## Lipin1 and ARF1 inhibition induce lipid accumulation and SREBP activation

SREBP activation downstream of mechanical cues bears multiple similarities with their regulation by sterols, but is apparently independent on sterol levels: regulation of SREBP occurs in cells that have excess lipids in their medium, and remains sensitive to sterol levels (as demonstrated by late inhibition of SREBP, after sterol accumulation). We initially tested the involvement of known upstream regulators of SREBP activity and lipogenesis, including AMPK and mTOR. For this we treated cells with a powerful mTOR inhibitor, Torin1, or used mouse embryonic fibroblasts (MEFs) knockout for both AMPK $\alpha$  subunits. In both cases, however, treatment of cells with ROCK/MLCK inhibitors was equally able to induce activation of SREBP, ruling out a primary involvement of either AMPK or mTOR.

We thus searched the literature for other mechanisms able to regulate SREBP independently of sterols. One of such mechanisms is based on the small GTPase ARF1 (ADP ribosylation factor 1), which regulates Golgi dynamics and has been isolated in unbiased screen in *C.elegans* as an inhibitor of SREBP<sup>69,92</sup>. Moreover, inhibition of ARF1, of its GEF GBF1, and of its downstream effector COPI (mediating retrograde trafficking from the Golgi to the ER) all cause SREBP activation in mammalian cells<sup>41,69,93</sup>. The other is based on LIPIN1, a lipid phosphatase that converts phosphatidates into diacylglycerols (DAG) at intracellular membranes (FIG. 11a), and that can also inhibit SREBP activation<sup>50,63</sup>. Interestingly, the activity of these two factors can be linked because inhibition of Lipin1 activity can lead to low levels of DAG at the Golgi apparatus, which is known to inhibit the recruitment of ARF1-GAP at Golgi membranes, which in turn causes an impairment in the formation of COPI-coated vesicles for retrograde protein transport<sup>60</sup> (FIG. 11a). Thus, we tested the idea that in conditions of high contractility Lipin1 sustains ARF1/COPI activity at the Golgi, thus continuously transporting SCAP/SREBP complexes back to the ER. This is possible, since very old studies already reported that a small portion of SCAP can shuttle through the Golgi apparatus in cells with normal lipid levels, as showed by the presence of Golgi-dependent

glycosylation patterns<sup>94</sup>. Moreover, SCAP is a KDEL client protein and it is thus likely that a portion of SCAP can shuttle to the Golgi and back to the ER even in conditions when the bulk pool of SCAP is at the ER. In this model, conditions of low contractility would cause inhibition of Lipin1 and of retrograde trafficking of SCAP/SREBP, causing their accumulation at the Golgi and finally SREBP activation.

To test this model we first checked whether Lipin1 regulates SREBP in our cells in conditions of high contractility. Inhibition of LIPIN1 by independent techniques (either by using siRNA or by treating cells with the small-molecule Lipin1 inhibitor propranolol) caused accumulation of cholesterol, as shown by filipin staining (FIG. 11b), and upregulation of SREBP target genes (FIG. 11c/d). Of note, the downregulation of SCAP by siRNA transfection prevented activation of SREBP in cells treated with Propranolol (FIG. 11e), indicating that in our cell systems Lipin1 acts on SREBP through SCAP, and not by alternative mechanisms<sup>61</sup>.

We also looked at SREBP localization, and we confirmed the coherent accumulation of SREBP2 in the nucleus upon LIPIN1 and ARF1 inhibition (FIG. 12a). Furthermore, by following SCAP localization, we observed the same results (FIG. 12b).

## ECM mechanical cues regulate Lipin1 and ARF1 activity

Our model poses that inhibition of actomyosin contractility causes inhibition of LIPIN1 and ARF1 activity. Lipin1 associates to intracellular membranes when it is active, prompting us to visualize membrane association in conditions of high vs. low actomyosin tension. We isolated microsomes by ultra-centrifugation and visualized endogenous co-purifying Lipin1 by western blot, and found lower amounts of LIPIN1 upon inhibition of cell contractility (FIG.13a). To reinforce this result we also used an indirect approach to measure DAG levels at the Golgi apparatus as a proxy for Lipin1 activity. For this we took advantage of an established sensor of Golgi DAG levels based on the DAG-binding domain of PKD (FIG. 13b). Protein kinase D (PKD) is a cytosolic serine-threonine kinase that binds to the trans-Golgi network and regulates vesicles formation and protein secretion. Of note, PKD binds DAG, and this binding is necessary for its recruitment to the Golgi, such that reduction of DAG inhibits PKD recruitment and blocked protein transport towards the cell surface<sup>93,95</sup>.

We thus transfected in HEK293 cells the GFP-PKD-KD DAG sensor, and observed that inhibition of LIPIN1 and of ROCK/MLCK caused a similar inhibition of the co-localization of GFP-PKD-KD and GM130, a widely used marker for the trans-Golgi network (FIG.13b). Moreover, both treatments also decreased the association of ARF1 with Golgi membranes, as assayed by immunofluorescence for endogenous ARF1 (FIG. 13c). Collectively these data validated our model and showed that inhibition of actomyosin contractility inhibits the activity of Lipin1 and or ARF1.

## LIPIN1 mediates the effects of tension on SREBP activity

We then wanted to understand how mechanical cues regulate LIPIN1. LIPIN1 activity can be regulated by phosphorylation<sup>61</sup> by mTOR and other kinases, which correlates with differential ability of Lipin1 to associate with membranes, prompting us to look for changes in the phosphorylation pattern of Lipin-1. For this we transfected cells with FLAG-tagged LIPIN1 and treated them with DMSO or ROCK/MCLK inhibitors for 24h. Then, by western blot analysis, we checked for a differential migratory pattern, that we however failed to observe (FIG. 14a). As positive control we transfected cells with a mutant of LIPIN1 with 17S/A mutation of all known phosphorylation sites<sup>50</sup>, which migrated faster than WT Lipin1. We then checked subcellular localization of LIPIN1, as this has been reported as an additional mechanism to control its activity<sup>96</sup>. By using transfected FLAG-tagged Lipin1 we observed a partial shift of LIPIN1 towards the nucleus (FIG. 14e). Nuclear LIPIN1 is induced by mTOR inhibition and associated with a decreased activity of SREBP<sup>61</sup>, which was discordant with our results (we observed nuclear Lipin1 in conditions of enhanced SREBP); we thus made the hypothesis that increased nuclear localization of Lipin1 was a secondary consequence of decreased retention of Lipin1 on intracellular membranes, as observed by microsome ultracentrifugation. To test the idea that localization of LIPIN1 at membranes is important downstream of mechanical inputs, we then designed a mutant form of the protein that is anchored to intracellular membranes by fusing it to the Golgi-localization domain of Syntaxin5. We developed two alternative constructs, bearing two different Syntaxin portions, one spanning the sole identified Golgi-localization domain, the other a longer portion of the protein<sup>97</sup>. By immunofluorescence, we verified that these

membrane-bound LIPIN1 isoforms (MB-Lipin1) were always found attached to intracellular membranes, including the Golgi and the ER, even in YM-treated cells (FIG. 14e). We then challenged activation of LDLR-luciferase by inhibition of ROCK and MLCK with WT, MB and 17S/A Lipin1 isoforms, and found that only the membrane-bound isoforms were able to prevent SREBP activation (FIG. 14f). Coherently, MB LIPIN1 expression in cells also dominantly inhibited lipid accumulation in condition of low actomyosin contractility (FIG. 14g). Thus, ECM mechanical cues regulate Lipin1 association with intracellular membranes independently of its phosphorylation. We finally used the same luciferase assay to probe the role of other recently reported post-translational modifications potentially affecting Lipin1 activity, but neither the sumoylation-insensitive nor the acetylation-insensitive Lipin1 mutants<sup>98,99</sup> were able to counteract SREBP activation by ROCK/MLCK inhibition, excluding also these mechanisms. In absence of other candidate mechanisms, we were thus left without a precise characterization of how actomyosin contractility regulates Lipin1, which will be the focus of future studies.

## The Golgi apparatus: a mechanosensitive organelle?

Even if we lacked of a precise mechanism, our data indicated that ECM mechanical cues regulate a key processes occurring at the Golgi apparatus. ECM mechanical forces can influence intracellular events through either the activation of signaling pathway at focal adhesions, or by more direct mechanisms, for example by stretching the plasma membrane, or owing to anchoring of stress fibers to the nuclear lamina<sup>100,101</sup>. Whether the Golgi apparatus might respond in a similar fashion has not been explored, but Golgi cisternae are embedded in a complex cytoskeletal network, and strikingly, the Golgi microenvironment is endowed of an intrinsic mechanical rigidity which depends on ROCK/MLCK<sup>102</sup>. Thus, in order to measure a possible change in the rigidity of the Golgi microenvironment upon changing external physical cues, we plated cells on fibronectin-coated micropatterns, where cells can be plated as single cells on adhesive islands of different size<sup>103</sup>. On large islands, cells spread against the surface and develop high cytoskeletal contractility; on small islands cells cannot spread and display reduced actomyosin contractility<sup>104</sup>. Importantly, we validated this experimental set-up as we observed accumulation of SCAP to the Golgi

apparatus in cells plated on small islands (FIG. 15a). We then measured Golgi rheology by pushing towards the Golgi apparatus a cytoplasmic bead immobilized in a laser optical trap (FIG. 15b). Analysis of the averaged relaxation curves indicated a lower rigidity of the Golgi apparatus in micropatterned cells, apparent from reduction of the bead step amplitude, the rigidity index, and the frequency of bead ejection (FIG. 15c). This experiment indicates that Golgi stiffness is coupled, directly or indirectly, to the mechanical properties of the ECM.

Strikingly, with this same experimental set-up we also observed that direct application of force to the Golgi apparatus, by repeatedly and steadily pushing the trapped beads towards the Golgi, was sufficient to induce recruitment of the GFP-PKD-KD reporter (FIG. 15d), a proxy for Lipin1 activity. As a control, moving the bead away from the Golgi apparatus showed that the overall cytoplasmic stiffness is not altered (FIG. 15e). This result is in line with higher Lipin-1 activity in cells developing higher contractile forces. Moreover, this may suggest that the cytoskeleton surrounding the Golgi is in principle able to respond to forces transmitted to it by the rest of the cell, including perhaps traction forces developed through stress fibers.

In future it will be important to understand how the F-actin cytoskeleton surrounding the Golgi is regulated, and how the organization of this cytoskeleton is connected to the rest of the cell and to focal adhesions.

## DISCUSSION AND FUTURE DIRECTIONS

In this work we sought to understand and characterize possible links between ECM mechanical cues and cell metabolism. We started the study by the unbiased observation that inhibition of ROCK and MLCK activity, i.e. when cells experience decreased actomyosin contractility, induces accumulation of neutral lipids and cholesterol inside the cells. We then showed this phenotype is a bona-fide response to cell tension dictated by the mechanical properties of the ECM, and a general phenotype that can be observed in multiple cell lines irrespective of their morphology (i.e. epithelial or mesenchymal) and transformation (i.e. primary or transformed). We also provided evidence this regulation occurs in human tissues, as we found that stiffened keloid scar tissues display reduced expression of SREBP target genes, which may now explain the observation that keloid scars have reduced cholesterol and triglyceride content. Moreover, we provided evidence that hPSCs survival as single cells promoted by ROCK inhibition is tightly linked to the ability of ROCK inhibition to induce SREBP activity and lipid synthesis. Given the extensive use of ROCK inhibitors in the stem cell and organoid fields, our observation might provide both a rationale for its use and some hints on how to optimize further isolation and culture conditions. Finally, a very similar phenotype was recently observed by another group<sup>105</sup>, indicating that regulation of lipid metabolism by ECM mechanical cues is a relevant phenotype.

Mechanistically, we propose that low levels of actomyosin contractility inhibit LIPIN1 phosphatidate phosphatase activity at intracellular membranes, which then causes reduced level of diacylglycerols at the Golgi apparatus. In turn, reduced diacylglycerols modulate the recruitment and activity of the ARF1 small GTPase, affecting COPI-dependent trafficking of SCAP/SREBP complexes between the Golgi apparatus and the ER. As a consequence, low levels of actomyosin contractility lead to SREBPs accumulation at the Golgi, the cleavage of their cytoplasmic domain and activation of SREBP-dependent transcription. SREBP regulation occurs in parallel to the homeostatic control of sterol levels at ER membranes; we thus propose that ECM mechanical cues can shift the “tone” of lipid synthesis, which is then maintained by sterol-dependent feedback control of Insig and SCAP activity. Indeed lipid accumulation upon inhibition of ROCK/MLCK was sustained for at

least three days, when SREBP nuclear activation was already normalized. Of note, we also observed SREBF1 and SREBF2 mRNA upregulation at late time points, and this was observed after inhibition of both LIPIN1 and actomyosin (data not shown). We interpret this regulation as a secondary event, and not the primary cause of SREBP1/2 activation in response to mechanical cues, because: (i) we detect nuclear SREBP2 also in cells treated with cycloheximide, which shows that direct SREBP2 regulation can occur in absence of transcription/translation; (ii) SREBP1/2 are known in the literature to regulate their own expression directly, as well as expression of LIPIN1 (see our data), which are common feedback mechanisms in every signalling pathway. So, at best this delayed effect can be interpreted as an additional mechanism that may contribute in supporting lipid accumulation. Our study also shed light on previous observations on Lipin-1, ARF1, and COPI-dependent trafficking of SREBP: while their effects on SREBP had been already described, and the possible links between each and any of them already demonstrated experimentally, it remained unclear whether this represented a coherent pathway as we now propose. Moreover, we now provide a physiologically-relevant upstream input for this atypical SREBP-regulatory module which was missing in previous studies.

The precise mechanism by which Lipin1 activity is regulated remains unknown; in future, we plan to investigate deeper how LIPIN1 is regulated by mechanical stimuli by performing a proximity proteomic study (by fusing Lipin1 to the BirA biotin ligase). This might be useful to identify new upstream regulators of Lipin1 connecting its activity to the cytoskeleton, or to tension-regulated signaling molecules (e.g. Src, FAK etc), but also to better understand where Lipin1 is active in cells. The current understanding of Lipin1 subcellular distribution, i.e. that it is an ER-bound enzyme, is based on microsomal ultracentrifugation; indeed many assume this fraction only contains ER vesicles, but we actually found it also contains abundant Golgi cisternae. The ER localization of phosphatidate phosphatase (PAP) enzymatic activity has been classically linked to production of DAG precursors for TAG synthesis and lipid droplet formation, which is thought to occur at the / from the ER. Multiple observations indicate that Lipin1 activity influences the concentration of DAG at the Golgi membranes<sup>106,107</sup>, even if this has not been measured directly due to lack of techniques to specifically isolate Golgi cisternae for mass-

spectrometry lipidomic analyses. Nonetheless, accumulation of DAG at the Golgi might be due to localization of Lipin-1 at the Golgi surface directly, or to indirect transport of DAG from the ER through contact sites / lipid carrier proteins. In addition, Lipin1 was also shown to shuttle into the nucleus, but the function of this pool, including a possible transcriptional-regulatory activity, remains poorly characterized. Thus, our understanding on how Lipin1 is regulated is very rough, and further studies on it might hold interesting surprises.

More in general, our data suggest that actin dynamics around the Golgi apparatus can be regulated by extracellular forces, opening the interesting possibility that the Golgi is a mechanosensitive organelle. The idea of an intracellular “antenna” for extracellular mechanics is not new in itself, but has been proposed for the nucleus a long time ago: cytoplasmic actin is directly connected to the nuclear envelope through sun/nesprin complexes, which bridge the nuclear envelope itself and connect to the nuclear lamina, which is now considered an important interface mediating the effects of extracellular forces on chromatin dynamics and gene expression. However, our observations might indicate that other processes occurring at the Golgi and that depend on DAG levels and ARF1 activity might be equally regulated. For example, the observation that inhibition of ROCK/MLCK causes increased ceramide content, which remains unexplained, might indicate regulation of sphingolipid metabolism, a pathway whose main steps occur at the ER/Golgi interface. Thus, in the future we plan to explore what other processes that occur at the Golgi apparatus are regulated by ECM mechanical cues.

Finally, our initial metabolomic analysis indicates other metabolic pathways besides lipids might be regulated by ECM mechanical cues. It will thus be interesting to obtain a more precise view on how ECM mechanical cues alter metabolic fluxes of the main carbon sources, and whether this may indicate other metabolic traits imposed by the mechanical microenvironment on cells.

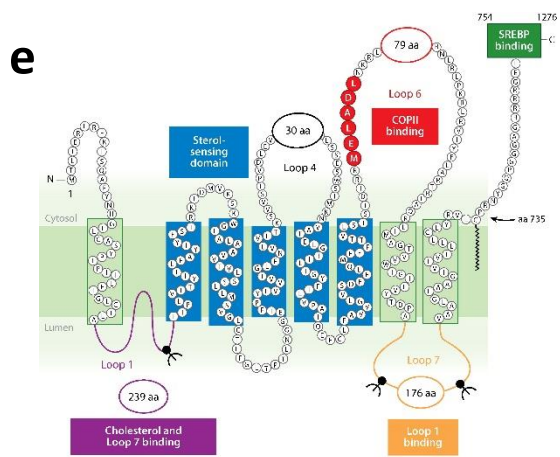
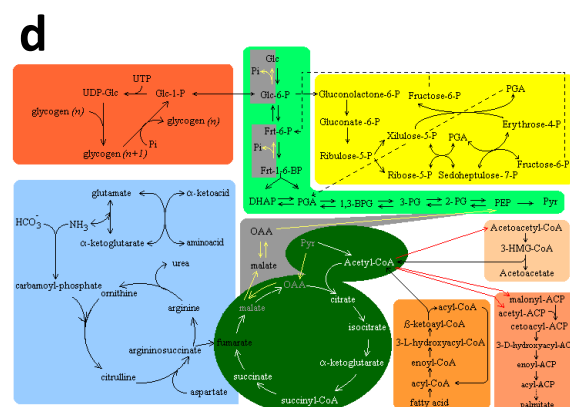
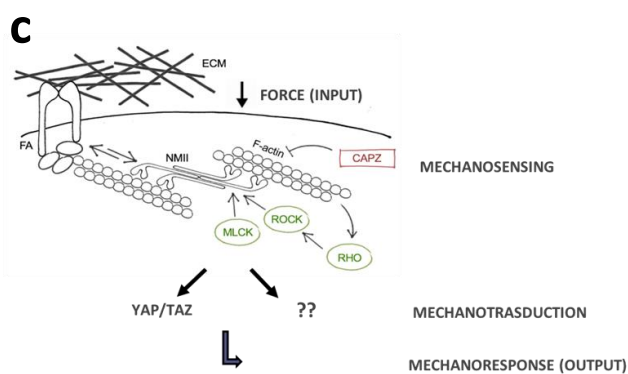
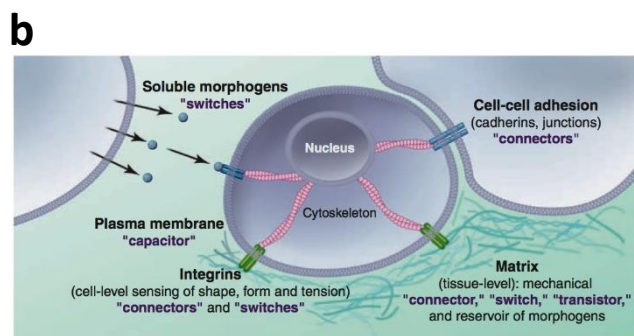
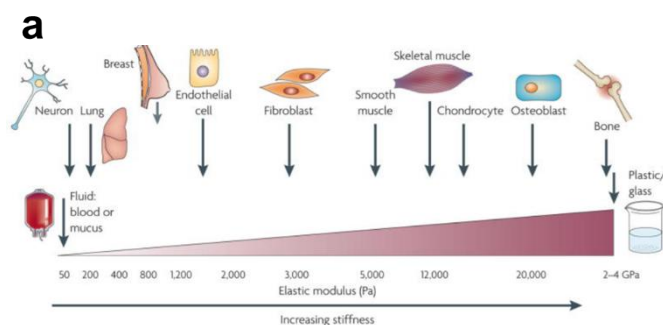
One open question that remains unanswered is the functional significance of the phenotype we described: why cells on a soft ECM accumulate neutral lipids? For sure this phenotype is conserved across multiple cell types, independent on the tissue type (i.e. epithelial or mesenchymal) or on oncogenic transformation, indicating it must have a general purpose.

From a metabolic and energetic point of view, this represents an anabolic reaction, i.e. cells are using energy and carbons to build up lipid droplets and to increase cholesterol content. This is however different from the known role of SREBP in the context of cancer cells, where SREBP-induced lipid synthesis is skewed towards the production of phospholipids (PE and PC) to form new membranes and to support proliferation. The accumulation of lipid droplets may represent a mechanism by which cells in a physiologically-normal (soft) ECM and in presence of excess nutrients (as in cell culture) store energy in the form of triglycerides. This is not allowed on a stiff ECM, which may be perceived by cells as a stress situation (in tissues, ECM stiffening is usually associated to wound healing and regeneration, or to inflammation), and where cells may want to maximize energy production instead of storage. Another possibility is that accumulation of lipid droplets is a trade-off, while the driving phenotype is production of cholesterol. Cholesterol is important to regulate important lipid bilayer biophysical parameters, including the fluidity of the membranes and their rigidity. In this view, one possibility may be that increased cholesterol synthesis when cells are on a soft ECM is needed to maintain the tensional homeostasis of the plasma membrane, which is key for several processes (for example endocytosis, ion channel activity, and the formation of “signaling hubs” at cholesterol-rich lipid rafts) in physiological conditions as well as for survival to stressful situations.

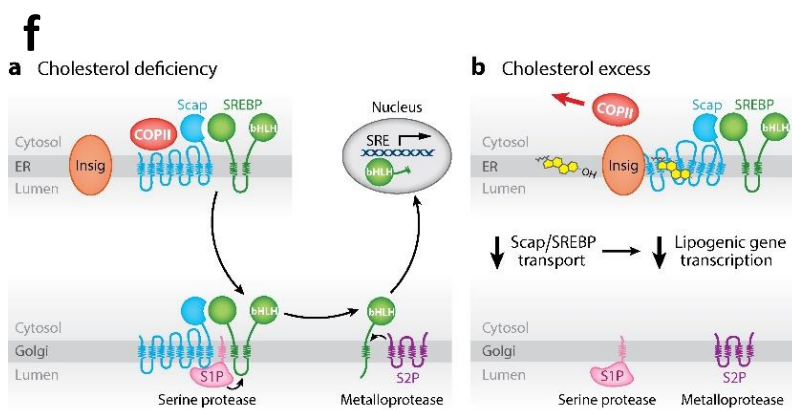
As already mentioned above, our findings indicate that SREBP lipogenic activity is skewed specifically towards neutral lipid synthesis, at difference with oncogenic stimulation of SREBP favoring the production of new membranes. Along this direction, it would be interesting to determine what is the functional significance of this metabolic phenotype, in physiology and in cancer.

# FIGURES

# FIGURE 1



Brown MS, et al. 2018. *Annu. Rev. Biochem.* 87:783-807



Brown MS, et al. 2018. *Annu. Rev. Biochem.* 87:783-807

## FIGURE 1

**a** Cells perceive their microenvironment not only through soluble signals but also in term of physical and mechanical cues, such as extracellular matrix (ECM) stiffness or confined adhesiveness. Cells sense these mechanical cues through integrins and focal adhesions and measure external resisting forces by developing internal pulling forces through their actomyosin cytoskeleton.

**b** All cells, are exposed to forces and tension that is generated locally by cell-cell or cell-ECM interactions and that influences cell function through actomyosin contractility and actin dynamics. Moreover, each cell type is specifically tuned to the specific tissue in which it resides. The brain, for instance, is infinitely softer than bone tissue. Consequently, neural cell growth, survival, differentiation and morphogenesis are optimally supported by interaction with a soft matrix. Following transformation, breast tissue becomes progressively stiffer and tumor cells become significantly more contractile and hyper-responsive to matrix compliance cues<sup>108</sup> Solid tissue exhibit a range of stiffness, as measured by the elastic modulus.

**c** Cells are able to sense and respond to the stiffness of the ECM thanks to mechanosensing mechanisms based on integrins, focal adhesion complexes and the contractile F-actin cytoskeleton. This system in turn transduces physical forces into biochemical signals, regulating intracellular signalling pathways and orchestrating a cell response.

**d** The complex network of the main metabolic pathways

**e** SCAP protein structure in detail

**f** A simplified scheme illustrating how SREBP is regulated by lipids (see text). Left: sterols retain SCAP/SREBP at the ER by binding SCAP and Insig1 proteins; a minor portion of SCAP/SREBP complexes continuously shuttles through the Golgi apparatus and is transported back to the ER<sup>5</sup>. Right: absence of sterols induces SCAP/SREBP accumulation at the Golgi apparatus where SREBP are cleaved, releasing the transcriptionally-active nuclear form of SREBP .

**FIGURE 2**

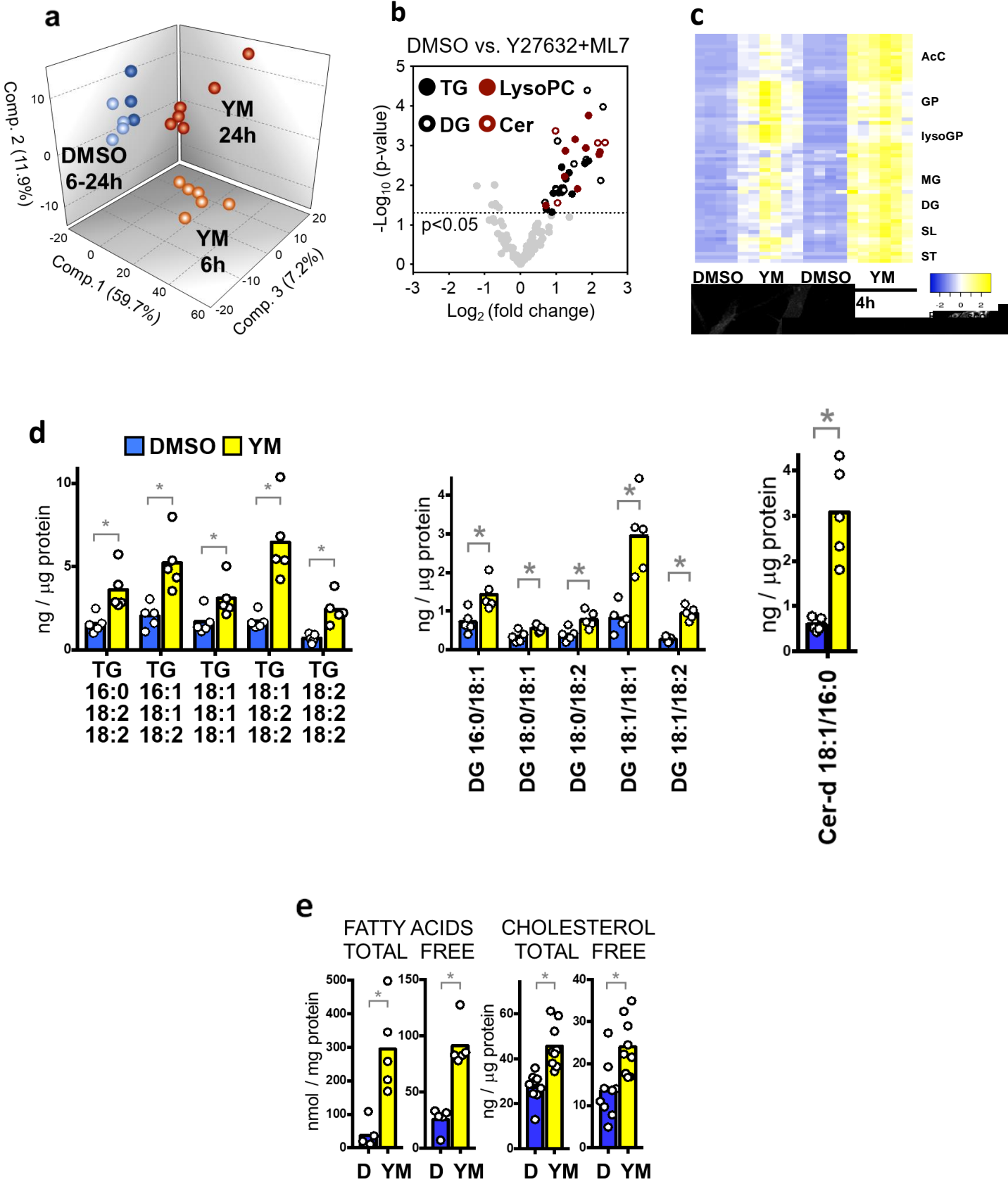


## FIGURE 2

### **Actomyosin contractility and ECM mechanical cues regulate lipid synthesis:**

**a** Principal component analysis of metabolites altered by global metabolomics in MCF10ATk1 human mammary epithelial cells treated for 6 or 24 h with 20  $\mu$  M Y27632 ROCK inhibitor and 20  $\mu$  M ML7 MLCK inhibitor to inhibit actomyosin contractility (hereafter YM,  $n = 6$  biologically independent samples), as compared to vehicle (DMSO,  $n = 4$  biologically independent samples).

**b** Volcano plot of lipid molecules altered in MCF10ATk1 cells treated for 24 h with YM, as measured by targeted lipidomics.  $n = 5$  biologically independent samples per condition. TG, triacylglycerols; DG, diacylglycerols; LysoPC, lyso-phosphatidylcholines; Cer, ceramides.

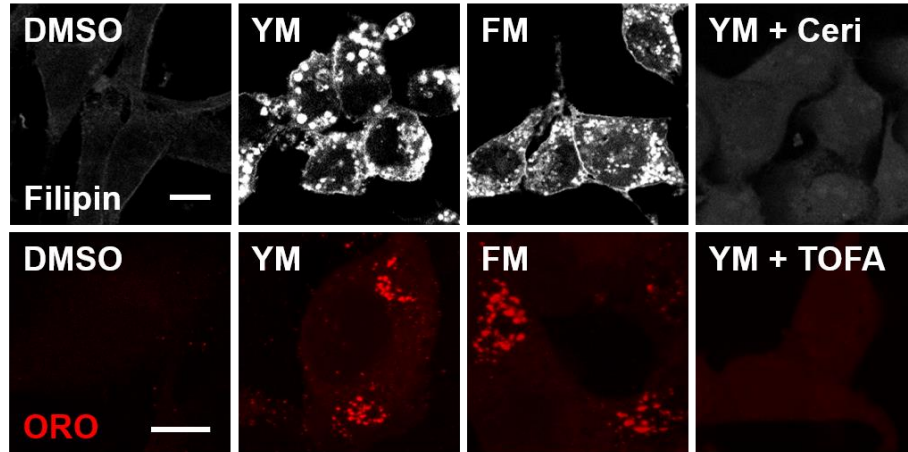
**c** Heatmap of lipid molecules displaying significant accumulation by global metabolomics in MCF10ATk1 Ras-transformed mammary epithelial cells treated for 6 or 24 hours with 20 $\mu$ M Y27632 ROCK inhibitor and 20 $\mu$ M ML7 MLCK inhibitor, as compared to an equivalent dose of vehicle (DMSO). Each column represents an independent biological replicate; each line to a single metabolite (mean fold>2.5  $p < 0.05$ ). AcC acylcarnitines; GP phospholipids; LysGP lyso-phospholipids; MG monoacylglycerols; DG diacylglycerols; SL sphingolipid metabolism; ST sterols. Triglycerides were not part of the analysis.

**d** Triglycerides (TG) and diacylglycerols (DG) levels in MCF10ATk1 cells treated with YM for 24 h, as measured by mass spectrometry. Only the five most abundant species are shown.

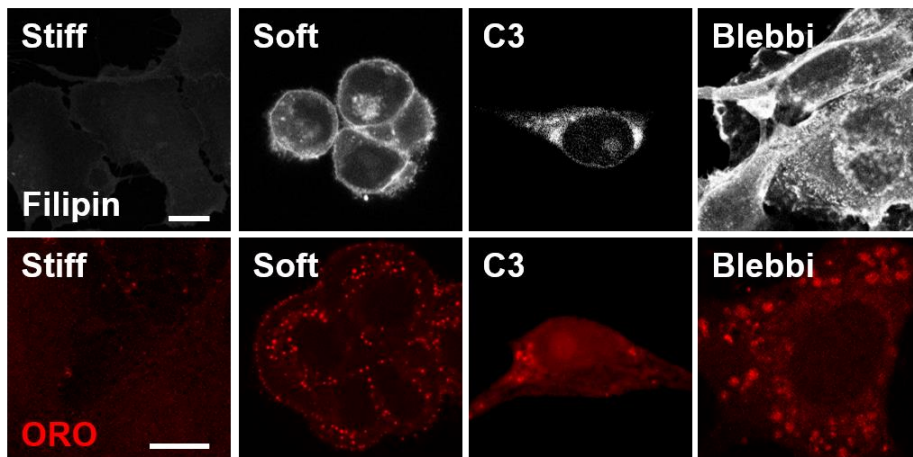
**e** Fatty acids and cholesterol in MCF10ATk1 cells treated with YM, assayed by standard colorimetric assays

**FIGURE 3**

**a**



**b**



**c**

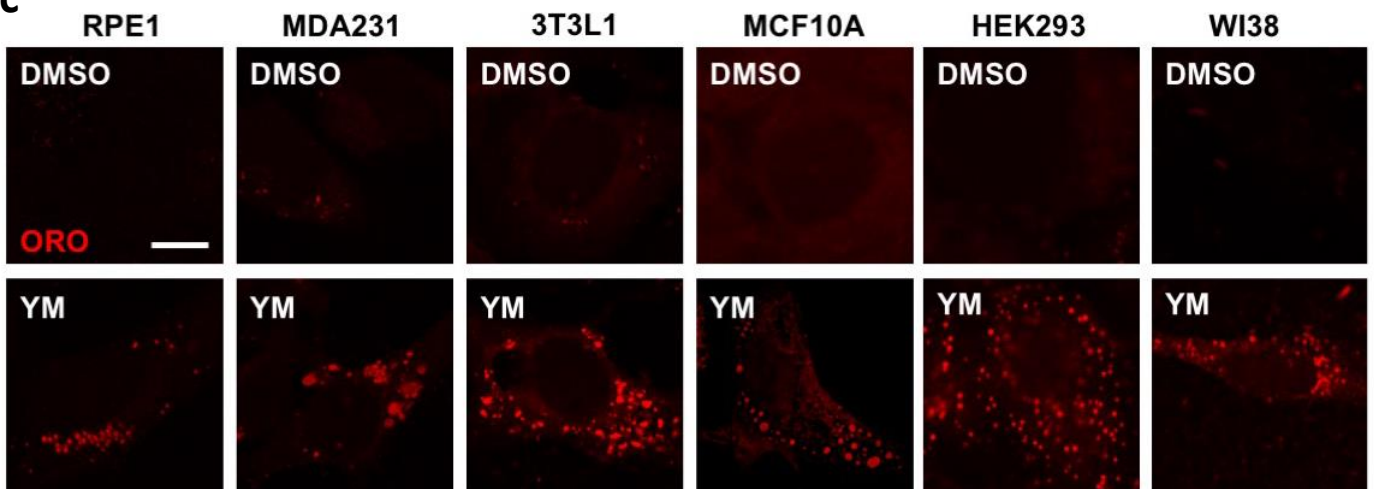


## FIGURE 3

### **Actin contractility and ECM mechanical cues regulate lipid accumulation:**

**a** Inhibition of ROCK and MLCK with YM or FM (Fasudil+ML7) induces lipid accumulation in MCF10ATk1 cells, as assayed by Filipin staining for cholesterol and Oil-Red-O (ORO) for neutral lipids. Inhibition of cholesterol and fatty acid synthesis with 10  $\mu$  M cerivastatin (Ceri) or with 15  $\mu$  M TOFA prevents accumulation. Scale bar: 5 $\mu$ m.

**b** Accumulation of cholesterol and neutral lipids in MCF10ATk1 cells on inhibition of RHO (C3 transferase transfection), non-muscle myosin II (20  $\mu$  M blebbistatin) or by plating cells on soft ( $E \approx 0.5$  kPa) fibronectin-coated polyacrylamide hydrogels, compared to stiff ( $E \approx 15$  kPa) hydrogels. Scale bars, 5  $\mu$  m

**c** Neutral lipid accumulation observed in different cell types upon DMSO and YM treatment.

**FIGURE 4**

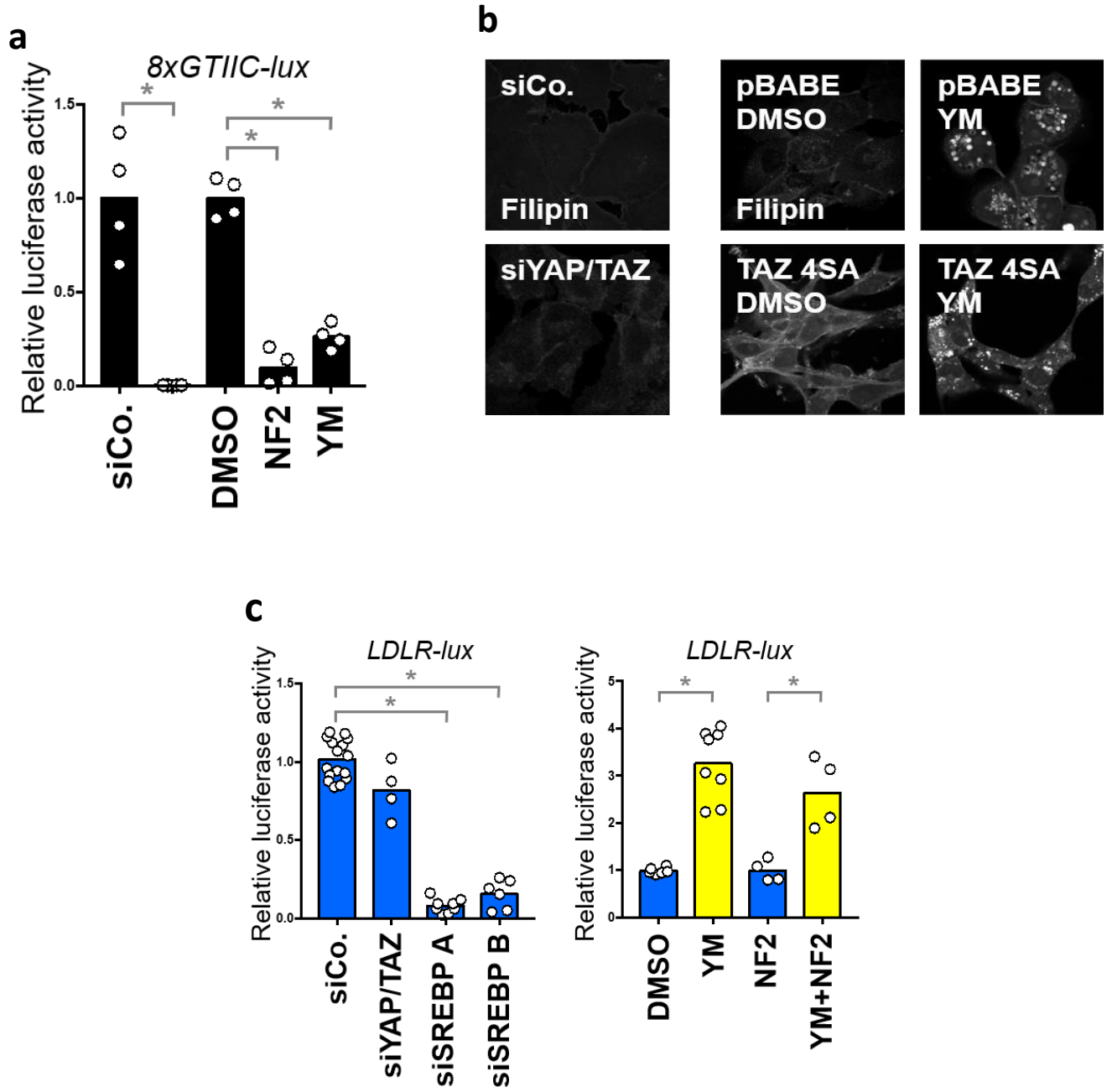


## FIGURE 4

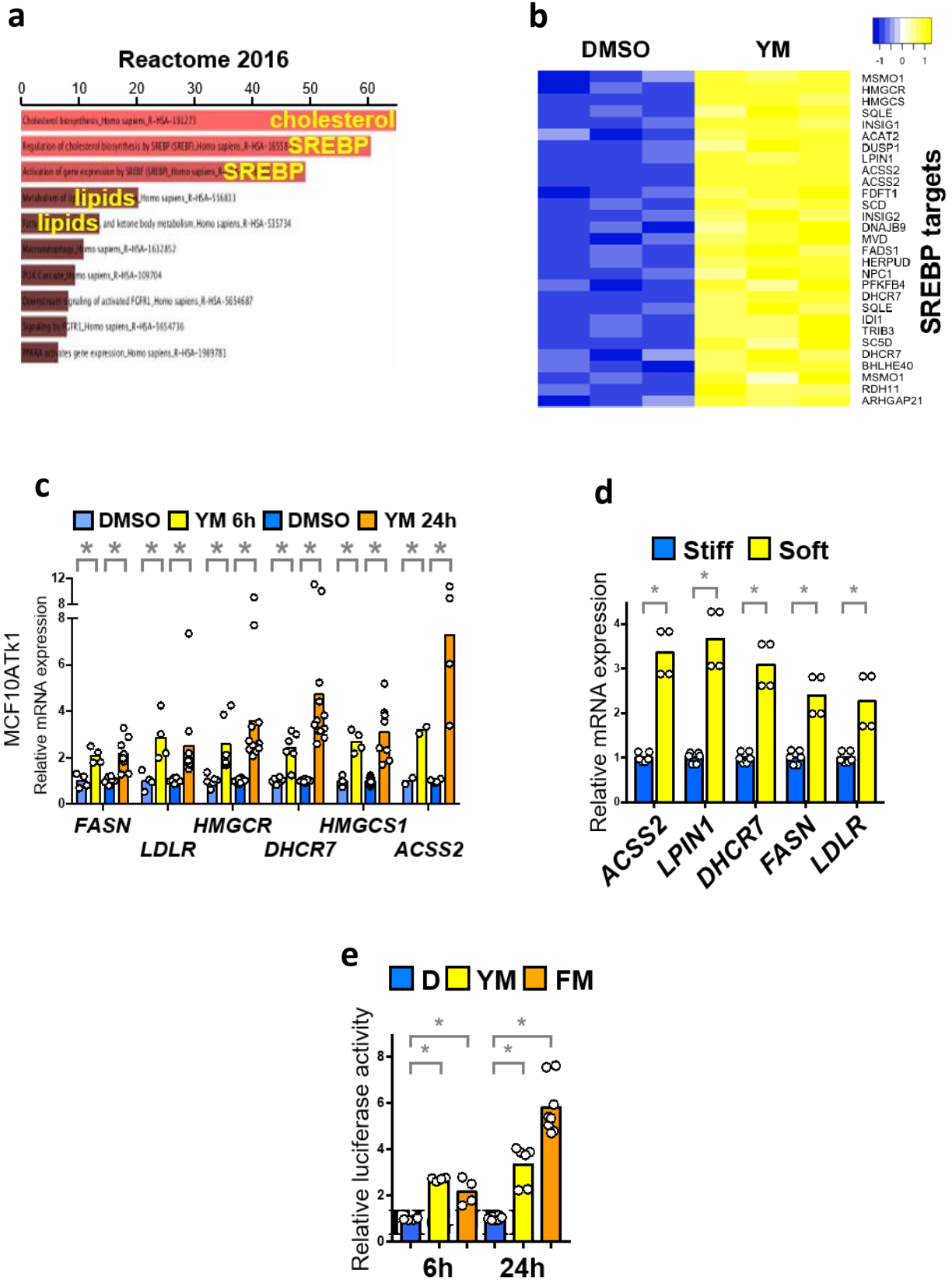
### **YAP/TAZ activity is inconsequential for lipid accumulation and SREBP activation in response to inhibition of ROCK/MLCK:**

**a** *8XGTIIIC-luciferase* reporter assay for YAP/TAZ activity in MDA231 cells transfected with control siRNA (siCO.), YAP/TAZ siRNA (siYT), cotransfected with the YAP/TAZ inhibitor NF2/Merlin expression plasmid, or treated with YM. Mean expression in the control was set to 1, and all other samples are relative to this

**b** Filipin staining for cholesterol in MCF10ATk1 depleted of YAP/TAZ and in MCF10ATk1 stably infected with pBABE TAZ 4SA or empty pBABE control, and treated with Y27632+ML7 (YM) for 24 hours. Scale bar: 10 $\mu$ m.

**c** Effect on YAP/TAZ inhibition on SREBP activity, as judged by luciferase in MDA 231 cells

**FIGURE 5**



### **ECM mechanical cues modulates the SREBP pathway:**

**a** Gene list enrichment analysis on probes significantly upregulated (mean fold > 1.3,  $P < 0.05$ ) in microarrays of MCF10ATk1 cells treated with DMSO or Y27632+ ML7 (YM) for 6 h. The graphs display the 10 most significantly overrepresented gene sets for each of the indicated databases, analysed with Enrichr and ranked according to combined score ( $x$  axis). Gene sets related to cholesterol, lipids and SREBP are highlighted in orange.

**b** Heatmap of SREBP target expression levels in microarrays of MCF10ATk1 cells treated with DMSO or with the ROCK/MLCK inhibitors Y27632+ML7 (YM) for 6 hours to inhibit actin tension. Each column represents an independent biological replicate; each line corresponds to a single gene probe indicated on the right (mean fold>1.3  $q < 0.05$ )

**c** qPCR for established SREBP targets in RPE1 cells treated for 6 or 24 h with DMSO, YM or FM

**d** Real-time PCR for established SREBP target genes (indicated above the corresponding control bars) in MCF10ATk1 cells plated on stiff ( $E \approx 15\text{kPa}$ ) or soft ( $E \approx 0.5\text{kPa}$ ) ECM for 24 hours. Data are relative to *GAPDH* levels; mean expression levels in control cells were set to 1, and all other samples are expressed relative to this.

**e** Inhibition of actin tension by treatment with YM or Fasudil+ML7 (FM) activates SREBP activity in MDA231 cells, as judged by *LDLR*-luciferase reporter assay. Mean expression levels in control cells were set to 1, and all other samples are expressed relative to this.

**FIGURE 6**

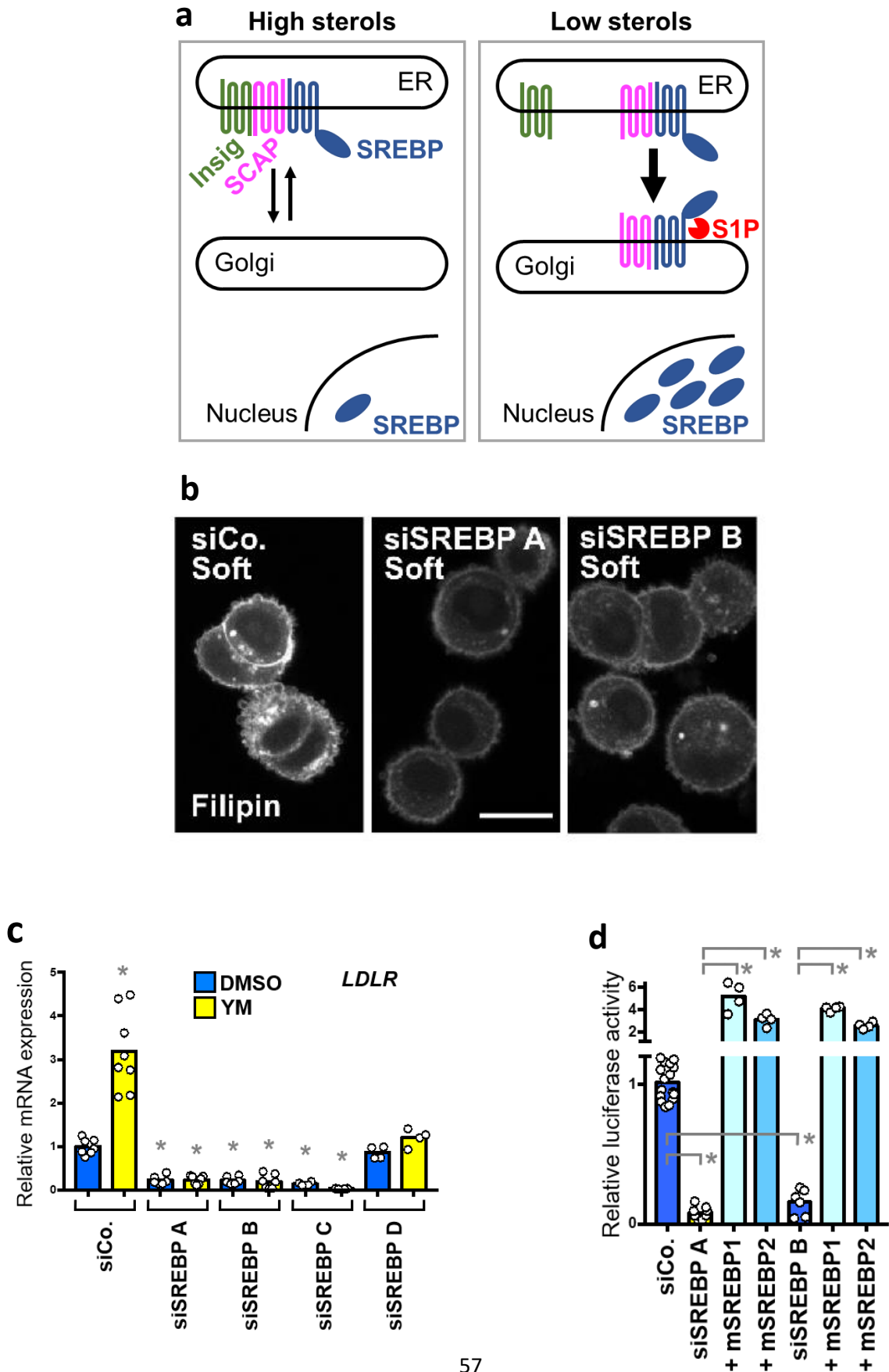


## FIGURE 6

### ECM mechanical cues regulate lipid synthesis through SREBP1/2:

**a** A simplified scheme illustrating how SREBP is regulated by lipids (see text). Left: sterols retain SCAP/SREBP at the ER by binding SCAP and Insig1 proteins; a minor portion of SCAP/SREBP complexes continuously shuttles through the Golgi apparatus and is transported back to the ER<sup>5</sup>. Right: absence of sterols induces SCAP/SREBP accumulation at the Golgi apparatus where SREBP are cleaved, releasing the transcriptionally-active nuclear form of SREBP

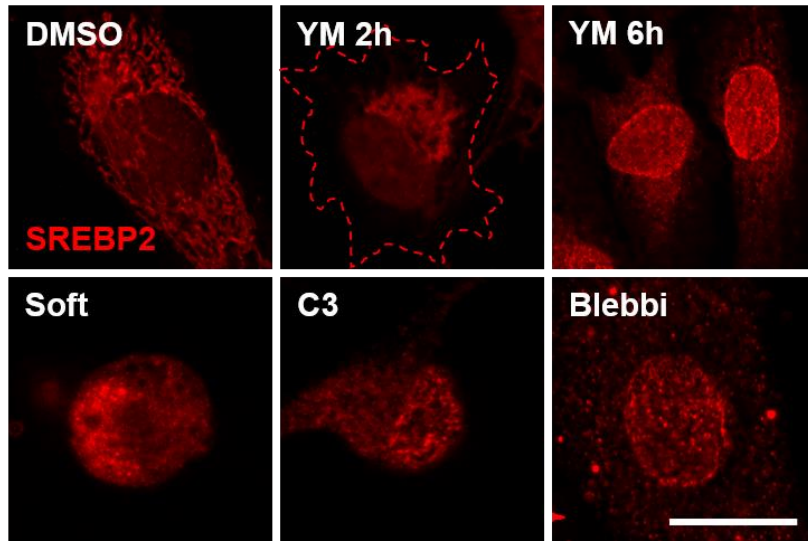
**b** Knockdown of SREBP1/2 by two independent siRNA mixes (siSREBP A and B) inhibits lipid accumulation in MCF10ATk1 cells plated on soft ECM for 24 hours.

**c** qPCR analysis of SREBP1/2 targets in MCF10ATk1 transfected as in **a** and treated with DMSO or YM for 24 h. mRNA expression data are relative to *GAPDH* levels; mean expression levels in controls were set to 1, and all other samples are expressed relative to this

**d** *LDLR-luciferase* in MDA231 cells transfected with the indicated siRNAs in combination with expression plasmids encoding for mouse full-length SREBP1 or SREBP2, whose cDNA is insensitive to siSREBP mixes A and B. Mean expression in the control was set to 1, and all other samples are relative to this

# FIGURE 7

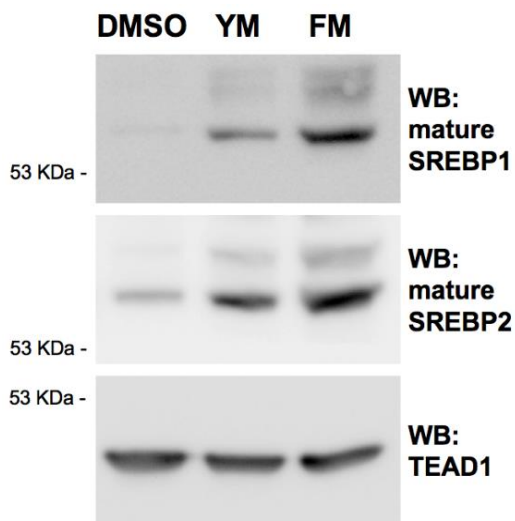
a



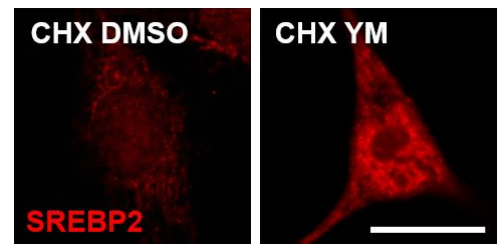
b



c



d



e

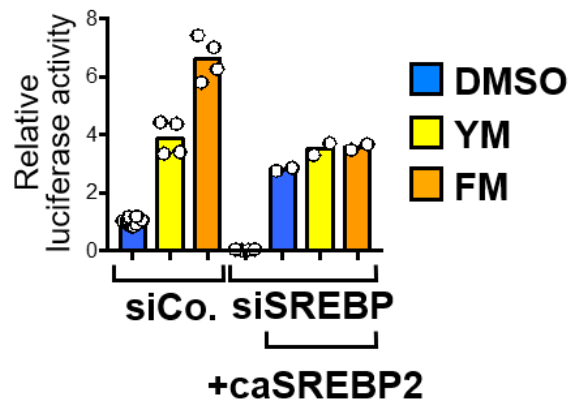


## FIGURE 7

### **ECM mechanical cues act through the direct processing of SREBPs:**

**a** Immunofluorescence for endogenous SREBP2 in MCF10ATk1 cells treated with YM (ROCK/MLCK inhibitor) for 2h and 6h, Blebbistatin, transfected with C3 RHO inhibitor, or plated on soft ECM for the indicated times. Cell contour is indicated in the second panel to visualize SREBP2 concentration in the Golgi region.

**b** Immunofluorescence for endogenous SREBP2 in MCF10ATk1 cells treated with YM (ROCK/MLCK inhibitor) for 24h and 48h, and with an 1h wash out of the treatment.

**c** Western blotting on nuclear extracts for the mature form of endogenous SREBP1 and SREBP2 in MCF10ATk1 cells treated with YM or FM (4 h). TEAD1 transcription factor serves as loading control.

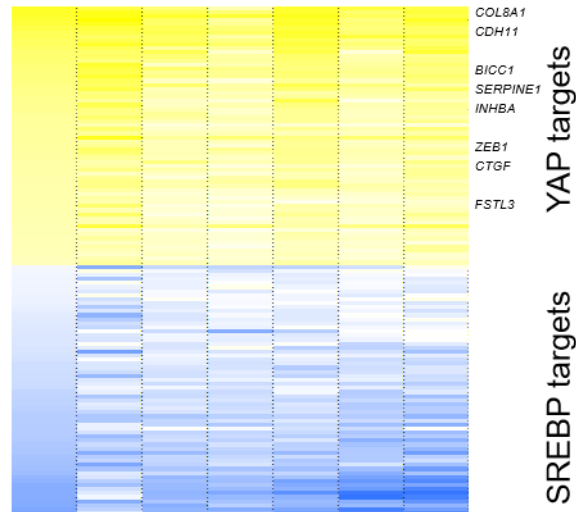
**d** Immunofluorescence for endogenous SREBP2 in MCF10ATk1 cells treated for 4 h with YM in the presence of 100  $\mu$ g ml<sup>-1</sup> cycloheximide (CHX). Scale bar, 10  $\mu$ m.

**e** YM and FM treatment activates endogenous SREBP activity, but have no effects in cells transfected with SREBP1/2 siRNA and reconstituted with a siRNAinsensitive, cleaved mature SREBP2 cDNA (CA SREBP2), as judged by *LDLR* luciferase reporter assay in MDA231 cells.

## FIGURE 8

### keloid scars vs. normal skin

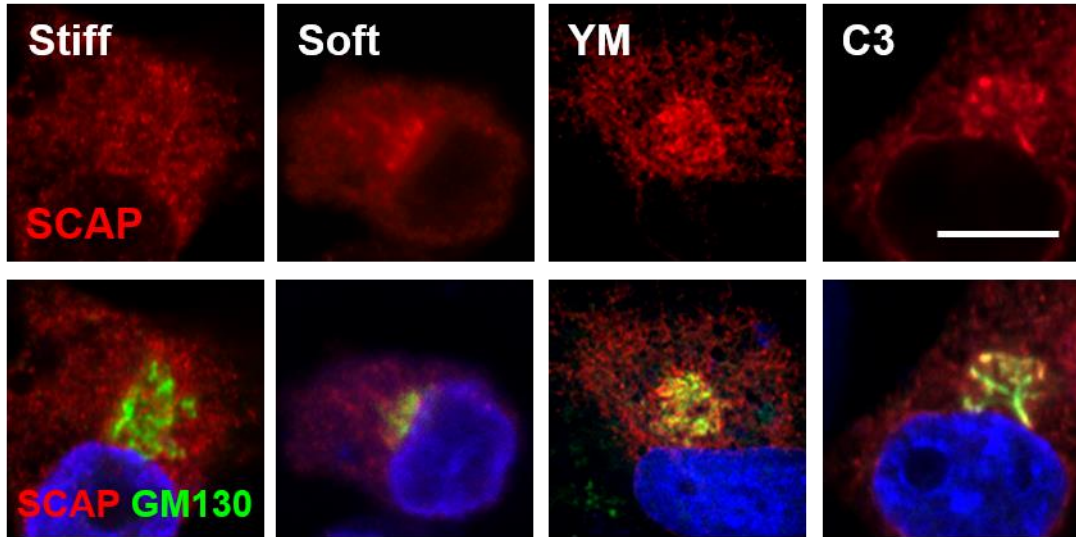
#1 #2 #3 #4 #5 #6 #7



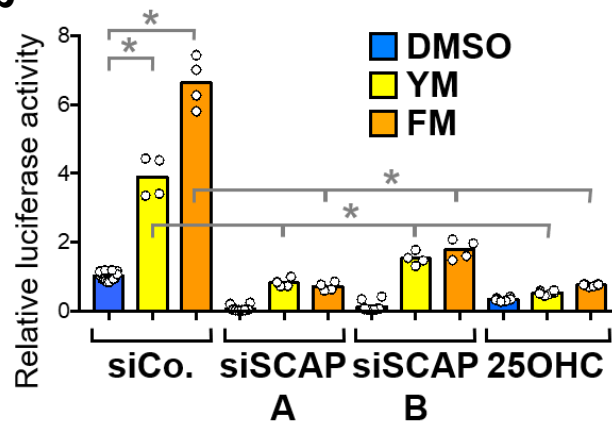
Heatmap of SREBP and YAP target levels in  $n = 7$  patient-matched soft normal skin versus stiff keloid tissue. Each column represents  $-\log_2(\text{keloid/skin})$  values for a single patient; each line is a single gene probe; genes ranked according to expression in patient #1. Selected gene names are indicated on the right; only the 60 most up- or downregulated genes ( $P < 0.05$ ) are included

**FIGURE 9**

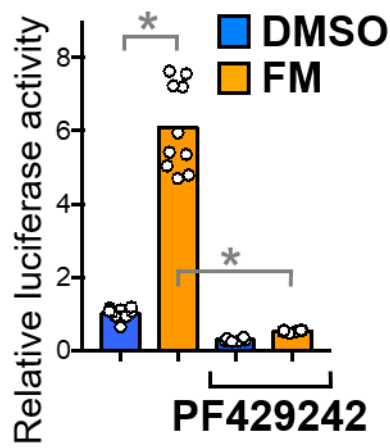
**a**



**b**



**c**



**d**

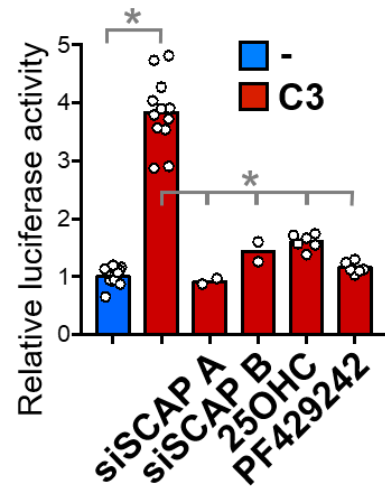


## FIGURE 9

### ECM mechanical cues regulate SREBP through SCAP and S1P:

**a** Co-localization of transfected MYC-tagged SCAP with a Golgi marker (GM130) in MCF10ATk1 cells treated with Y27632+ML7 (YM), transfected with C3 RHO inhibitor, or cultured on soft ( $E \approx 0.5$  kPa) fibronectin-coated hydrogels 6 h).

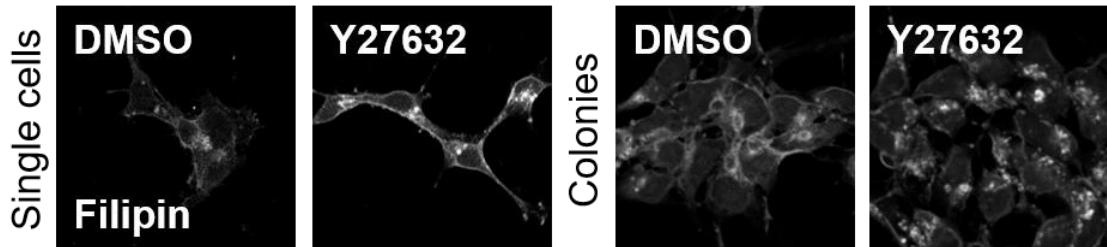
**b** Knockdown of endogenous SCAP by two independent siRNA oligos (siSCAP A and B) inhibits SREBP activity induced by YM or Fasudil+ML7 (FM) treatment (24 h), as judged by *LDLR* luciferase reporter assay in MDA231 cells. D is for DMSO, siCo. for control siRNA. Mean expression levels in control cells were set to 1, and all other samples are expressed relative to this.

**c** Treatment with S1P protease inhibitor, inhibit the activation of the LDLR reporter, on YM treated cells

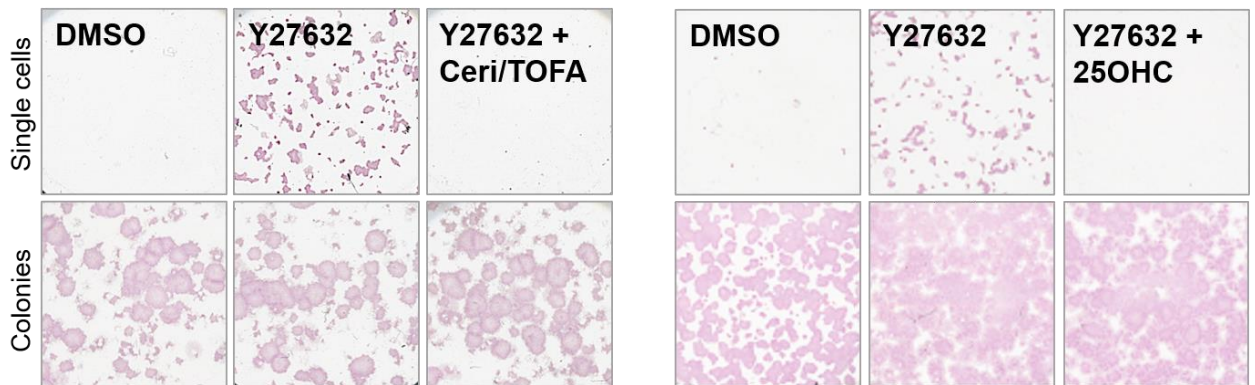
**d** Treatment with S1P protease inhibitor, inhibit the activation of the LDLR reporter, on C3 transfected cells

**FIGURE 10**

**a**



**b**



**c**



## FIGURE 10

### **hPSCs survival depends on lipid synthesis and in part on SREBP activity:**

**a** Filipin staining of hPSC plated as single-cells or cultured as multicellular aggregates and treated for 24 hours with the Y27632 ROCK inhibitor.

**b** human Pluripotent Stem Cells (hPSC) were plated as single cells in the absence (DMSO, D) or presence of 10 $\mu$ M Y27632 ROCK inhibitor (Y) for 24 hours to enable survival, released in medium without Y27632 for 4 days, and stained for alkaline phosphatase to visualize self-renewing colonies. Treatment with titrated doses of Cerivastatin (Ceri 25nM) and TOFA (75nM) for 24 hours together with Y27632 (Y+Ceri/TOFA) inhibits single cell survival. Lower panels: treatment on already established colonies does not have any effect. Higher doses of Ceri/TOFA (10 $\mu$ M and 15 $\mu$ M) inhibit also established colonies in line with Ref104. Representative pictures from two biological replicates. The experiment was repeated 3 times.

**c** hPSC were transfected with the indicated siRNAs and plated as above as single cells. Representative pictures from two biological replicates. The experiment was repeated 3 times. Scale bars: 5 $\mu$ m.

**FIGURE 11**

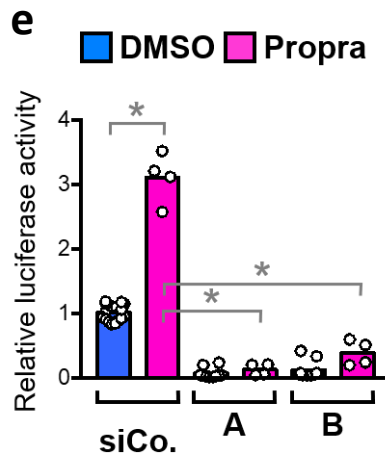
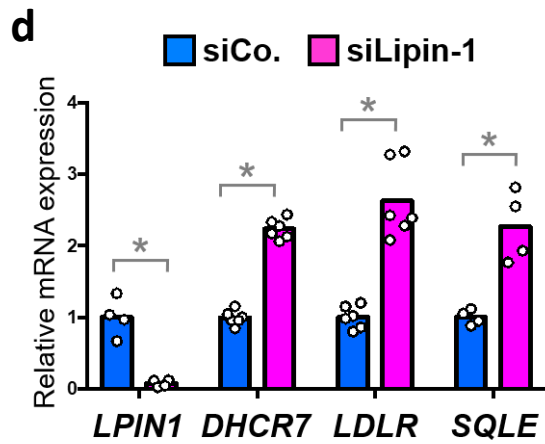
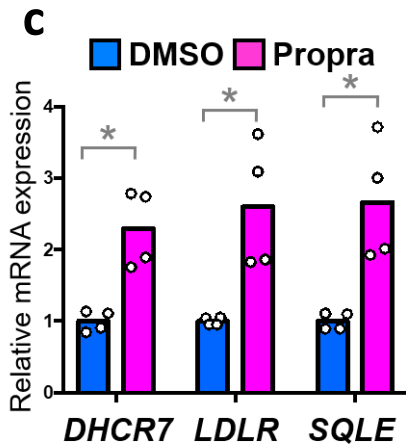
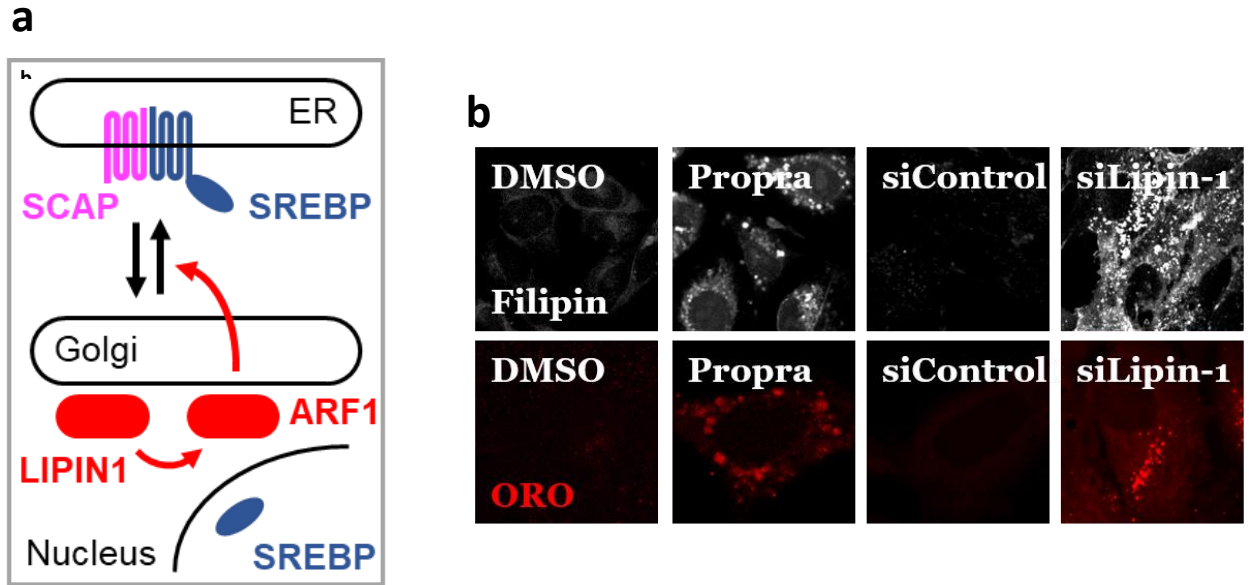


## FIGURE 11

### **Lipin1 inhibition induces lipid accumulation and SREBP activation:**

**a** A simplified scheme illustrating how SREBP is regulated by Lipin-1 and ARF1 (see text)

**b** Filipin and ORO staining of MCF10ATk1 cells treated with YM for 24h and with 100 microM of propranolol for 24h, or transfected with control and Lipin1 siRNA. Lipid accumulation in condition of low contractility is comparable with Lipin1 inhibition.

**c e d** qPCR for SREBP target genes in MCF10ATk1 cells treated with 100 microM of propranolol for 24h, or transfected with control and Lipin1 siRNA. In both condition, we confirmed activation of the SREBP pathway.

**e** *LDLR-luciferase* in MDA231 cells transfected with the indicated siRNA and treated with 100  $\mu$  M propranolol. Mean expression in the control was set to 1, and all other samples are relative to this

**FIGURE 12**

**a**



**b**

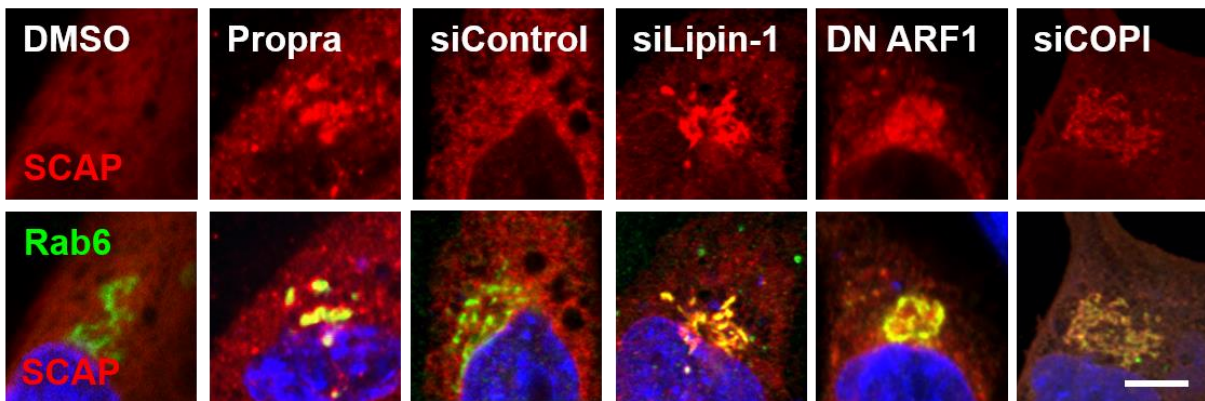


## FIGURE 12

### **Lipin1 and ARF1 inhibition activate the SREBP-SCAP pathway:**

**a** Immunofluorescence of SREBP localization in RPE1 htert cells treated with 100 microM of Propranolol for 24h, or transfected with control and Lipin1 siRNA, or with a dominant negative mutant for ARF1 (ARF1-T31N-GFP) and finally transfected with a siRNA for COPI. All conditions results in a consistent accumulation of SREBP in the nucleus.

**b** Immunofluorescence of SCAP localization in the same condition of (A). Coherently, we observed SCAP translocation towards the golgi membranes.

**FIGURE 13**

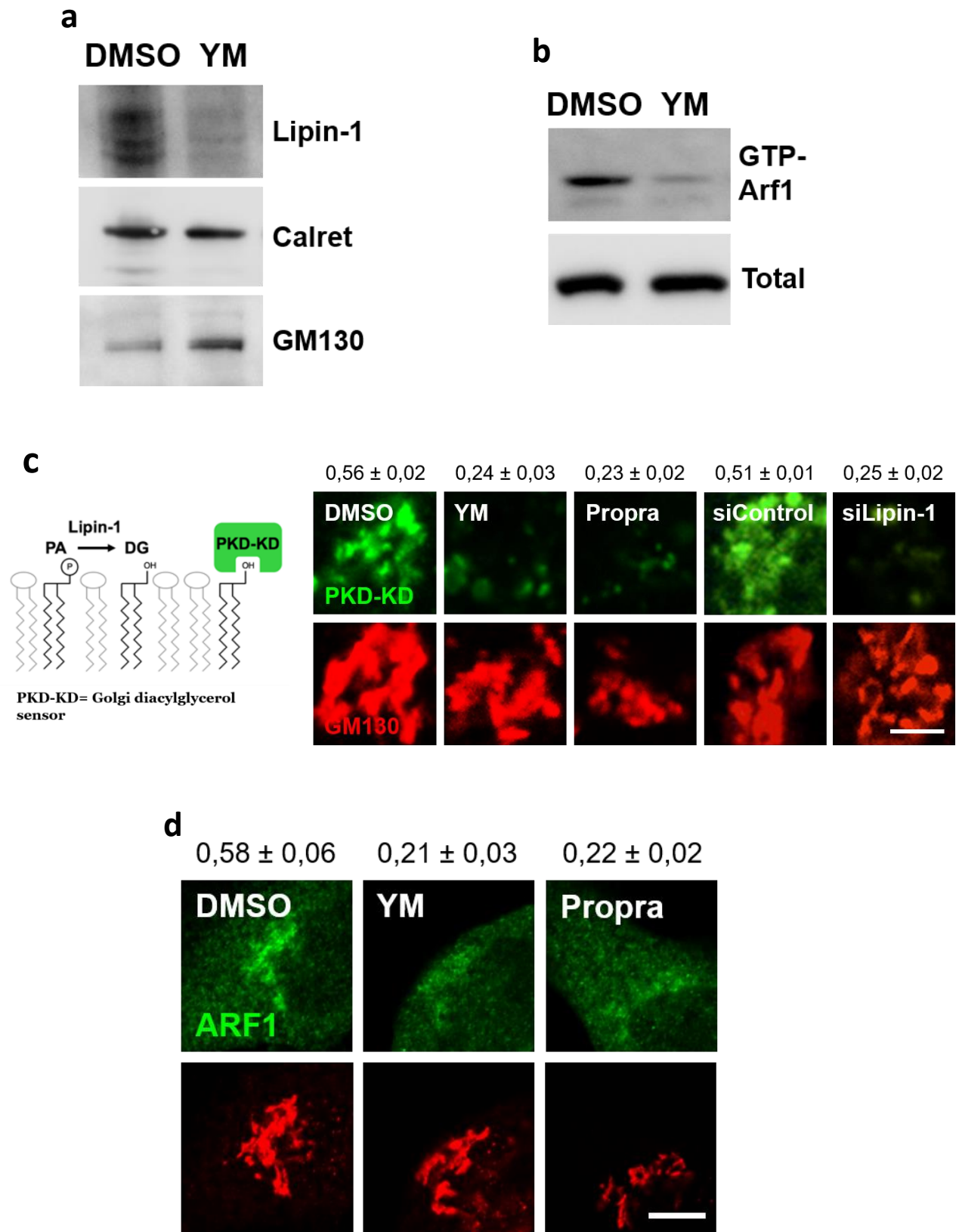


## FIGURE 13

### ECM mechanical cues regulate Lipin1 and ARF1 activity:

**a** Western blot performed on microsomal fractions of MCF10ATk1 cells. Lipin1 levels in cells treated for 3h with DMSO or YM was detected. Calreticulin is used as ER loading, GM130 as golgi loading.

**b** GST-GGA3-PBD pulldown for GTP-bound active ARF1 (GTP-Arf1) and western blotting for ARF1 in the total extracts (Total Arf1). MCF10ATk1 cells were treated 3 hours with DMSO or YM.

**c** Co-localization of transfected GFP-PKD-KD with the GM130 Golgi marker in HEK293 cells treated for 30 min with YM, with 100  $\mu$ M Propranolol, or transfected with control (siCo.) and Lipin-1 siRNAs. Scale bar 10  $\mu$ m. Mean Pearson's correlation coefficient and SD for co-localization is indicated above each panel ( $n \geq 10$  cells were measured for each condition).

**d** Co-localization of endogenous ARF1 with a Golgi marker (GM130) in MCF10ATk1 cells treated 6 hours with YM or Propranolol. Scale bar 10  $\mu$ m. Mean Pearson's correlation coefficient and SD for co-localization is indicated above each panel ( $n \geq 10$  cells were measured for each condition).

**FIGURE 14**

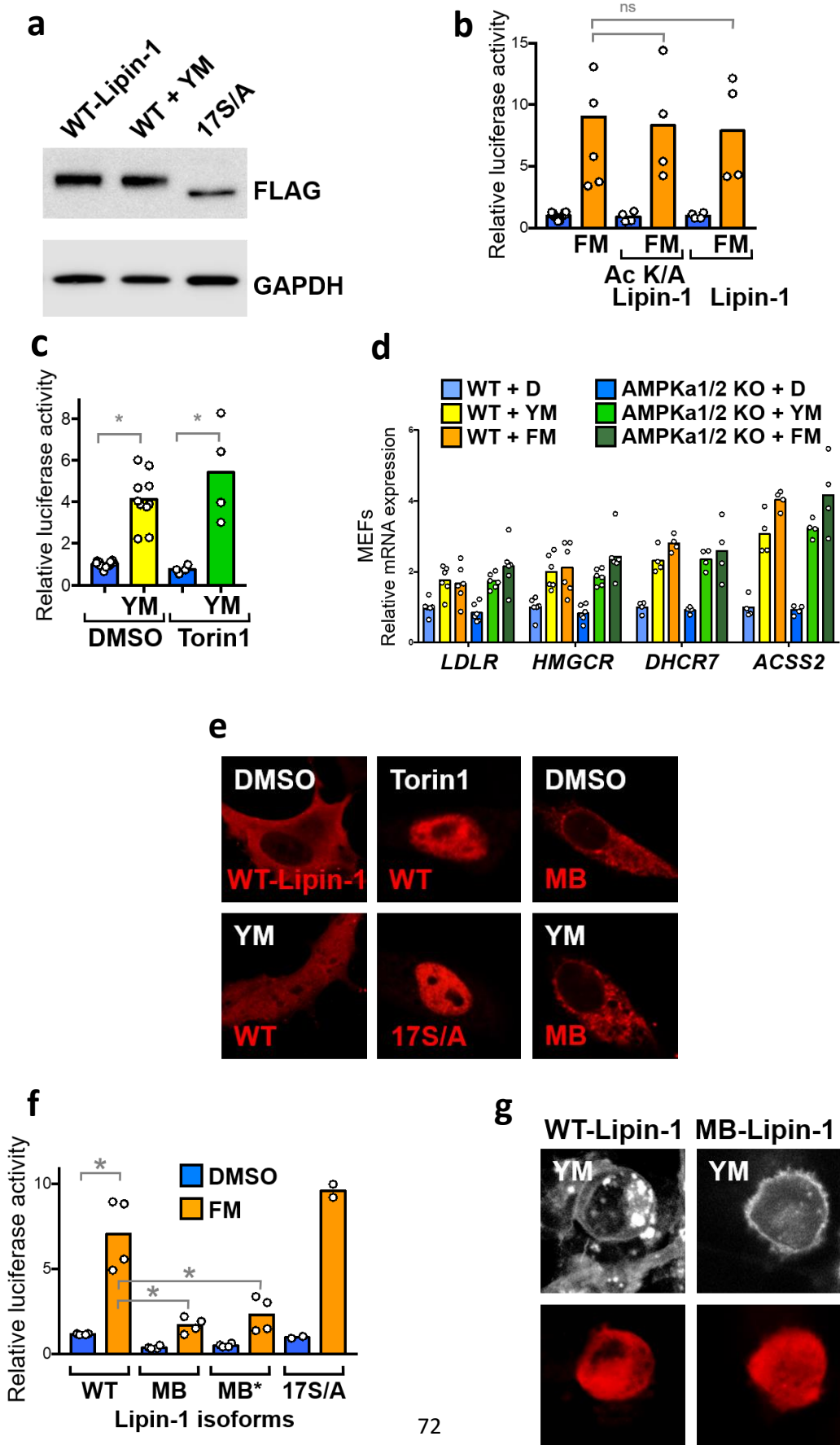


## FIGURE 14

### ECM mechanical cues regulate lipid accumulation through LIPIN1:

**a** Western blot of HEK 293 cells transfected with the wild type form of LIPIN1 and treated for 6h with DMSO and YM. The two condition do not show different pattern of protein migration, suggesting that phosphorylation is not implicated in the regulation of LIPIN1 by low contractility. Trasfection of the 17S/A mutated form of LIPIN1 is used of positive control of differential migration.

**b** *LDLR-luciferase* in MDA231 cells expressing Lipin-1 isoforms mutated in the known acetylation (Ac K/A, K476/646A) or SUMOylation (SUMO K/A, K616/646A) sites and treated with DMSO or FM. Mean expression in the control was set to 1, and all other samples are relative to this.

**c** *LDLR-luciferase* in MDA231 cells treated with DMSO, YM and Torin1 (500nM). Mean expression in the control was set to 1, and all other samples are relative to this.

**d** qPCR for established SREBP target genes in MCF10ATk1 cells. Data are relative to *GAPDH* levels; mean expression controls was set to 1, and all other samples are relative to this.

**e** Immunofluorescence for transfected wild-type (WT) or 17S/A FLAG-tagged Lipin-1 isoforms in RPE1 cells, treated with DMSO, YM or Torin1 (500 nM) for 6 h. Fusion with the membrane-localization domain of Syntaxin5 tethers MB-Lipin-1 to cytoplasmic membranes. Scale bar, 10  $\mu$  m. At least 50 cells per condition. Similar results were obtained with MB\*-Lipin-1

**f** Luciferase assay using LDLR reporter gene in MDA 231 cells. Here, we compare SREBP transcriptional activity in cells expressing the wild type form of Lipin1 and the membrane bound Lipin1 (MB-Lipin1). WT Lipin1 has not effect on YM dependent SREBP activation, MB-Lipin1 instead, is able to inhibit the effect of low contractility (YM).

**g** MDA231 cells were transfected with WT-Lipin-1 or MB-Lipin-1 together with mCherry (RFP), treated with YM, and stained for cholesterol. n>30 cells per condition. Graph: cells were scored positive (+ve) for Filipin based on the presence/absence of cytoplasmic cholesterol accumulation.

**FIGURE 15**

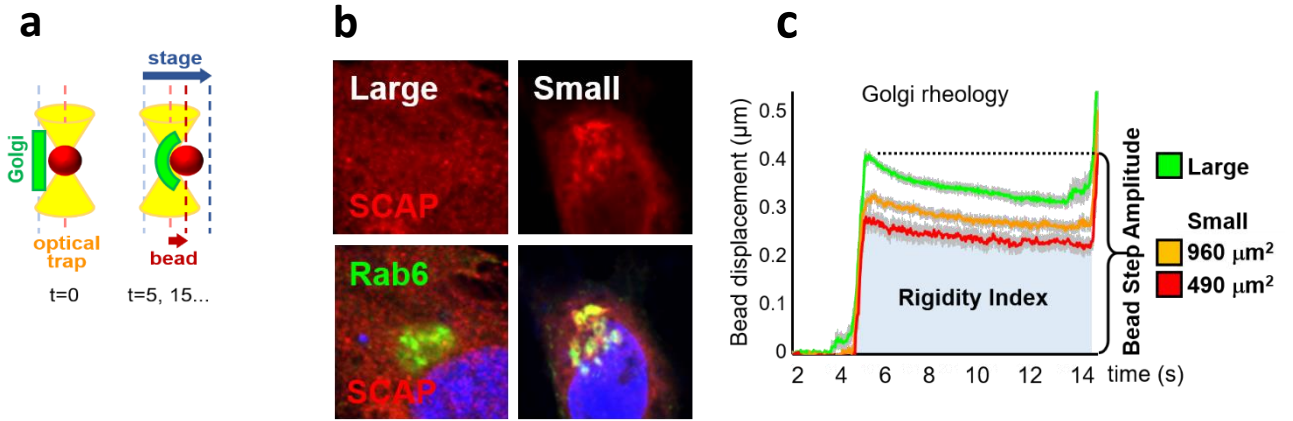


## FIGURE 15

### **The Golgi apparatus responds to extracellular physical cues and intracellular force application:**

**a** Simplified diagram illustrating the technique to measure Golgi rheology. Left: an internalized bead (red) is immobilized in proximity to the Golgi membranes (green) by a laser optical trap (yellow cones). Right: when the stage and thus the whole cell is moved towards the bead (blue arrow), the Golgi apparatus displaces the bead away from the trap center (red arrow). Since the Golgi microenvironment has visco-elastic properties, the bead position partially relaxes in time attracted towards the trap center.

**b** Co-localization of transfected MYC-SCAP with the GFP-Rab6 Golgi marker in RPE1 cells freely spreading on fibronectin-coated glass (Large) or plated on micropatterned fibronectin islands restraining cell area and inducing low F-actin tension (Small, 960  $\mu\text{m}^2$  or 490  $\mu\text{m}^2$ ). Scale bar, 10  $\mu\text{m}$ . At least 30 cells per condition.

**c** Golgi rheology was measured in RPE1 cells plated as in **a**. GFP-Rab6-positive Golgi membranes were pushed towards a cytoplasmic bead immobilized by an optical trap in a series of five 0.5  $\mu\text{m}$  steps in 1 min (Supplementary Fig. 7a and Methods). The graph shows the averaged displacements of the bead during the first step. Green line: large unconfined cells, conditions of high tension ( $n = 39$  cells). The Golgi microenvironment displays a visco-elastic behaviour as the bead is first maximally displaced (bead step amplitude), and then slowly relaxes back due to attraction from the optical trap. Orange and red lines: micropatterned small ECM ( $n = 28, 21$  cells). Gray shading: s.e.m. error. A smaller displacement and a faster relaxation of the bead indicate a lower rigidity of the Golgi apparatus.

**d** Time-lapse confocal images of a representative RPE1 cell transfected with the GFP-PKD-KD diacylglycerol sensor and with Golgi-localized mCherry. A 2- $\mu\text{m}$ -diameter cytoplasmic bead (yellow dotted circle) was immobilized by an optical trap in the proximity of the Golgi apparatus ( $t = 0$ ) and then pushed every 5 min towards the Golgi (white arrow, direction of compressive constraint).

e Normalized intensity of the GFP-PKD-KD signal before and after application of force ( $n = 19$  cells). In the control the bead was moved away from the Golgi towards the cytoplasm ( $n = 18$  cells).

## MATERIALS AND METHODS

### Plasmids and recombinant plasmids

Plasmids encoding for SCAP-MYC, HA-S1P and HA-S2P were from Y. Chen (SIBS Shanghai), perilipin3-RFP from L. Scorrano (UniPd), kinase-dead GFP-PKD1-K612W from A. Hausser (UniStuttgart), ARF1-T31N-GFP from A. DeMatteis (TIGEM Naples), KDEL-mCherry from E. Greotti (UniPd) and GFP-OSBP from N. Ridgway (UniGlasgow). Addgene plasmids: FASN-lux #8890; LDLR-lux #14940; 8XGTIIC-lux #34615; NF2 #19701; CMV-Luc2P\_ARE #62857; constitutive-active FLAG-SREBP2 #26807; FLAG-Lipin-1 WT #32005 and 17S/A #32007; mCherry-Golgi(B4GALT1) #55052. Full-length SREBP1 and SREBP2 were subcloned from Addgene plasmids #32017 and #32018. ER/Golgi membrane-tethered Lipin-1 isoforms were obtained by in-frame fusion of the Syntaxin5 delta220 or TMD fragments to FLAG-Lipin-1 WT and have been deposited as Addgene plasmids #120277 and #120278. SUMOylation (K616/646A) and acetylation (K476/646A) FLAG-Lipin-1 mutants were obtained by targeted mutagenesis. All plasmids were sequence-verified before use and transfected as endotoxin-free maxi preps.

### Recombinant retrovirus for stable transduction

Retroviral particles were prepared by transiently transfecting HEK293gp cells with retroviral vectors together with packaging vector (pMD2-env).

Plasmid DNA transfections were done with Transit-LT1 (MirusBio).

At 48 hours after transfection, culture medium containing the recombinant viral particles, was collected, filtered (filter with a 0,45  $\mu\text{m}$ ) and used to infect cells (viral particles are diluted 1:4 in complete medium). The cells are previously plated at 25% confluence and are left 24 hours in contact with the viral particles. Retroviral vectors contain a gene for resistance to puromycin, which allows the selection of only the infected cells. Therefore, cells have been maintained in culture in the presence of puromycin. Not transduced control cells were killed in 48 hours in the presence of puromycin, indicating the proper functioning of selection agent. The selection of the transduced cells was maintained until the control

cells die, in order to be sure that in culture there were only properly infected cells. Authorized people generated retroviral particles in a dedicated room.

## Cell cultures

MCF10A, MCF10ATk1 and MCF10ATk1 pBABE mTAZ 4SA were cultured in DMEM/F12 5% HS insulin (Sigma), cholera toxin (Sigma), hEGF (PeproTech) and hydrocortisone (Sigma), GFP-Rab6 and parental RPE1 in DMEM/F12 10% FBS (neomycin for GFP-Rab6), MDA-MB-231 in DMEM/F12 10% FBS, HEK293 in DMEM 10% FBS, WI-38 in MEM 10% FBS 5% oxygen, 3T3-L1 in DMEM 10% FBS 5% oxygen, H9 hPSC in E8 medium (DMEM/F12, NaHCO<sub>3</sub>, insulin, selenium, transferrin, L-ascorbic acid, FGF2, TGFβ1) 5% oxygen, and WT and AMPKα1/2<sup>-/-</sup> MEFs in DMEM 20% FBS. Glutamine was freshly added to a final concentration of 2 mM to all media. General media, serum and supplements were from Thermo. All cell lines were routinely tested with an ATCC Universal Mycoplasma Detection kit to exclude contaminations. FBS was previously decontaminated for one hour at 56 °C.

hPSCs were dissociated with Tryple (Thermo) and plated as single cells (2,500 cells per 2 cm<sup>2</sup> well) in the presence or absence of the indicated small molecules for 24 h; medium was then changed and cells were left growing for 4–5 days, until the appearance of macroscopic colonies. Treatment of colonies was done on colonies grown from single cells as above, and then treating for 24 h. Cell transfections were carried out with Transit-LT1 (MirusBio) or with Lipofectamine RNAi-MAX (Thermo).

## siRNA transfection

siRNAs were selected among FlexiTube GeneSolution 4 siRNA sets (Qiagen) and reordered after validation as dTdT-overhanging 19 nt RNA duplexes (Thermo). siRNA transfections were performed with Lipofectamine RNAi MAX (Invitrogen) in antibiotics-free medium, at a cell confluence of 20% and according to manufacturer instructions. At the proper time point, cells were washed with HBSS and harvested for the subsequent analysis. Control

siRNAs were Qiagen AllStars Negative Control siRNA, with results comparable to non-transfected cells.

Hereafter, targeted sense sequence of the mRNA:

SiRNA target gene	Interfering sequence
SREBF1 a	CGGAGAAGCUGCCUAUCAA
SREBF1 b	GCGCACUGCUGUCCACAAA
SREBF1 c	GCGCACUGCUGUCCACAAA
SREBF1 d	ACAGCAACCAGAAACTCAA
SREBF2 a	GCAGUGUCCUGUCAUUCGA
SREBF2 b	GCAAUUUGUCAGUAAUCAA
SREBF2 c	GGCCAUUGAUUACAUCAAA
SREBF2 d	CGAUAUCGCUCCUCCAUCA
SCAP a	GGAAGAUCGACAUGGUCAA

SCAP b	GGCCGACGCUCUUCAGCUA
LIPIN1	GUUCGGAUACCUUCAGUAA
YAP	CUGGUCAGAGAUACUUCUU
TAZ	AGGUACUCCUCAAUUCACA
COPI a	GAUUUACCGAGGAGCAUUA
COPI b	GGAUCGCUUGAUAGAAUUA

## Reagents

The small molecule inhibitors were Y27632 (Axon 1683, 20  $\mu$ M, 10  $\mu$ M on hPSC), Fasudil/HA1077 (SantaCruzBiotechnology sc358231, 20  $\mu$ M), ML7 (Sigma I2764, 20  $\mu$ M), blebbistatin (Sigma B0560, 20  $\mu$ M), propranolol (Sigma P0884, 100  $\mu$ M), cycloheximide (Sigma C1988, 100  $\mu$ g ml<sup>-1</sup>), TOFA (Sigma T6575, 15  $\mu$ M, 75 nM on hPSC), cerivastatin (Sigma SML0005, 10  $\mu$ M, 25 nM on hPSC), 25-hydroxycholesterol (Sigma SML2042, 30  $\mu$ M, 1.25  $\mu$ M on hPSC), U18666A (SantaCruzBioTechnology sc203306, 3  $\mu$ M), PF429242 (Sigma SML0667, 10  $\mu$ M), Z-VAD-FMK (Sigma V116, 30  $\mu$ M), Torin1 (Axon 1833, 500 nM), MG132 (Sigma C2211, 10  $\mu$ M) and MG115 (Sigma C6706, 10  $\mu$ M).

## RNA extraction

For RNA extraction RNeasy Mini kit (Qiagen) is used. 350  $\mu$ l of Lysis buffer is added to each well plate containing cells. Lysis buffer is prepared in advanced by the addition of DTT 2M ( 10  $\mu$ l for each ml of Lysis buffer). Lysate cells are detached from the plate by using a scraper and transferred in a clean eppendorf, in which an equal volume of 70% ethanol is added. Each sample is vortexed until the solution becomes homogeneous. The mixture is then transferred to the RNeasy Mini spin column and centrifuged for 30 seconds at 10000rcf. The flow-through id discard and 350  $\mu$ l of wash buffer is added to the columns. After centrifugation, a mix of DNAsi I and RDD buffer is added and left incubate for 15 minutes at room temperature. The mix is prepared in advanced, blending 10  $\mu$ l of DNAsi I to 70  $\mu$ l of RDD buffer for each sample. 350  $\mu$ l of wash buffer is then added to the column. After centrifugation, 2 washing steps with RPE buffer are performed, the first followed by a 30 seconds centrifugation, and the second by a 2 minutes centrifugation, both at 10000 rcf. A new collection tube is then used for an 1 minute full speed centrifugation to dry the membrane of the column. Finally, the column is moved to a new supplied collection tube and 35  $\mu$ l of RNase-free water is added directly to the spin column. The RNA is elute by centrifuging 1 minute at 10000 rcf and quantified.

## Retrotranscription protocol

0,5-5  $\mu$ g of extracted RNA is used for generation of cDNA. RNA is heated for 5 minutes at 70 °C and immediately moved on ice for 2 minutes, in order to denature the secondary structures. The retrotranscription master mix contains FS buffer 5X, DTT 0,1 M 10X, dNTPs mix (5 mM each), oligo-d(T) primers 20X( 5mM each) and Mo-MLV RT (Invitrogen). The mix is added to each RNA sample and the reactions are then incubated for 2 hours at 37 °C. After incubation, Mo-MLV RT is inactivated for 10 minutes at 70 °C.

## RT-PCR

cDNAs samples are properly diluted and run in triplicate. The amplification reaction contains the cDNA of interest, forward and reverse primers (5mM each) and the Mastermix FastStart SYBR Green (Roche). Amplification program used is the following: inicial

detaturation step: 95 °C for 10 minutes - Cycle repeated 50 times: Denaturation: 95 °C for 10 seconds, Annealing: 60 °C for 15 seconds, Elongation: 72 °C for 20 seconds. Experiment were performed with QuantStudio6Flex thermal cycler (Thermo).

The expression levels are always normalized to GAPDH, based on  $\frac{\text{eff}^{-\Delta C_t \text{gene}}}{\text{eff}^{-\Delta C_t \text{GAPDH}}}$  where eff is the primer amplification efficiency, calculated from three consecutive five fold dilutions of one control sample cDNA, centred on the dilution used for all other samples

Sequences of primers are the following:

<b>Gene</b>	<b>Forward primer</b>	<b>Reverse primer</b>
<i>GAPDH</i>	CTCCTGCACCACCAACTGCT	GGCCATCCACAGTCTTCTG
<i>ACSS2</i>	GTT GAC TCC CCT TCC TGG TG	CTT CCA ACT CTT CCC CGG AC
<i>CTGF</i>	AGG AGT GGG TGT GTG ACG A	CCAGGCAGTTGGCTCTAATC
<i>DHCR7</i>	CCG CCC AGC TCT ATA CCT TG	ACT TGT TCA CAA CCC CTG CA
<i>FASN</i>	GGA GGA GTG TAA ACA GCG CT	TTG GCA AAC ACA CCC TCC TT
<i>HMGCR</i>	TGC AGC AAA CAT TGT CAC CG	CAC CAC CCA CCG TTC CTA TC
<i>HMGCS1</i>	ACA CAA GAT GCT ACA CCG GG	ATG GGT GTC CTC TCT GAG CT
<i>LDLR</i>	AAG GAC ACA GCA CAC AAC CA	AAA GGA AGA CGA GGA GCA CG
<i>LPN1</i>	ACA TGG ATC CTG AAG TGG CG	GAG ATG GCG ATG GAA GGG AG
<i>SQLE</i>	AGG CGC AGA AAA GGA ACC AA	GCC AGC TCC CAC GAT GAT AA
<i>SCD</i>	CCA CTT GCT GCA GGA CGA TA	CCA AGT AGA GGG GCA TCG TC
<i>SREBF1</i>	CGT TTC TTC GTG GAT GGG GA	CCC GGA ATA GCT GAG TCA CC
<i>SREBF2</i>	GGG CTG GTT TGA CTG GAT GA	AGA TCT GCC TGT TTC CGG TG

<i>SCAP</i>	CAG CAG CAA CAC AGT GAC CT	TAT GGT CTT GGC TCC CTG TC
<i>COPI</i>	AGT ACA GCC TGA TGA CCC CA	TGC TGC CTC TTT CCT CTG TG
<i>AMPK<math>\alpha</math>1</i>	CTT GCC AAA GGA GTG ATT CAG ATG C	AGG TCA ACA GGA GAA GAG TCA AGT GT
<i>AMPK<math>\alpha</math>2</i>	AGC GTT CCT GTT CTG CTG CT	TCC ATG GTG TGA CTG CCC AG

## Western blot

Cells were washed with HBSS and harvested using a specific lysis buffer (50 mM Hepes pH 7,8, 200 mM NaCl, 5 mM EDTA, 1% NP40, 5% glycerol) through a cell scraper. For the optimization of cell membranes lysis, the extracts were exposed to ultrasound in a sonicator (Diagenode Bioruptor). The lysate were centrifuged for 10 minutes at 4 °C to remove the insoluble fraction. Then, the samples are boiled at 95 °C for 3 minutes in 1X FSB (50 mM Tris pH 6.8, 2% SDS, 0.1% Bromophenol Blue, 10% glycerol). Total protein concentration of the lysate was determined by Bradford measuring the absorbance of the solution at 595 nm. Proteins were stained with Coomassie Blue and a calibration line was prepared, using different BSA quantities. After the determination of the desired volume of cellular extracts, each sample was run in an NuPAGE Novex 10% or 4-12% Bis/Trylacrylamide gel (Invitrogen) with Tri-Glycine buffer (30 g Tris, 144 g Glycine, 5 g SDS/liter). Thus, the separated proteins were electrophoretically transferred on a PVDF membrane (Millipore) in a transfer solution (50 mM Tris, 40 mM glycine, 20% methanol, 0.04% SDS). After incubating for one hour at room temperature in a range of 0,1-0,5% milk powder in TBST (8 g NaCl, 2.4 g Tris, 0.1% Tween20/liter, pH 7.5), the membrane was incubated overnight at 4°C with the primary antibody diluted in a range of 0,1-0,5% milk powder (depending on antibody) in TBST. After three washes of 10 minutes with TBST at room temperature, the membrane was incubated 60 minutes with the secondary antibody conjugated to peroxidase, diluted in 0,1% (anti-mouse, diluted 1:5000) or 0,5% (anti-rabbit or anti-goat, both diluted 1:1000) milk in TBST. After three washes of 10 minutes with TBST at room temperature,

the bands were visualized by incubating the membrane of substrate containing luminol (Thermo Scientific) and chemiluminescence is digitally acquired by ImageQuant LAS 4000. Cells were incubated with 10  $\mu$ M MG132/MG115 proteasome inhibitors during treatment to prevent degradation of cleaved SREBPs.

## Cell fractionation and pulldown

Nuclear extracts and microsomes were obtained by resuspending cells in lysis buffer (250 mM sucrose, 10 mM triethanolamine pH 7.4, 10 mM acetic acid, 1 mM EDTA, 10 mM KCl) and passing cells eight times (that is, complete lysis at the microscope) through an Isobiotec Cell Homogenizer with a 6  $\mu$ m clearance sphere. Lysates were centrifuged at 800 r.c.f. to isolate nuclei, and then at 100,000 r.c.f. to isolate microsomes. Active GTP-bound ARF1 pulldown was performed with a commercial kit following the manufacturer's instructions (Cytoskeleton BK032).

Cytoskeleton's Arf1 Activation Assay Biochem Kit™ utilizes the Arf1 protein binding domain (PBD) of the effector protein GGA3 (Golgi-localized  $\gamma$ -ear containing, Arf-binding protein 3), which has been shown to specifically bind the GTP-bound form of Arf1. The purified GGA3-PBD (amino acids 1-316) expressed in *E. coli*, is covalently conjugated to the colored sepharose beads provided in the kit. Using these beads, is possible to “pull-down” Arf1-GTP and quantify the level of active Arf1 with a subsequent Western blotting step using the Arf1 specific antibody provided in the kit.

## Luciferase Assay

Luciferase assays were performed in MDA-MB-231 cells. Cells, were typically plated in 24-well format and luciferase reporter plasmids were transfected with CMV-lacZ to normalize for transfection efficiency based on CPRG (Merck) colorimetric assay, together with plasmids encoding for the indicated proteins; DNA content was kept uniform by using pKS Bluescript. Cells were harvested in Luc lysis buffer (25mM Tris pH 7.8, 2.5mM EDTA, 10% glycerol, 1% NP40). Luciferase activity was determined in a Tecan plate luminometer with freshly reconstituted assay reagent (0.5mM DLuciferin, 20mM Tricine, 1mM

(MgCO<sub>3</sub>)<sub>4</sub>Mg(OH)<sub>2</sub>, 2.7mM MgSO<sub>4</sub>, 0.1mM EDTA, 33mM DTT, 0.27mM CoA, 0.53mM ATP). Each sample was transfected at least in two biological duplicates in each experiment to determine the experimental variability; each experiment was repeated independently with consistent results.

## Antibody and Microscopy

For the SREBP2 antibodies, independent lots were used with consistent results. Immunofluorescence was performed as follow: 10 min 1.5 mg ml<sup>-1</sup> glycine in PBS before permeabilization to reduce background, and blocking in 1–2% BSA. Primary antibodies were incubated overnight in PBS+0,1% Triton and 2% BSA or Goat Serum. Secondary antibodies were suscitated in Goat and conjugated with different fluorocromes (Alexa488, Alexa568 and Alexa647, Invitrogen).

Cells for immunofluorescence in a stiff microenvironment were plated on fibronectin-coated glass coverslips. Stiff ( $E \approx 15$  kPa) and soft ( $E \approx 0.5$  kPa) fibronectin-coated polyacrylamide hydrogels were assembled in-house by standard protocols. Annular-shaped micropatterns (25 or 35  $\mu$ m diameter, 5  $\mu$ m line thickness) were printed on PEG-coated glass coverslips by deep ultraviolet photolithography and coated with 50  $\mu$ g ml<sup>-1</sup> fibronectin supplemented with 20  $\mu$ g ml<sup>-1</sup> Alexa647-fibrinogen (Sigma).

Images were acquired sequentially with a Zeiss LSN700 or a Leica SP5 confocal microscope equipped with a charge-coupled device camera using ZEN 2 or Leica LAS AF software. Typical acquisition settings for IF were as follows: image size 1,024  $\times$  1,024 pixels; acquisition mode *xyz*; pixel size 0.15  $\mu$ m; image depth 8 bits; acquisition speed 5/10, with average 2; Plan-Apochromat  $\times$ 63/1.40 oil DIC M27 objective. For multichannel acquisitions, we used a main beamsplitter 405/488/555/639. Raw images (saved in .czi or .lif formats) were opened in ImageJ and saved in exportable formats. If needed, colours were changed (for example, red to green) with Photoshop CC.

Antibodies catalogue numbers, dilutions and validations are the following:

<b>Epitope</b>	<b>Antibody Catalog/Brand</b>	<b>Dilution</b>	<b>Antibody validation</b>
SREBP2	BD 557037	IF 1:100 WB 1:500	Staining is diffuse cytoplasmic in full serum and shifts to the nucleus upon serum/lipid deprivation. WB on siRNA-transfected cells.
SREBP2	Cayman 10007663	IF 1:100 WB 1:500	Staining colocalizes with ER membranes (KDEL-mCherry) in full serum and shifts to the nucleus (with unstained nucleoli) upon serum/lipid deprivation. WB on siRNA-transfected cells.
SREBP1	SCBT sc13551X	WB 1:1000	WB on SREBP1 siRNA-transfected cells
Insig1	Proteintech 22115-1-AP	IF 1:200 WB 1:1000	Staining colocalizes with ER membranes and recognizes a band of the expected molecular weight in WB.
GM130	BD 610822	IF 1:100 WB 1:500	Vesicular cytoplasmic staining colocalizes with other Golgi markers but not with ER.
Calreticulin	n.a. (E. Greotti)	IF 1:200 WB 1:1000	Vesicular cytoplasmic staining colocalizes with transfected KDEL-mCherry but not with Golgi.
Giantin	n.a. (E. Greotti)	IF 1:100	Vesicular cytoplasmic staining colocalizes with other Golgi markers but not with ER.
Golgin97	n.a. (E. Greotti)	IF 1:100	Vesicular cytoplasmic staining colocalizes with other Golgi markers but not with ER.

ARF1	Pierce MA3-060	IF 1:20	Colocalization with Golgi markers is lost upon propranolol treatment. Staining increased in cells transfected with GFP-ARF1.
LAMP2	Abcam ab25631	IF 1:200	Staining encircles cytoplasmic Filipin-positive dots in cells treated with the U18666A NPC1 inhibitor.
GAPDH	Millipore MAB374	IF 1:25.000	Recognizes a unique band of the expected molecular weight in WB.
FLAG	Sigma M2	IF 1:200 WB 1:500	WB and IF on cells with/without transfected FLAG-tagged protein.
MYC	SCBT sc789	IF 1:200	WB and IF on cells with/without transfected MYC-tagged protein.
HA	SCBT sc805	IF 1:200	WB and IF on cells with/without transfected HA-tagged protein.
Puromycin	Millipore MABE343	WB 1:1000	WB on cells with/without puromycin treatment.
Phalloidin-FITC	Thermo	IF 1:100	Detects filamentous cytoplasmic structures that are lost upon treatment of cells with F-actin inhibitory drugs.
TOTO-3	Thermo	IF 1:2000	Nuclear counterstain
Propidium Iodide	Sigma P4178	IF 1:500	Nuclear counterstain
DAPI	Thermo	IF 1:2000	Nuclear counterstain

## Oil red O and Filipin Staining

Oil Red-O staining is used to detect neutral lipids, based on a lysochrome, fat soluble dye, which has greater solubility in neutral fats, than in the solvent in which it is dissolved. Usually, the ORO solution is dissolved in ethanol or alcoholic solvents, such that in fat containing

tissues or cells, the fat soluble dye, moves from the staining solution towards the fats present. Filipin staining instead, is based on filipin, which is a naturally fluorescence cholesterol binding molecule. It comes from a mixture of chemical compound isolated from actinomicetes bacteria discovered in a soil sample collected in Philippines islands.

Oil Red-O staining (Sigma) was carried out after fixation, in 60% vol/vol isopropanol/water. Filipin staining was acquired using an ultraviolet filter set (340/380 nm excitation, 40 nm dichroic, 430 nm long pass filter) by prefocusing cells based on TOTO3 nuclear counterstain (633/647 nm) and then acquiring the ultravioletUV channel without prior observation to avoid photobleaching. Typical acquisition settings for Filipin were as follows: image size 1,024 × 1,024 pixels; acquisition mode *xyz*; pixel size 0.15 μm; image depth 8 bits; acquisition speed 5/10, with average 2; Plan-Apochromat ×63/1.40 oil DIC M27 objective. Pictures were always taken using the same acquisition conditions for all different experimental samples; panels are representative pictures based on at least two independent experiments.

## Alkaline Phosphatase Staining

Alkaline phosphatase (AP) is a universal pluripotent marker for all types of pluripotent stem cells including embryonic stem cells, embryonic germ cells, and induced pluripotent stem cells. Alkaline phosphatase staining was carried out with a Leukocyte AP kit (Sigma). Cells on 24 well plate were treated with different agents and time. Then, they were washed from the medium and fixed 2 minutes with a fix solution supplied by the kit, with addition of formaldehyde and acetone. After a quick wash in water, the AP staining was applied at cells for 2 minutes in the dark. At last, after another wash with water, plates with cells were leaved to dry out.

Panels shown are representative pictures of one biological replicate of one experiment; each experiment was repeated three times independently.

## EdU Incorporation Assay

Cell proliferation ability was determined by directly measuring DNA synthesis using Click-iT EdU Imaging Kits (Invitrogen). EdU (5-ethynyl-2'-deoxyuridine) provided in the kit is a nucleoside analogue of thymidine and it is incorporated into DNA during active DNA synthesis. The EdU detection is based on the click reaction of a copper-catalyzed covalent reaction between an alkyne molecule of EdU and an azide group of the Alexa Fluor dye. The small size of the dye allows the efficient detection of the incorporated EdU without the need of DNA denaturation (usually required with BrdU).

At the proper time, cells, previously plated in 24-wells containing fibronectin-coated 13mm glass slides, were incubated with EdU (for analysis of the S-phase) for 1h and then fixed for 15min at room temperature with 3,7% formaldehyde diluted in PBS. The fixative is then removed and cells were washed with 3% BSA, diluted in PBS. Permeabilization step was pursued by adding 0.5% Triton X-100 in PBS to each well and by letting it incubate for 20 minutes at room temperature. Cells were then either left in PBS at 4°C (for few days only) or analyzed according to manufacturer's instructions (Invitrogen). Click-iT reaction cocktail for EdU detection contains: Click-iT reaction buffer, CuSO<sub>4</sub>, Alexa Fluor azide, EdU buffer additive and water up to the desired volume. The reaction is incubated for 30 minutes at room temperature, protected from light and paying attention that the solution is homogeneously distributed over the cells. Click-iT reaction cocktail was then removed and cells were washed with PBS. The DNA staining was performed by incubation of DAPI (protected from light) and cells were analyzed with a fluorescent microscope.

## Hydrogel Preparation

Cover slips of the desired diameter are washed in ethanol and then water. When they dried out, 3-aminopropyl-trimethoxysilane (APTMS) is applied for 3 minutes on glasses to functionalize the plastic surface. After 4-5 water washes, 2.5% glutaraldehyde is utilized to fix the APTMS for 30 mins, and this is instrumental for the chemical crosslinking of the PAA gel. After the removal of the glutaraldehyde, cover slips are deeply washed for 3-4 times with water.

Gel preparation step: 500  $\mu$ l of 40% acrylamide + 65  $\mu$ l of 100% hydroxyl-acrylamide. Vortex the solution and remove 65  $\mu$ l to obtain 500  $\mu$ l of total solution. After that, 280  $\mu$ l of 2% acrylamide is added. Different quantity of this premix can be diluted in PBS1X in order to obtain different stiffness of the gel. In 500  $\mu$ l of total solution we usually mix 58  $\mu$ l of gel premix with 442  $\mu$ l of PBS1X in order to have 0,5 KPa soft hydrogels. For 10 KPa stiff hydrogels instead, we mix the solutions respectively in 1:2 ratio. To induce gel polymerization, ammonium persulfate (APS) and Tetramethylethylenediamine (TEMED) are added to the mix, respectively 5  $\mu$ l and 1,5  $\mu$ l. Mix the solution gently and quickly. The gel solution is then pipette in small drops on top of coverslips and gently lower top coverslips onto gel drops. Top coverslips were pretreated with RainX solution which makes them antiadhesive. After short time, when gel is polymerized, they are moved into a well plate filled with PBS1X and leaved to gently shake. Lastly, top coverslips are removed and hydrogels are washed several times with PBS1X and sterilized with UV light.

## Metabolomics and metabolic analyses

Large-scale metabolic analysis (global metabolomics) and principal component analysis of the results were carried out by Metabolon. Mechanosensitive MCF10Tk1 cells<sup>56</sup> were washed once in warm 1 $\times$  PBS, and metabolites were extracted for 5 min at room temperature on 15 cm plates with 80% vol/vol methanol/water extraction buffer with internal standards. We harvested cells on plate to specifically avoid alteration of actin tension and metabolism due to cell detachment. Metabolites were normalized to protein content. This analysis did not focus on triglyceride content. Clustering of selected lipid metabolites (fold change > 2.5,  $P < 0.05$ ) shown in Supplementary Fig. [1e](#) was carried out with Heatmapper.

Targeted lipidomic analysis was carried out on MCF10Tk1 cells lysed in 1:1 vol/vol MeOH/acetonitrile extraction buffer by tissue lyser and spun at 20,000g for 5 min at 4  $^{\circ}$ C. Supernatants were then passed through a regenerated cellulose filter, dried, and resuspended in 100  $\mu$ l MeOH.

For quantification of the different phospholipid species, liquid chromatography tandem mass spectrometry LC-MS/MS analysis was performed on an API-4000 triple quadrupole mass spectrometer (AB Sciex) coupled with an HPLC system (Agilent) and CTC PAL HTS autosampler (PAL System). The identity of the different phospholipid families was confirmed using pure standards, namely one for each family. Methanolic extracts were analysed with a 5 min run in both positive and negative ion mode with 275 multiple reaction monitoring (MRM) transitions in positive mode and 92 MRM transitions in negative mode. Quantification of different phospholipids in positive ion mode was performed using a Synergi 4 $\mu$  Hydro-RP (50 mm  $\times$  2.0 mm, 4  $\mu$ m; Phenomenex) and in negative ion mode using a Cyano-phase LUNA column (50 mm  $\times$  4.6 mm, 5  $\mu$ m; Phenomenex). The mobile phase for positive ion mode was 0.1% formic acid in MeOH and 5 mM ammonium acetate pH 7 in MeOH for negative ion mode, both with a flow rate of 500  $\mu$ l min<sup>-1</sup>. MultiQuant software version 3.0.2 was used for data analysis and peak review of chromatograms. Semi-quantitative evaluation of different phospholipids was performed based on external standards, then the data were normalized on protein content assessed by the BCA (bicinchoninic acid assay) method.

For quantification of the different diacylglycerol and triacylglycerol species the LC-MS/MS analysis was performed on an API-4000 triple quadrupole mass spectrometer (AB Sciex) coupled with an HPLC system (Agilent) and a CTC PAL HTS autosampler (PAL System). Methanolic extracts were dried under nitrogen and resuspended in 100  $\mu$ l of 65% acetonitrile/30% isopropanol/5% water. Samples were then analysed with a 10 min run in positive ion mode with 92 MRM transitions. Quantification of different diacylglycerols and triacylglycerols was performed using an XBridge C-18 column (100 mm  $\times$  2.1 mm, 3.5  $\mu$ m; Waters). Column temperature was set at 55  $^{\circ}$ C. The mobile phases were as follows—phase A: 40% acetonitrile, 0.1% formic acid and 10 mM ammonium acetate in water; phase B: isopropanol 90%, acetonitrile 10%, 0.1% formic acid and 10 mM ammonium acetate;  $T_0$ : 55% A;  $T_{2\text{min}}$ : 55% A;  $T_{4\text{min}}$ : 3% A;  $T_{7\text{min}}$ : 3% A;  $T_{7.1\text{min}}$ : 55% A;  $T_{10\text{min}}$ : 55% A; with a flow rate of 260  $\mu$ l min<sup>-1</sup>. MultiQuant software version 3.0.2 was used for data analysis and peak review of chromatograms. Semi-quantitative evaluation of different diacylglycerols and

triacylglycerols was performed based on external standards, then data were normalized on protein content assessed by the BCA method.

For the quantification of free and total fatty acids and cholesterol levels, we used an aliquot of extracts as described above and commercial kits (Sigma MAK044 and MAK043), following the manufacturer's instructions.

## Microarray

Microarray probe synthesis, hybridization and detection were performed at CMB Trieste on HumanHT-12 v4 Expression BeadChips with an Illumina Hiscan system. Data analyses were performed in R (version 3.0.2) using Bioconductor libraries (BioC 2.13) and R statistical packages. Probe level signals were converted to expression values using the Robust Multi-array Average procedure RMA of the Bioconductor Affymetrix package. Differentially expressed genes were identified using the Significance Analysis of Microarray (SAM) algorithm coded in the same R package. In SAM, we estimated the percentage of false-positive predictions (that is, false discovery rate, FDR) with 100 permutations. Genes activated or inhibited upon YM treatment and used for gene list enrichment analysis were filtered based on  $P < 0.05$  and fold change  $> 1.3$ . Gene list enrichment analysis was performed with Enrichr. SREBP target genes were defined based on literature.

## Intracellular optical micromanipulation, microrheological measurements and analysis

The set-up combining optical trapping and confocal imaging has been described previously. Briefly, red fluorescent 580/605 nm 2- $\mu$ m-diameter latex beads (Thermo F88265) were endocytosed overnight in RPE1 cells stably expressing the Golgi marker GFP-Rab6. The incubation time and bead concentration were adjusted so that cells typically contained one or two beads before optical micromanipulation. Cells were plated on 18-mm-diameter coverslips uniformly coated with fibronectin, or with annular-shaped adhesive fluorescent micropatterns of different diameters (25 or 35  $\mu$ m), for 6 h. Non-adherent cells were washed

off by rinsing with culture medium. The coverslip was then mounted in a Ludin chamber and the culture medium was supplemented with 20 mM HEPES before the experiment.

Force was applied on GFP-positive Golgi membranes by first trapping a bead located close to the Golgi apparatus and then displacing the microscope stage to push the organelle against the trapped bead. Trapping was not possible on polyacrylamide hydrogels because of the excessive distance between the lens and cells in this set-up. The applied force  $F$  was deduced from the bead displacement relative to the trap centre,  $\Delta x$ , after calibration of the trap stiffness  $k_{\text{trap}}$  using  $F = k_{\text{trap}}\Delta x$  with  $k_{\text{trap}} = 280 \text{ pN } \mu\text{m}^{-1}$ . The output power of the infra-red laser at the objective aperture was 150 mW. Stage displacement was performed using a nanopositioning piezo-stage (Nanobio 200, Mad City Labs) controlled by NanoRoute3D software (Mad City Labs). The stage displacement consisted of five consecutive  $0.5 \mu\text{m}$  steps with a 10 s pause between each step to allow visco-elastic relaxation of the bead position towards the trap centre. The total duration of optical trapping was limited to 1 min for a given cell to ensure cell viability.

To characterize the rigidity of the microenvironment surrounding the bead, we used a phenomenological analysis of the relaxation curves to measure three parameters: the frequency of bead ejection, the bead step amplitude and the rigidity index. Qualitatively, in a low rigidity microenvironment, friction on the bead is low and the bead does not move much from the trap centre during the step displacement and relaxes rapidly towards the trap centre. In a rigid microenvironment, the bead experiences a high friction and its initial displacement is larger and closer to the step displacement ( $0.5 \mu\text{m}$ ) and the relaxation is slower. If the force acting on the bead is too large (typically above 300–400 pN), the bead falls off the trap and subsequently follows the displacement of the stage. We termed such events ‘ejections’ and scored their frequency (defined as the ratio between the number of experiments in which ejection occurred and the total number of experiments) and the step at which ejection occurred. The bead step amplitude  $X_b$  corresponds to the displacement of the bead after a  $0.5 \mu\text{m}$  step of the piezo stage. Values of  $X_b$  close to  $0.5 \mu\text{m}$  indicate a high rigidity of the bead microenvironment. Lower values indicate softer microenvironments. The rigidity index (RI) is defined as

$$RI = \frac{\int_{t_i}^{t_i+T} \dot{x}_b(t) dt}{\int_{t_i}^{t_i+T} \dot{x}_s(t) dt} = \frac{\int_{t_i}^{t_i+T} \dot{x}_b(t) dt}{X_s T} \quad RI = \frac{\int_{t_i}^{t_i+T} \dot{x}_b(t) dt}{\int_{t_i}^{t_i+T} \dot{x}_s(t) dt} = \frac{\int_{t_i}^{t_i+T} \dot{x}_b(t) dt}{X_s T}$$

where  $t_i$  is the time when the  $i$ th  $0.5 \mu\text{m}$  step displacement of the piezo stage occurs,  $x_b$  and  $x_s$  are, respectively, the displacement of the bead relative to the trap centre and the displacement of the piezo stage,  $X_s = 0.5 \mu\text{m}$  is the amplitude of the piezo-stage step and  $T = 10 \text{ s}$  is the duration of the step. The rigidity index is a phenomenological parameter that allows us to compare the rigidity of the microenvironment surrounding the bead in various conditions. The value of rigidity index falls between 0 (the microenvironment does not exert any friction on the bead) and 1 (the microenvironment is not deformable). The values of the rigidity index for each step displacement were averaged.

To measure GFP-PKD-KD recruitment on force application, cells were plated at day 1 in a 12-well plate to reach around 75% confluence on day 2. At day 2, cells were transfected with GFP-PKD-KD and mCherry-Golgi (B4GALT1) plasmids. At the end of day 2, the cells were incubated with  $2\text{-}\mu\text{m}$ -diameter fluorescent beads overnight. At day 3, cells were transferred to fibronectin-coated coverslips for the experiment. The evolution of normalized intensity of GFP-PKD-KD in the region of the Golgi apparatus, visualized by the mCherry-Golgi marker, was monitored after application of a mechanical constraint exerted by internalized beads trapped with optical tweezers. A bead located near the Golgi apparatus was selected in a cell expressing GFP-PKD-KD and the mCherry-Golgi marker. A first image was taken at  $t = 0 \text{ min}$ . The bead was then trapped with the optical tweezers and the microscope stage manually displaced to bring the Golgi apparatus in contact with the bead and apply a compressive constraint on the Golgi apparatus during 1 min. The same protocol was repeated every 5 min until  $t = 30 \text{ min}$ . The duration of the compressive constraint was reduced to 30 s after  $t = 10 \text{ min}$  to avoid cellular damage due to prolonged laser exposure. As a control, the same protocol was used but the microscope stage was displaced to move the bead away from the Golgi apparatus.

To quantify the fluorescence intensity of GFP-PKD-KD in each of the seven images taken every 5 min, the Golgi apparatus was delimited using the mCherry Golgi marker. The total

intensities of the mCherry Golgi marker ( $I_r$ ) and GFP-PKD-Kd ( $I_g$ ) were measured as well as the mean intensity of the background for each channel ( $\langle I_{rback} \rangle$  for the mCherry Golgi marker;  $\langle I_{gback} \rangle$  for GFP-PKD-KD) and the area of the Golgi apparatus,  $A_{Golgi}$ . The total intensity of the background in the Golgi apparatus region for each channel was then estimated by multiplying the mean background intensity by the Golgi area:

$$I_{rback} = A_{Golgi} \langle I_{rback} \rangle$$

$$I_{gback} = A_{Golgi} \langle I_{gback} \rangle$$

The fluorescence intensity of GFP-PKD-KD was normalized by the fluorescence intensity of the mCherry Golgi marker:

$$I = \frac{I_g - I_{gback}}{I_r - I_{rback}}$$

to account for slight changes in the imaging plane from one image to the next. The relative temporal variations of the GFP-PKD-KD fluorescence were obtained by normalizing the intensity  $I$  measured from each image taken every 5 min by its initial value  $I_0$ :  $I(t) = I/I_0$ .

## REFERENCES

1. Antoni, M. H. *et al.* The influence of bio-behavioural factors on tumour biology: pathways and mechanisms. *Nat. Rev. Cancer* **6**, 240–248 (2006).
2. Shirakawa, J. *et al.* Insulin Signaling Regulates the FoxM1/PLK1/CENP-A Pathway to Promote Adaptive Pancreatic  $\beta$  Cell Proliferation. *Cell Metab.* **25**, 868-882.e5 (2017).
3. Mammoto, T. & Ingber, D. E. Mechanical control of tissue and organ development. *Development* **137**, 1407–1420 (2010).
4. Chen, C. S. Mechanotransduction - a field pulling together? *J. Cell Sci.* **121**, 3285–3292 (2008).
5. Handorf, A. M., Zhou, Y., Halanski, M. A. & Li, W.-J. Tissue Stiffness Dictates Development, Homeostasis, and Disease Progression. *Organogenesis* **11**, 1–15 (2015).
6. Engler, A. J., Sen, S., Sweeney, H. L. & Discher, D. E. Matrix Elasticity Directs Stem Cell Lineage Specification. *Cell* **126**, 677–689 (2006).
7. Janmey, P. A. & Miller, R. T. Mechanisms of mechanical signaling in development and disease. *J. Cell Sci.* **124**, 9–18 (2011).
8. McBeath, R., Pirone, D. M., Nelson, C. M., Bhadriraju, K. & Chen, C. S. Cell Shape, Cytoskeletal Tension, and RhoA Regulate Stem Cell Lineage Commitment. *Dev. Cell* **6**, 483–495 (2004).
9. Vining, K. H. & Mooney, D. J. Mechanical forces direct stem cell behaviour in development and regeneration. *Nat. Rev. Mol. Cell Biol.* **18**, 728–742 (2017).
10. Dupont, S. *et al.* Role of YAP/TAZ in mechanotransduction. *Nature* **474**, 179 (2011).
11. Mitchell, M. J. *et al.* Polymeric mechanical amplifiers of immune cytokine-mediated apoptosis. *Nat. Commun.* **8**, 14179 (2017).
12. Paluch, E. K. *et al.* Mechanotransduction: Use the force(s). *BMC Biol.* **13**, 1–14 (2015).

13. Yano, H., Choudhury, M. E., Islam, A., Kobayashi, K. & Tanaka, J. Cellular mechanotransduction of physical force and organ response to exercise-induced mechanical stimuli. *J. Phys. Fit. Sport. Med.* **4**, 83–91 (2015).
14. Alonso Wolfgang H., J. L. Cellular mechanotransduction. *AIMS Biophys.* **3**, 50–62
15. Isermann, P. & Lammerding, J. Nuclear mechanics and mechanotransduction in health and disease. *Curr. Biol.* **23**, R1113–R1121 (2013).
16. Martino, F., Perestrelo, A. R., Vinarský, V., Pagliari, S. & Forte, G. Cellular mechanotransduction: From tension to function. *Front. Physiol.* **9**, 1–21 (2018).
17. Spinale, F. G. Myocardial Matrix Remodeling and the Matrix Metalloproteinases: Influence on Cardiac Form and Function. *Physiol. Rev.* **87**, 1285–1342 (2007).
18. Dupont, S. Regulation of YAP/TAZ Activity by Mechanical Cues: An Experimental Overview. in *The Hippo Pathway: Methods and Protocols* (ed. Hergovich, A.) 183–202 (Springer New York, 2019). doi:10.1007/978-1-4939-8910-2\_15
19. Fukata, Y., Kaibuchi, K., Amano, M. & Kaibuchi, K. Rho–Rho-kinase pathway in smooth muscle contraction and cytoskeletal reorganization of non-muscle cells. *Trends Pharmacol. Sci.* **22**, 32–39 (2001).
20. Sit, S.-T. & Manser, E. Rho GTPases and their role in organizing the actin cytoskeleton. *J. Cell Sci.* **124**, 679 LP – 683 (2011).
21. Hoon, J., Tan, M. & Koh, C.-G. The Regulation of Cellular Responses to Mechanical Cues by Rho GTPases. *Cells* **5**, 17 (2016).
22. Folkman, J. & Moscona, A. Role of cell shape in growth control. *Nature* **273**, 345–349 (1978).
23. Watt, F. M., Jordan, P. W. & Neill, C. H. Cell shape controls terminal differentiation of human epidermal keratinocytes. *Proc. Natl. Acad. Sci.* **85**, 5576 LP – 5580 (1988).
24. Mooney, D. *et al.* Switching from differentiation to growth in hepatocytes: Control by

- extracellular matrix. *J. Cell. Physiol.* **151**, 497–505 (1992).
25. Chen, C. S., Mrksich, M., Huang, S., Whitesides, G. M. & Ingber, D. E. Geometric Control of Cell Life and Death. *Science* (80-. ). **276**, 1425 LP – 1428 (1997).
  26. Brock, I. C. *et al.* Luminosity measurement in the L3 detector at LEP. *Nucl. Instruments Methods Phys. Res. Sect. A Accel. Spectrometers, Detect. Assoc. Equip.* **381**, 236–266 (1996).
  27. Galbraith, C. G. & Sheetz, M. P. Forces on adhesive contacts affect cell function. *Curr. Opin. Cell Biol.* **10**, 566–571 (1998).
  28. Lewis, J. M., Cheresch, D. A. & Schwartz, M. A. Protein kinase C regulates alpha v beta 5-dependent cytoskeletal associations and focal adhesion kinase phosphorylation. *J. Cell Biol.* **134**, 1323 LP – 1332 (1996).
  29. Esnault, C. *et al.* Rho-actin signaling to the MRTF coactivators dominates the immediate transcriptional response to serum in fibroblasts. *Genes Dev.* **28**, 943–958 (2014).
  30. Miralles, F., Posern, G., Zaromytidou, A.-I. & Treisman, R. Actin Dynamics Control SRF Activity by Regulation of Its Coactivator MAL. *Cell* **113**, 329–342 (2003).
  31. Piccolo, S., Dupont, S. & Cordenonsi, M. The Biology of YAP/TAZ: Hippo Signaling and Beyond. *Physiol. Rev.* **94**, 1287–1312 (2014).
  32. Zhao, B., Li, L., Lei, Q. & Guan, K.-L. The Hippo-YAP pathway in organ size control and tumorigenesis: an updated version. *Genes Dev.* **24**, 862–874 (2010).
  33. Santinon, G. *et al.* dNTP metabolism links mechanical cues and YAP/TAZ to cell growth and oncogene-induced senescence. *EMBO J.* **37**, e97780 (2018).
  34. Panciera, T., Azzolin, L., Cordenonsi, M. & Piccolo, S. Mechanobiology of YAP and TAZ in physiology and disease. *Nat. Rev. Mol. Cell Biol.* **18**, 758 (2017).
  35. Maxfield, F. R. & van Meer, G. Cholesterol, the central lipid of mammalian cells. *Curr. Opin. Cell Biol.* **22**, 422–429 (2010).
  36. Lande, M. B., Donovan, J. M. & Zeidel, M. L. The relationship between membrane fluidity

- and permeabilities to water, solutes, ammonia, and protons. *J. Gen. Physiol.* **106**, 67–84 (1995).
37. Jedlovszky, P. & Mezei, M. Effect of Cholesterol on the Properties of Phospholipid Membranes. 2. Free Energy Profile of Small Molecules. *J. Phys. Chem. B* **107**, 5322–5332 (2003).
  38. Incardona, J. P. & Eaton, S. Cholesterol in signal transduction. *Curr. Opin. Cell Biol.* **12**, 193–203 (2000).
  39. Goluszko, P. & Nowicki, B. Membrane cholesterol: a crucial molecule affecting interactions of microbial pathogens with mammalian cells. *Infect. Immun.* **73**, 7791–7796 (2005).
  40. Orth, M. & Bellosta, S. Cholesterol: its regulation and role in central nervous system disorders. *Cholesterol* **2012**, 292598 (2012).
  41. Walker, A. K. *et al.* A conserved SREBP-1/phosphatidylcholine feedback circuit regulates lipogenesis in metazoans. *Cell* **147**, 840–852 (2011).
  42. Brown, M. S. & Goldstein, J. L. The SREBP Pathway: Regulation of Cholesterol Metabolism by Proteolysis of a Membrane-Bound Transcription Factor. *Cell* **89**, 331–340 (1997).
  43. Schoenheimer, R. & Breusch, F. SYNTHESIS AND DESTRUCTION OF CHOLESTEROL IN THE ORGANISM. *J. Biol. Chem.* **103**, 439–448 (1933).
  44. Edwards, P. A., Muroya, H. & Gould, R. G. In vivo demonstration of the circadian rhythm of cholesterol biosynthesis in the liver and intestine of the rat. *J. Lipid Res.* **13**, 396–401 (1972).
  45. Horton, J. D., Goldstein, J. L. & Brown, M. S. SREBPs: activators of the complete program of cholesterol and fatty acid synthesis in the liver. *J. Clin. Invest.* **109**, 1125–1131 (2002).
  46. Brown, M. S., Radhakrishnan, A. & Goldstein, J. L. Retrospective on Cholesterol Homeostasis: The Central Role of Scap. *Annu. Rev. Biochem.* **87**, 783–807 (2018).
  47. Brown, A. J., Sun, L., Feramisco, J. D., Brown, M. S. & Goldstein, J. L. Cholesterol Addition to ER Membranes Alters Conformation of SCAP, the SREBP Escort Protein that Regulates

Cholesterol Metabolism. *Mol. Cell* **10**, 237–245 (2002).

48. Lee, J.-H. *et al.* SREBP-1a-stimulated lipid synthesis is required for macrophage phagocytosis downstream of TLR4-directed mTORC1. *Proc. Natl. Acad. Sci. U. S. A.* **115**, E12228–E12234 (2018).
49. Nohturfft, A., DeBose-Boyd, R. A., Scheek, S., Goldstein, J. L. & Brown, M. S. Sterols regulate cycling of SREBP cleavage-activating protein (SCAP) between endoplasmic reticulum and Golgi. *Proc. Natl. Acad. Sci.* **96**, 11235 LP – 11240 (1999).
50. Cheng, C. *et al.* Glucose-Mediated N-glycosylation of SCAP Is Essential for SREBP-1 Activation and Tumor Growth. *Cancer Cell* **28**, 569–581 (2015).
51. Wang, Y.-N. *et al.* COPI-mediated retrograde trafficking from the Golgi to the ER regulates EGFR nuclear transport. *Biochem. Biophys. Res. Commun.* **399**, 498–504 (2010).
52. Repa, J. J. *et al.* Regulation of mouse sterol regulatory element-binding protein-1c gene (SREBP-1c) by oxysterol receptors, LXRA and LXRβ. *Genes Dev.* **14**, 2819–2830 (2000).
53. Caron, A., Richard, D. & Laplante, M. The Roles of mTOR Complexes in Lipid Metabolism. *Annu. Rev. Nutr.* **35**, 321–348 (2015).
54. Porstmann, T. *et al.* SREBP activity is regulated by mTORC1 and contributes to Akt-dependent cell growth. *Cell Metab.* **8**, 224–236 (2008).
55. Düvel, K. *et al.* Activation of a Metabolic Gene Regulatory Network Downstream of mTOR Complex 1. *Mol. Cell* **39**, 171–183 (2010).
56. Peng, T., Golub, T. R. & Sabatini, D. M. The immunosuppressant rapamycin mimics a starvation-like signal distinct from amino acid and glucose deprivation. *Mol. Cell. Biol.* **22**, 5575–5584 (2002).
57. Yecies, J. L. *et al.* Akt stimulates hepatic SREBP1c and lipogenesis through parallel mTORC1-dependent and independent pathways. *Cell Metab.* **14**, 21–32 (2011).
58. Lee, G. *et al.* Post-transcriptional Regulation of *De Novo* Lipogenesis by

- mTORC1-S6K1-SRPK2 Signaling. *Cell* **171**, 1545-1558.e18 (2017).
59. Wan, W. *et al.* mTORC1 Phosphorylates Acetyltransferase p300 to Regulate Autophagy and Lipogenesis. *Mol. Cell* **68**, 323-335.e6 (2017).
  60. Eid, W. *et al.* mTORC1 activates SREBP-2 by suppressing cholesterol trafficking to lysosomes in mammalian cells. *Proc. Natl. Acad. Sci.* **114**, 7999 LP – 8004 (2017).
  61. Peterson, T. R. *et al.* mTOR complex 1 regulates lipin 1 localization to control the SREBP pathway. *Cell* **146**, 408–420 (2011).
  62. Kim, H. E. *et al.* Lipin1 regulates PPAR $\gamma$  transcriptional activity. *Biochem. J.* **453**, 49 LP – 60 (2013).
  63. Dwyer, J. R. *et al.* Mouse lipin-1 and lipin-2 cooperate to maintain glycerolipid homeostasis in liver and aging cerebellum. *Proc. Natl. Acad. Sci.* **109**, E2486 LP-E2495 (2012).
  64. Csaki, L. S. *et al.* Lipin-1 and lipin-3 together determine adiposity in vivo. *Mol. Metab.* **3**, 145–154 (2014).
  65. Mitra, M. S. *et al.* Mice with an adipocyte-specific lipin 1 separation-of-function allele reveal unexpected roles for phosphatidic acid in metabolic regulation. *Proc. Natl. Acad. Sci. U. S. A.* **110**, 642–647 (2013).
  66. Reue, K. & Dwyer, J. R. Lipin proteins and metabolic homeostasis. *J. Lipid Res.* **50 Suppl**, S109–S114 (2009).
  67. Donkor, J., Sariahmetoglu, M., Dewald, J., Brindley, D. N. & Reue, K. Three Mammalian Lipins Act as Phosphatidate Phosphatases with Distinct Tissue Expression Patterns. *J. Biol. Chem.* **282**, 3450–3457 (2007).
  68. Harris, E. N., Kyosseva, S. V., Weigel, J. A. & Weigel, P. H. Expression, Processing, and Glycosaminoglycan Binding Activity of the Recombinant Human 315-kDa Hyaluronic Acid Receptor for Endocytosis (HARE). *J. Biol. Chem.* **282**, 2785–2797 (2007).
  69. Smulan, L. J. *et al.* Cholesterol-Independent SREBP-1 Maturation Is Linked to ARF1 Inactivation. *Cell Rep.* **16**, 9–18 (2016).

70. Zhang, P. & Reue, K. Lipin proteins and glycerolipid metabolism: Roles at the ER membrane and beyond. *Biochim. Biophys. Acta. Biomembr.* **1859**, 1583–1595 (2017).
71. Fung, C., Lock, R., Gao, S., Salas, E. & Debnath, J. Induction of autophagy during extracellular matrix detachment promotes cell survival. *Mol. Biol. Cell* **19**, 797–806 (2008).
72. Avivar-Valderas, A. *et al.* PERK integrates autophagy and oxidative stress responses to promote survival during extracellular matrix detachment. *Mol. Cell. Biol.* **31**, 3616–3629 (2011).
73. Chen, N., Eritja, N., Lock, R. & Debnath, J. Autophagy restricts proliferation driven by oncogenic phosphatidylinositol 3-kinase in three-dimensional culture. *Oncogene* **32**, 2543–2554 (2013).
74. Pavel, M. *et al.* Contact inhibition controls cell survival and proliferation via YAP/TAZ-autophagy axis. *Nat. Commun.* **9**, 2961 (2018).
75. Grassian, A. R., Metallo, C. M., Coloff, J. L., Stephanopoulos, G. & Brugge, J. S. Erk regulation of pyruvate dehydrogenase flux through PDK4 modulates cell proliferation. *Genes Dev.* **25**, 1716–1733 (2011).
76. Schafer, Z. T. *et al.* Antioxidant and oncogene rescue of metabolic defects caused by loss of matrix attachment. *Nature* **461**, 109–113 (2009).
77. Gan, B. *et al.* Role of FIP200 in cardiac and liver development and its regulation of TNF $\alpha$  and TSC–mTOR signaling pathways. *J. Cell Biol.* **175**, 121 LP – 133 (2006).
78. Jiang, L. *et al.* Reductive carboxylation supports redox homeostasis during anchorage-independent growth. *Nature* **532**, 255 (2016).
79. Peck, B. *et al.* Inhibition of fatty acid desaturation is detrimental to cancer cell survival in metabolically compromised environments. *Cancer Metab.* **4**, 6 (2016).
80. Bertero, T. *et al.* Vascular stiffness mechanoactivates YAP/TAZ-dependent glutaminolysis to drive pulmonary hypertension. *J. Clin. Invest.* **126**, 3313–3335 (2016).
81. Bertero, T. *et al.* Tumor-Stroma Mechanics Coordinate Amino Acid Availability to Sustain

- Tumor Growth and Malignancy. *Cell Metab.* **29**, 124-140.e10 (2019).
82. Totaro, A. *et al.* Cell phenotypic plasticity requires autophagic flux driven by YAP/TAZ mechanotransduction. *Proc. Natl. Acad. Sci.* **116**, 17848 LP – 17857 (2019).
  83. Wu, J. *et al.* Intercellular interaction dictates cancer cell ferroptosis via NF2–YAP signalling. *Nature* **572**, 402–406 (2019).
  84. Bays, J. L., Campbell, H. K., Heidema, C., Sebbagh, M. & DeMali, K. A. Linking E-cadherin mechanotransduction to cell metabolism through force-mediated activation of AMPK. *Nat. Cell Biol.* **19**, 724–731 (2017).
  85. Ogawa, R. Mechanobiology of scarring. *Wound Repair Regen.* **19**, s2–s9 (2011).
  86. Aya, R. *et al.* The Shear Wave Velocity on Elastography Correlates with the Clinical Symptoms and Histopathological Features of Keloids. *Plast. Reconstr. surgery. Glob. open* **3**, e464–e464 (2015).
  87. Tachi, M. & Iwamori, M. Mass spectrometric characterization of cholesterol esters and wax esters in epidermis of fetal, adult and keloidal human skin. *Exp. Dermatol.* **17**, 318–323 (2008).
  88. Calvo, F. *et al.* Mechanotransduction and YAP-dependent matrix remodelling is required for the generation and maintenance of cancer-associated fibroblasts. *Nat. Cell Biol.* **15**, 637–646 (2013).
  89. Liu, F. *et al.* Mechanosignaling through YAP and TAZ drives fibroblast activation and fibrosis. *Am. J. Physiol. Lung Cell. Mol. Physiol.* **308**, L344–L357 (2015).
  90. Watanabe, K. *et al.* A ROCK inhibitor permits survival of dissociated human embryonic stem cells. *Nat. Biotechnol.* **25**, 681–686 (2007).
  91. Ohgushi, M. *et al.* Molecular Pathway and Cell State Responsible for Dissociation-Induced Apoptosis in Human Pluripotent Stem Cells. *Cell Stem Cell* **7**, 225–239 (2010).
  92. Takashima, K. *et al.* COPI-mediated retrieval of SCAP is crucial for regulating lipogenesis under basal and sterol-deficient conditions. *J. Cell Sci.* **128**, 2805 LP – 2815 (2015).

93. Takashima, K. *et al.* GBF1-Arf-COPI-ArfGAP-mediated Golgi-to-ER Transport Involved in Regulation of Lipid Homeostasis. *Cell Struct. Funct.* **36**, 223–235 (2011).
94. Goldstein, J. L., DeBose-Boyd, R. A. & Brown, M. S. Protein Sensors for Membrane Sterols. *Cell* **124**, 35–46 (2006).
95. Fernández-Ulibarri, I. *et al.* Diacylglycerol is required for the formation of COPI vesicles in the Golgi-to-ER transport pathway. *Mol. Biol. Cell* **18**, 3250–3263 (2007).
96. Baron, C. L. & Malhotra, V. Role of Diacylglycerol in PKD Recruitment to the TGN and Protein Transport to the Plasma Membrane. *Science (80-. )*. **295**, 325 LP – 328 (2002).
97. Hay, J. C. *et al.* Localization, dynamics, and protein interactions reveal distinct roles for ER and Golgi SNAREs. *J. Cell Biol.* **141**, 1489–1502 (1998).
98. Liu, G.-H. & Gerace, L. Sumoylation regulates nuclear localization of lipin-1alpha in neuronal cells. *PLoS One* **4**, e7031–e7031 (2009).
99. Li, T. Y. *et al.* Tip60-mediated lipin 1 acetylation and ER translocation determine triacylglycerol synthesis rate. *Nat. Commun.* **9**, 1916 (2018).
100. Jiang, M. *et al.* Changes in tension regulates proliferation and migration of fibroblasts by remodeling expression of ECM proteins. *Exp. Ther. Med.* **12**, 1542–1550 (2016).
101. Swift, J. & Discher, D. E. The nuclear lamina is mechano-responsive to ECM elasticity in mature tissue. *J. Cell Sci.* **127**, 3005–3015 (2014).
102. Guet, D. *et al.* Mechanical Role of Actin Dynamics in the Rheology of the Golgi Complex and in Golgi-Associated Trafficking Events. *Curr. Biol.* **24**, 1700–1711 (2014).
103. Fu, J. *et al.* Mechanical regulation of cell function with geometrically modulated elastomeric substrates. *Nat. Methods* **7**, 733–736 (2010).
104. Dumbauld, D. W. *et al.* How vinculin regulates force transmission. *Proc. Natl. Acad. Sci.* **110**, 9788 LP – 9793 (2013).
105. Bertolio, R. *et al.* Sterol regulatory element binding protein 1 couples mechanical cues and lipid metabolism. *Nat. Commun.* **10**, 1326 (2019).

106. Romani, P. *et al.* Extracellular matrix mechanical cues regulate lipid metabolism through Lipin-1 and SREBP. *Nat. Cell Biol.* **21**, 338–347 (2019).
107. Hausser, A. *et al.* Phospho-specific binding of 14-3-3 proteins to phosphatidylinositol 4-kinase III  $\beta$  protects from dephosphorylation and stabilizes lipid kinase activity. *J. Cell Sci.* **119**, 3613 LP – 3621 (2006).
108. Butcher, D. T., Alliston, T. & Weaver, V. M. A tense situation: forcing tumour progression. *Nat. Rev. Cancer* **9**, 108 (2009).